NEW MEXICO INSTITUTE OF MINING AND TECHNOLOGY

A MATHEMATICAL AND EXPERIMENTAL STUDY OF THE WATER-SILICATE INTERFACE IN POROUS MEDIA

BY

RAUL A. DEJU

Submitted to the faculty of the
New Mexico Institute of Mining & Technology
in partial fulfillment of the requirements
for the degree of Doctor of Philosophy
in Geoscience (Ground Water Hydrology)

March 1969

TABLE OF CONTENTS

Page

ABSTRACT i

GENERAL INTRODUCTION 1
Purpose
Outline of the Work
Acknowledgments

CHAPTER 1. SILICATE MINERALOGY 3
Structural Classification of the Silicates
Surface Mineralogy
Oxygen-Silicon Ratio
References

CHAPTER 2. MECHANISM OF SURFACE REACTIONS 18
Sorption Model
Experimental Procedure
Experiments on Sorption Rates
Effect of Detergent Concentration
Experiments to Relate Oxygen-Silicon
Ratio and Sorption
Reaction Mechanism
Summary
References

CHAPTER 3. ELECTRICAL PROPERTIES OF SILICATE MINERALS 34
Theoretical Considerations
Experimental
Summary
Symbols
References

CHAPTER 4. MATHEMATICAL TREATMENT OF SORPTION 71
Definitions
Kinetics
Mass Conservation
Boundary and Initial Conditions
Mathematical Solution
Summary
Symbols
References

CHAPTER 5. EXPERIMENTAL TREATMENT OF SORPTION 84
Experimental
Hydrogen Sorption
Desorption
Summary
References

Page

GENERAL SUMMARY AND CONCLUSIONS 107

RECOMMENDATIONS FOR FUTURE STUDY 109

APPENDIX 1. CHEMICAL ANALYSES PROCEDURES 110

APPENDIX 2. PPM-EPM CONVERSIONS 123

ABSTRACT

Static, electrokinetic, and column experiments were carried out to investigate sorption and to verify theoretical models. At the silicate-water interface, exchange of H^+ for metal cations takes place. The extent of such process (a sorption reaction) is related to the O:Si ratio of the silicate used. The rate of sorption increases with the ionic mobility. The region in which sorption occurs in the water-silicate system is determined by the isoelectric point of charge. In this report, a model of flow through porous media with sorption is developed. This model shows the difference between sorption and dispersion. Column experiments further illustrate this difference and give information about rates of sorption which can be correlated with the crystal structure.

GENERAL INTRODUCTION

Purpose

The purpose of this report is to discuss the basic properties of silicate minerals and to present a mathematical and experimental model of the flow of water through a silicate bed. The model includes not only the physical aspects of flow but also the chemical reactions taking place at the interface between a flowing liquid and a silicate bed. The model is restricted to the case of water and silicate minerals. Laboratory tests have been conducted to substantiate the model.

Outline of the Work

The problem of ground water contamination is one of growing concern, not only because of the increasing pressures on our sources of supply, but also because of the increasing necessity to find vehicles of waste disposal. Also, the hydrochemistry of waste waters must be understood in order to dispose properly of them. Similarly, knowledge of surface reactions is of critical importance in extractive metallurgy. This is especially true regarding the froth flotation process of mineral concentration and all phases of hydrometallurgical recovery of metals.

To understand these problems, we must obtain a better insight into the reactions that take place between water and the porous medium through which it flows. In this report, a model to explain the surface reaction mechanism between water and silicate minerals will be presented. Silicate minerals were selected because of their importance and abundance.

In order to understand the surface reaction mechanism, one must analyze the electrical properties of the silicate-water interface. The

electrical properties of interfaces are probably the most important single factor controlling surface reactions. A theoretical and experimental model of the electrical properties of the silicate-water interface is presented in Chapter 3. This model supports the proposed mechanism for the surface reactions taking place at the silicate-water interface.

Once the surface reactions and the electrical properties of the silicate-water interface are understood one can then construct a theoretical model to predict the fate of a chemical species in solution as it reacts with a solid through which the solution is percolating. This model includes the effects of surface reactions and the factors controlling them.

For the first time, the model proposed in this report attempts to combine surface chemistry with the equations of flow rather than considering only the physical aspects of flow as has been done by others.

Acknowledgments

The author is indebted to many people for their helpful comments while working on this project. Special thanks go to Dr. Gerardo Gross, Dr. Roshan Bhappu, Prof. Charles E. Jacob, and Dr. Dexter H. Reynolds for reading the manuscript and making helpful suggestions. Thanks also go to Dr. Geoffrey Purcell and Mr. A. J. Thompson for their assistance, comments, and encouragement. Miss Teri Ray helped with the editing and numerous people typed the manuscript.

The help of the many individuals who have not been mentioned by name is gratefully acknowledged.

CHAPTER 1

SILICATE MINERALOGY

The basic structural unit of all silicate minerals is a tetrahedron with a silicon atom at the center and four oxygen atoms at the corners. The oxygen-silicon distance is about 1.6 Å and the oxygen-oxygen distance about 2.6 Å. The different types of oxygen-silicon frameworks in the various silicates are based entirely on the combinations of the tetrahedral oxygen-silicon groups through sharing of oxygen atoms.

In recent years, infrared spectroscopy has permitted estimation of the ionic character of the oxygen-silicon bond to be 2.3 times that of the oxygen-carbon bond. Electronegativity measurements of the two bonds have substantiated this finding, since the ionic character amounts to 51 per cent for the oxygen-silicon bond and only 22 per cent for the oxygen-carbon bond; this means a ratio of 51 to 22, or 2.3 to 1. On this basis, it seems safe to assume that the oxygen-silicon bond is the strongest one occurring in silicate minerals.

The compositions and structures of the most important naturally occurring silicate minerals have been determined. Table 1 lists the accepted chemical compositions and some of the more important physical and optical properties of the silicates considered in this report. In a previous paper, Dejú and Bhappu (1965) presented a correlation of some of these properties to O:Si ratios. Others (DeVore, 1962; Hartman and Perdok, 1955; and Ramberg, 1952, and 1954) have correlated the properties listed in Table 1 to various stability criteria. DeVore (1962) presents a very good bibliography on silicate mineralogy.

Table 1. Physical and Optical Properties of Silicates

Sample	Formula	Specific Gravity	Hardness Index	Crystalline Form & Color	Index of Refraction (Na) (n,w,θ;α,β,γ)
livine	$(Mg,Fe)_2SiO_4$	3.26-3.40	6.5-7.0	Rhombic, olive green or grayish green.	1.662, 1.680, 1.699
orsterite	Mg_2SiO_4	3.19-3.33	6.0-7.0	Rhombic, white, greenish, yellowish.	1.635,1.651, 1.670
ayalite	Fe_2SiO_4	3.91-4.34	6.5	Rhombic, yellowish black.	1.835, 1.877, 1.886
ugite	$Ca(Mg\cdot Fe)(SiO_3)_2((Al\cdot Fe)_2O_3)_x$	3.20-3.60	5.0-6.0	Monoclinic dark green to black.	1.712, 1.717, 1.733
nstatite	$MgO\cdot SiO_2$	3.10-3.43	5.0-6.0	Rhombic grayish, or yellowish, or greenish.	1.650, 1.653, 1.658
podumene	$Li_2O\cdot Al_2O_3 4SiO_2$	2.64	5.5-6.0	Monoclinic, white, gray, green, pink, or purple.	1.660, 1.666, 1.676
rnblende	$Ca_2(Mg,Fe,Al)_5(OH)_2((Si,Al)_4O_{11})_2$	3.0 - 3.5	5.0-6.0	Monoclinic, dark green to black.	1.629, 1.642, 1.653
uscovite	$K_2O\cdot 3Al_2O_3 6SiO_2\cdot 2H_2O$	2.70-3.00	2.5-3.0	Monoclinic, colorless or pale yellow or gray.	1.561, 1.590, 1.594
eryl	$3BeO\cdot Al_2O_3 6SiO_2$	2.60-2.90	7.5-8.0	Hexagonal, green, blue, yellow, or reddish.	1.581, 1.575, -
bite	$Na_2OAl_2O_3 6SiO_2$	2.61-2.64	6.0-6.5	Triclinic, gray or colorless.	1.525, 1.529, 1.536
crocline	$K_2OAl_2O_3 6SiO_2$	2.54-2.57	6.0-6.5	Triclinic, white, yellowish, gray, green, or red.	1.522, 1.526, 1.530
artz	SiO_2	2.59-2.65	7.0	Hexagonal, trigonal, colorless or colored.	1.544, 1.553 -

STRUCTURAL CLASSIFICATION OF THE SILICATES

As pointed out in the previous section, the bonds between oxygen and silicon are so strong that the four oxygens are always found at the corners of a tetrahedron of nearly constant dimensions and very regular shape. All the various types of silicates arise from the various ways in which Si-O tetrahedra are related to one another. Various types of silicates are shown in Figures 1 through 4. The classification of silicates is based on the types of linkages. The structural classification of silicates is given in many books (Berry and Mason, 1959; Dana, 1955), and is depicted in Table 2.

Silicate structures also possess additional oxygen atoms, hydroxyl groups, water molecules, and cations which are arranged with the Si-O tetrahedra in such a way as to produce a mechanically stable and electrically neutral structure. Aluminum plays an important role in the structure of some silicates since it is stable in both fourfold and sixfold coordination. It sometimes replaces Si in an SiO_4 group and common six-coordination cations such as Mg^{+2} and Fe^{+2}. In some silicate minerals such as the feldspars, aluminum is present entirely in a single coordination; in others, like the amphiboles and pyroxenes, it may appear in both fourfold and sixfold coordination.

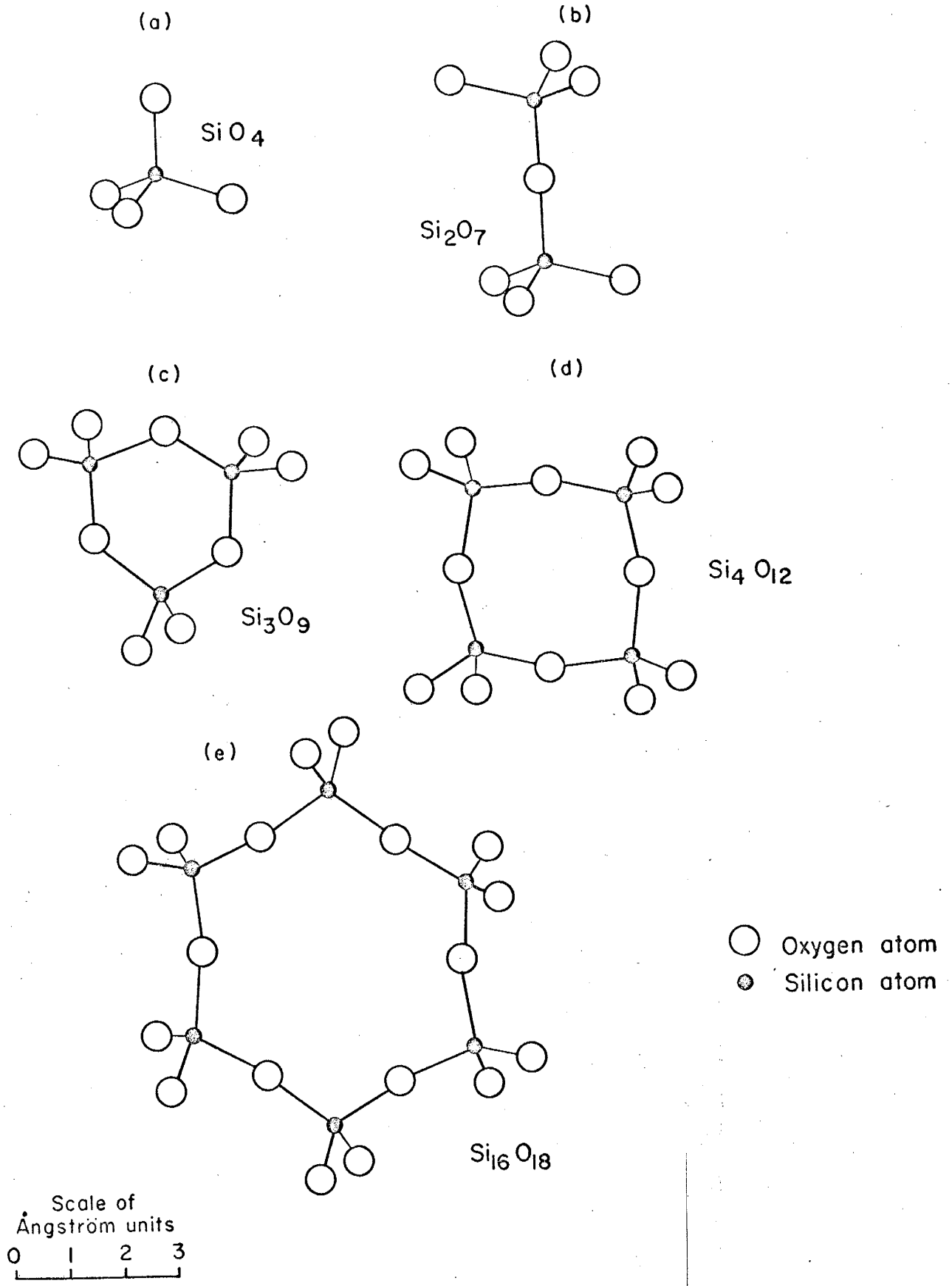

Figure 1. Types of linkage of silicon-oxygen tetrahedra. (a) Independent tetrahedra; (b) double tetrahedra, and (c), (d), and (e) ring structures. (After Berry and Mason, 1959.)

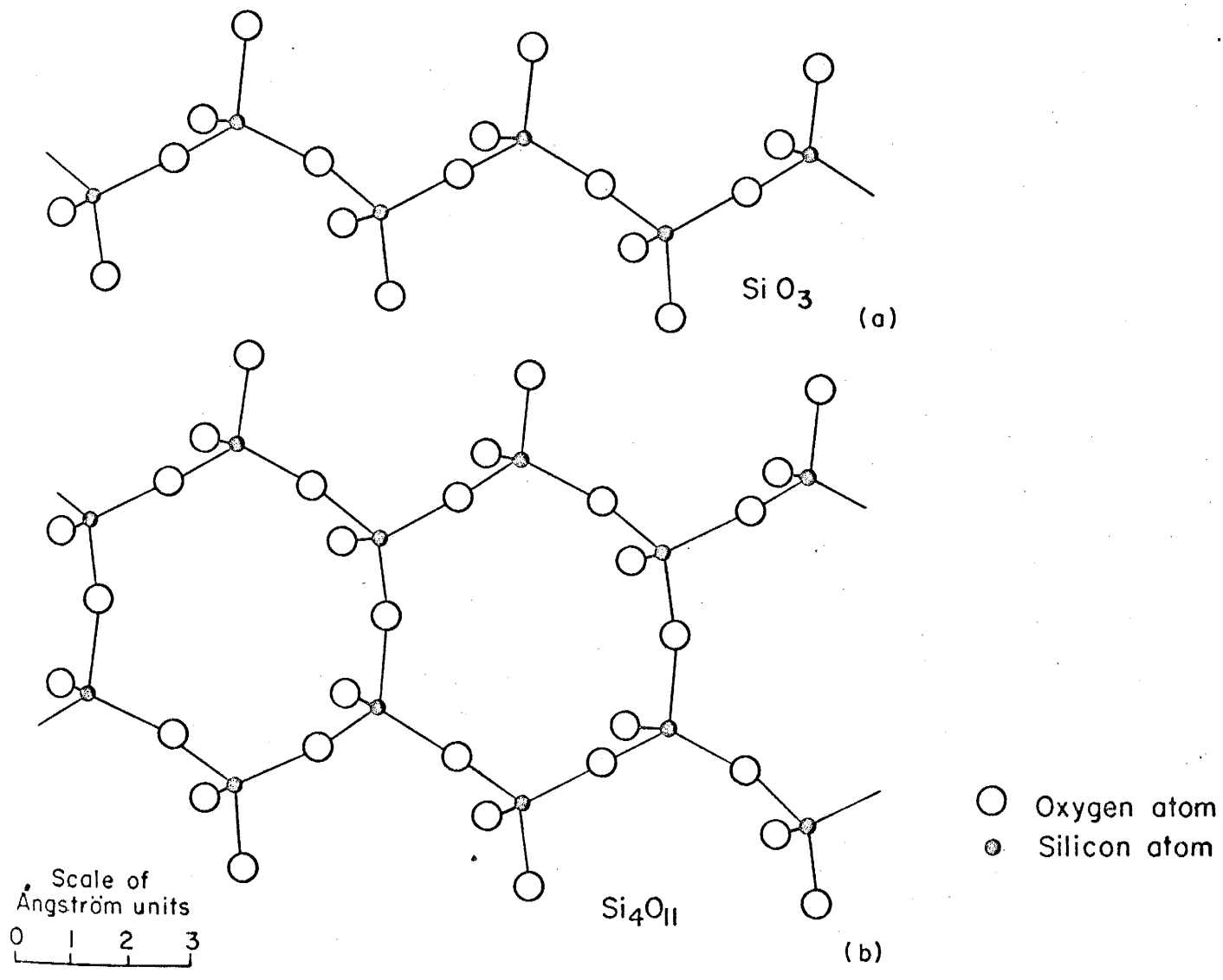

Figure 2. Types of linkage of silicon-oxygen tetrahedra. (a) Single chains; (b) double chains. (After Berry and Mason, 1959.)

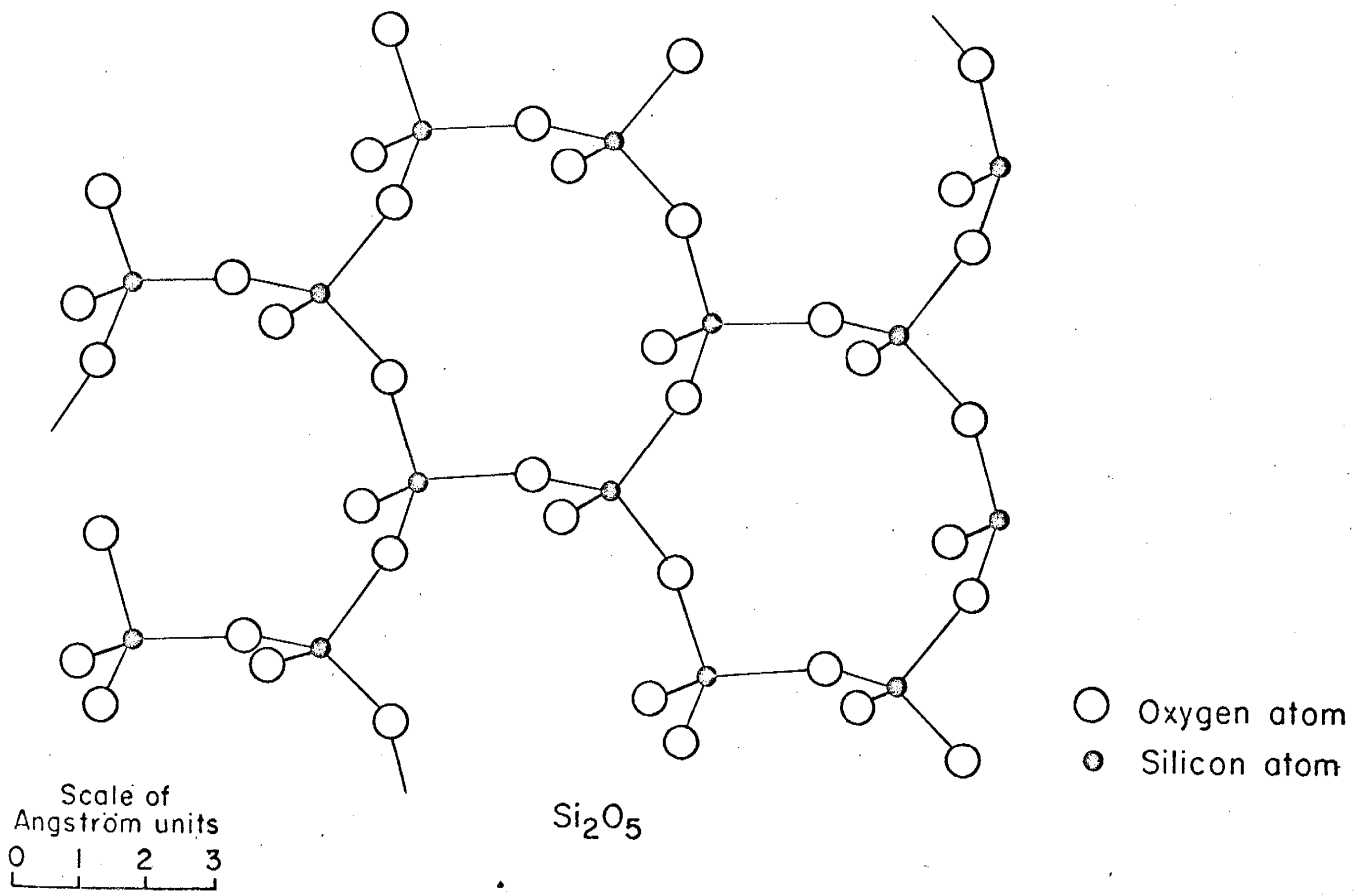

Figure 3. Type of linkage of oxygen-silicon tetrahedra. Sheet structure. (After Berry and Mason, 1959.)

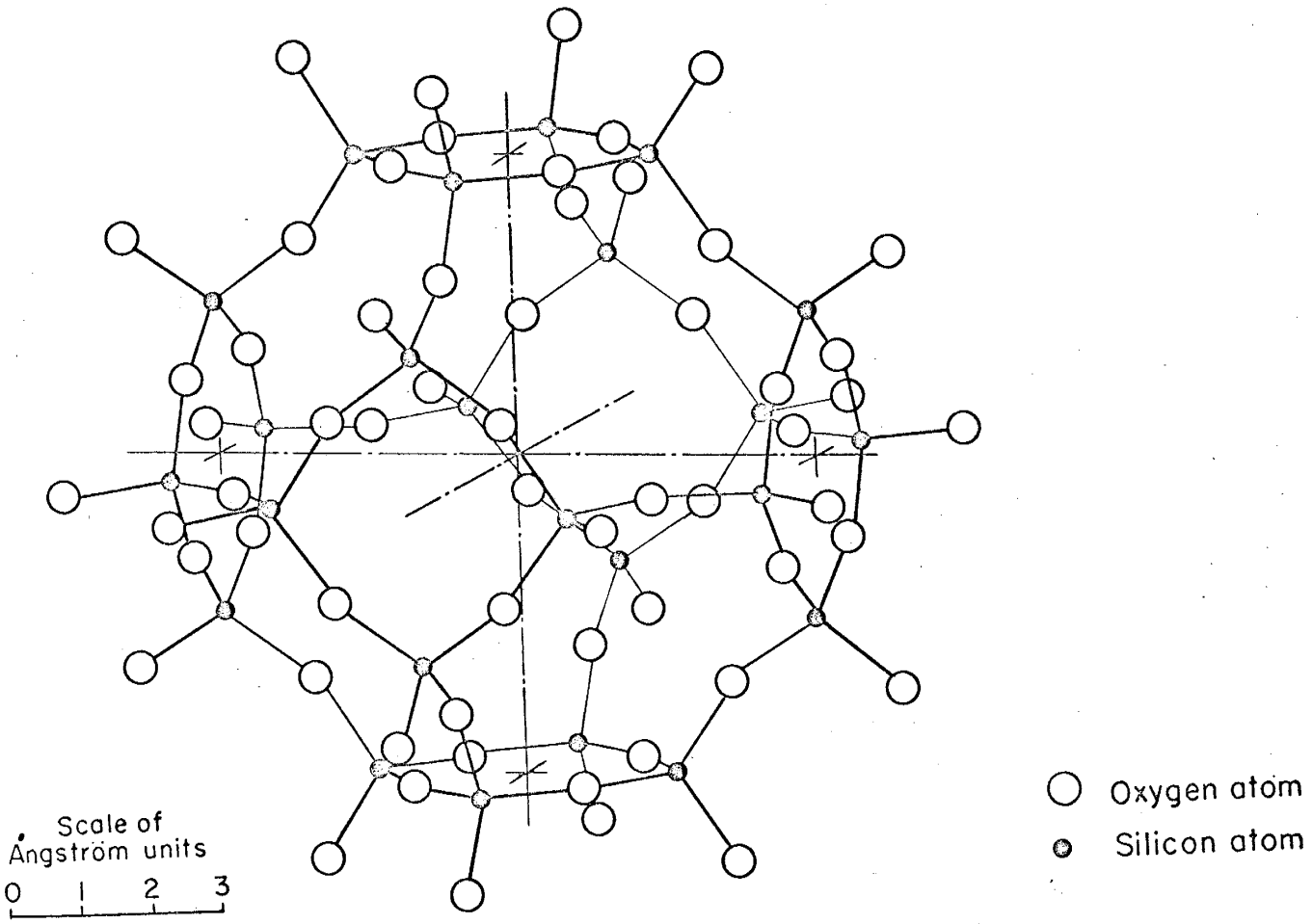

Figure 4. Type of linkage of oxygen-silicon tetrahedra. Three-dimensional network. (After Berry and Mason, 1959.)

Table 2. Structural Classification of the Silicates

Classification	Structural Arrangement	O:Si	Examples	Figure
Nesosilicates	Independent tetrahedra	4:1	Forsterite (Mg_2SiO_4)	1a
Sorosilicates	Two tetrahedra sharing one oxygen	7:2	Hemimorphite ($Zn_4Si_2O_7(OH)_2 \cdot H_zO$)	1b
Cyclosilicates	Closed rings of tetrahedra each sharing two oxygens	3:1	Beryl ($3BeO \cdot Al_2O_3 6SiO_2$)	1c,d,e
Inosilicates	Continuous single chains of tetrahedra each sharing two oxygens	3:1	Enstatite ($MgO \cdot SiO_2$)	2a
	Continuous double chains of tetrahedra sharing alternately two and three oxygens	11:4	Anthophyllite ($Mg_7(Si_4O_{11})_2(OH)_2$)	2b
Phyllosilicates	Continuous sheets of tetrahedra each sharing three oxygens	5:2	Talc ($Mg_3Si_4O_{10}(OH)_2$)	3
Tektosilicates	Continuous framework of tetrahedra each sharing all four oxygens	2:1	Quartz (SiO_2)	4

SURFACE MINERALOGY

The interruption of the atomic geometry at the crystal surface is the cause of many so-called surface phenomena. A crystal system must minimize all surface phenomena so that the system can accomodate the surface or interface with a minimum of additional energy. Thus, charge demands must be satisfied, and the atomic coordinations must be approximately complete to minimize the effects of the elastic strains, repulsions of similar charges, and the compositional interruption of the surface. These adjustments must also produce a minimum of free energy difference between the crystal, the surface, and the external environment. All adsorption phenomena can be thought of as a device adopted by a given crystal system in order to minimize the surface effects. Figure 5 indicates various atomic associations at the quartz surface, all of which tend to minimize effects caused by the interruption of the atomic geometry at the crystal surface.

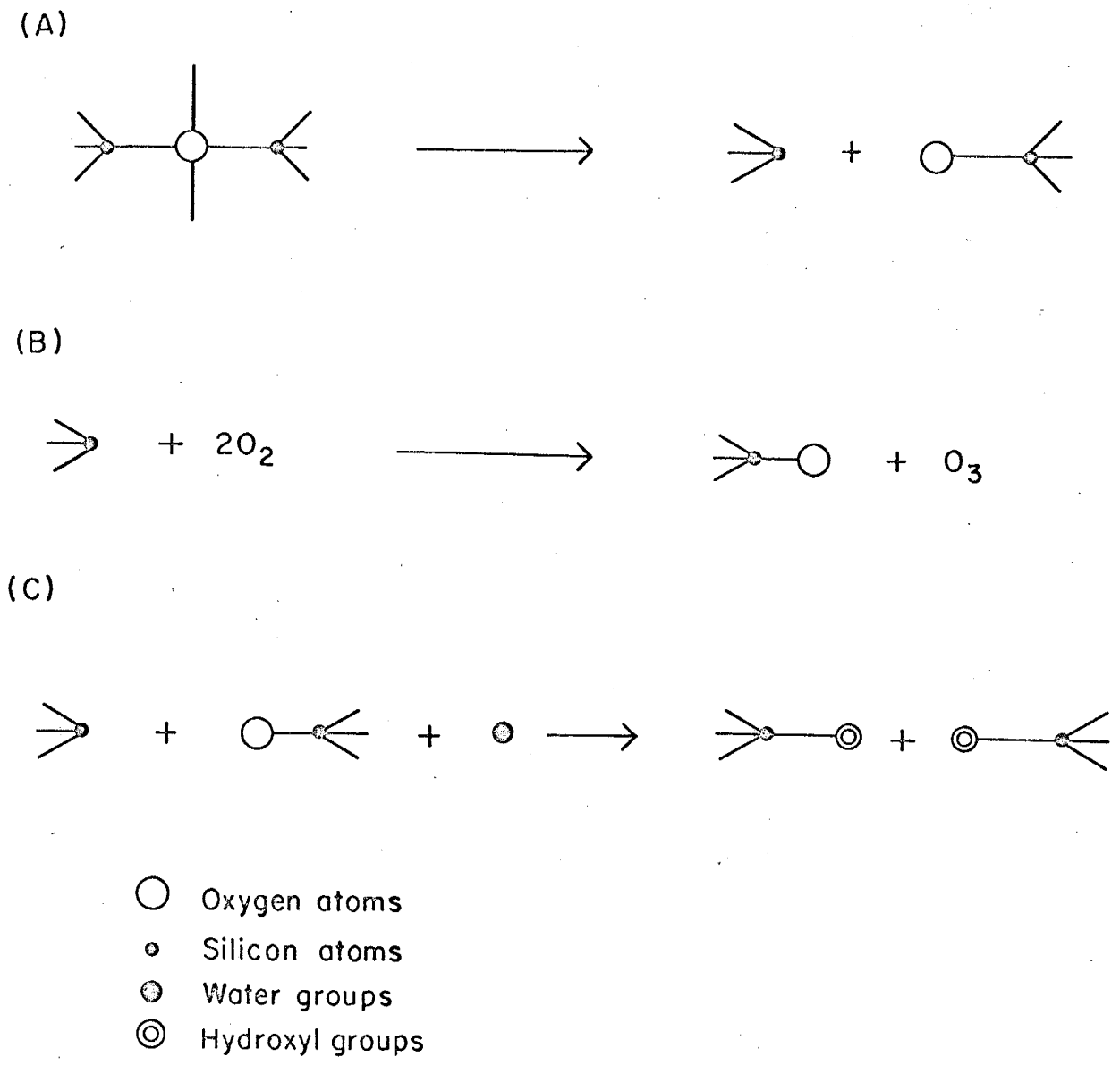

Figure 5. Various atomic associations at surfaces: (a) depicts the oxygen-silicon bonding at a fresh surface of quartz; (b) depicts the formation of ozone on a fresh surface of quartz; (c) depicts the possible hydration of a surface of quartz.

OXYGEN-SILICON RATIO

Except for the case of the nesosilicates, the oxygen-silicon polymerization is usually interrupted by the surface. This interruption, as shown by DeVore (1962), tends to increase the O:Si ratio and thus would change the "type" of Si-O tetrahedra present at the surface. Table 3 lists, and Figures 6 and 7 illustrate, the compositions of surface Si-O tetrahedra for various directions in the silicates. It is seen from Table 3 and Figures 6 and 7 that certain surface compositions deviate markedly from the mineral composition, and are related more closely to the compositions of other minerals than they are to their own interiors.

Table 3. Surface Oxygen-Silicon Ratios
(after DeVore, 1962)

Mineral	Surface	Composition Si-O Tetrahedra	Combined Composition Si-O Tetrahedra
Olivine	(hkl)	Si_2O_8*	Si_4O_{16}
Pyroxene	(001)	Si_2O_7	Si_4O_{14}
	(hk0)	Si_2O_6*	Si_4O_{12}
Amphibole	(001)	Si_2O_6 and Si_2O_7	Si_4O_{13}
	(010)	Si_2O_6*	Si_4O_{12}
	(100)	Si_2O_6* and Si_2O_5*	Si_4O_{11}
Mica	(010)	Si_2O_5*	Si_4O_{10}
	(hk0)	Si_2O_6 and Si_2O_5*	Si_4O_{11}
Quartz	(0001)	Si_2O_6 and Si_2O_4*	$Si_{12}O_{28}$
	(hh$\bar{2}$l)	Si_2O_5 and Si_2O_4*	$Si_{12}O_{28}$ and $Si_{12}O_{29}$

* Si-O tetrahedra with the mineral composition, i.e., no polymerization interruption. The surface Si-O tetrahedra are single but are listed in the table as complexes to give whole numbers.

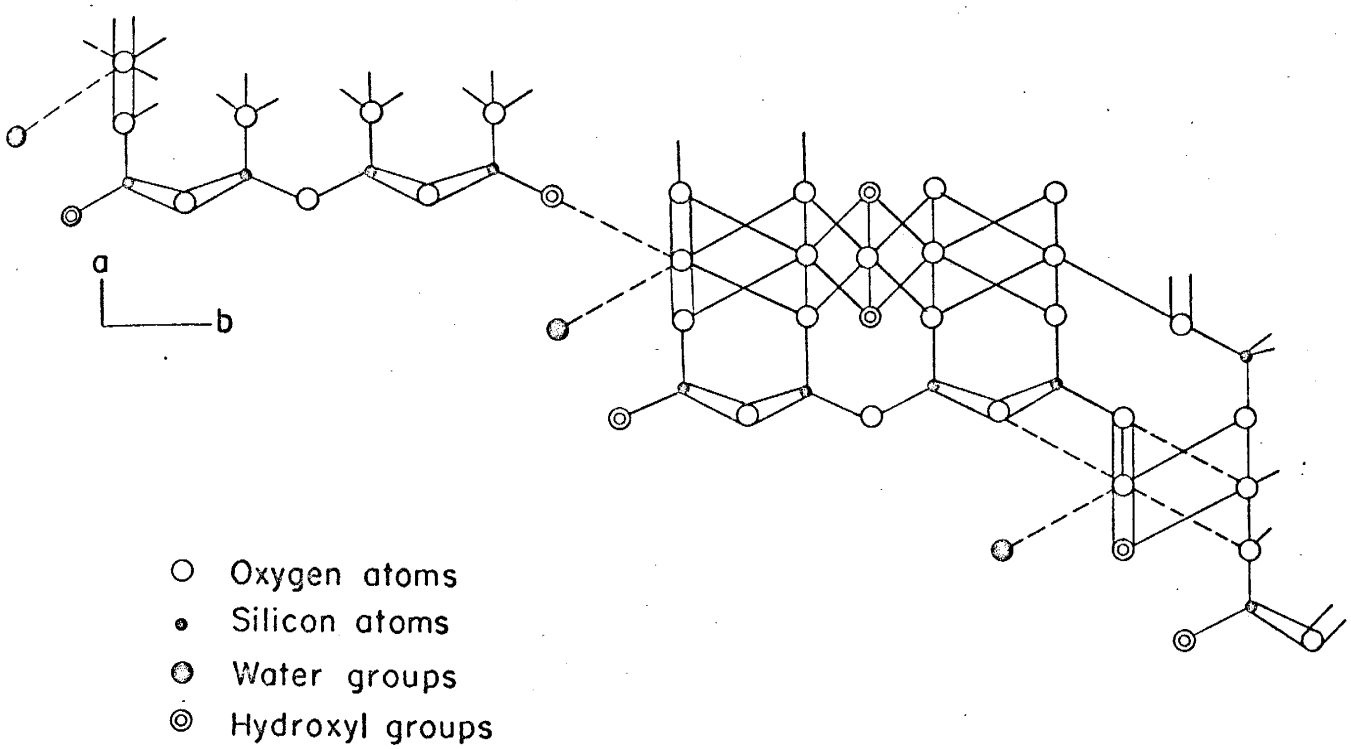

Figure 6. Atomic associations at the amphibole surface. The figure depicts the bonding relation and surface composition on (110) of amphibole. The left side of the diagram depicts composition with maximum hydrogen association with Si-O oxygens; right side illustrates the minimum hydrogen association with Si-O oxygens. Structure is schematic and projected on (001). Bond angles and bond lengths are not exact. (After DeVore, 1962.)

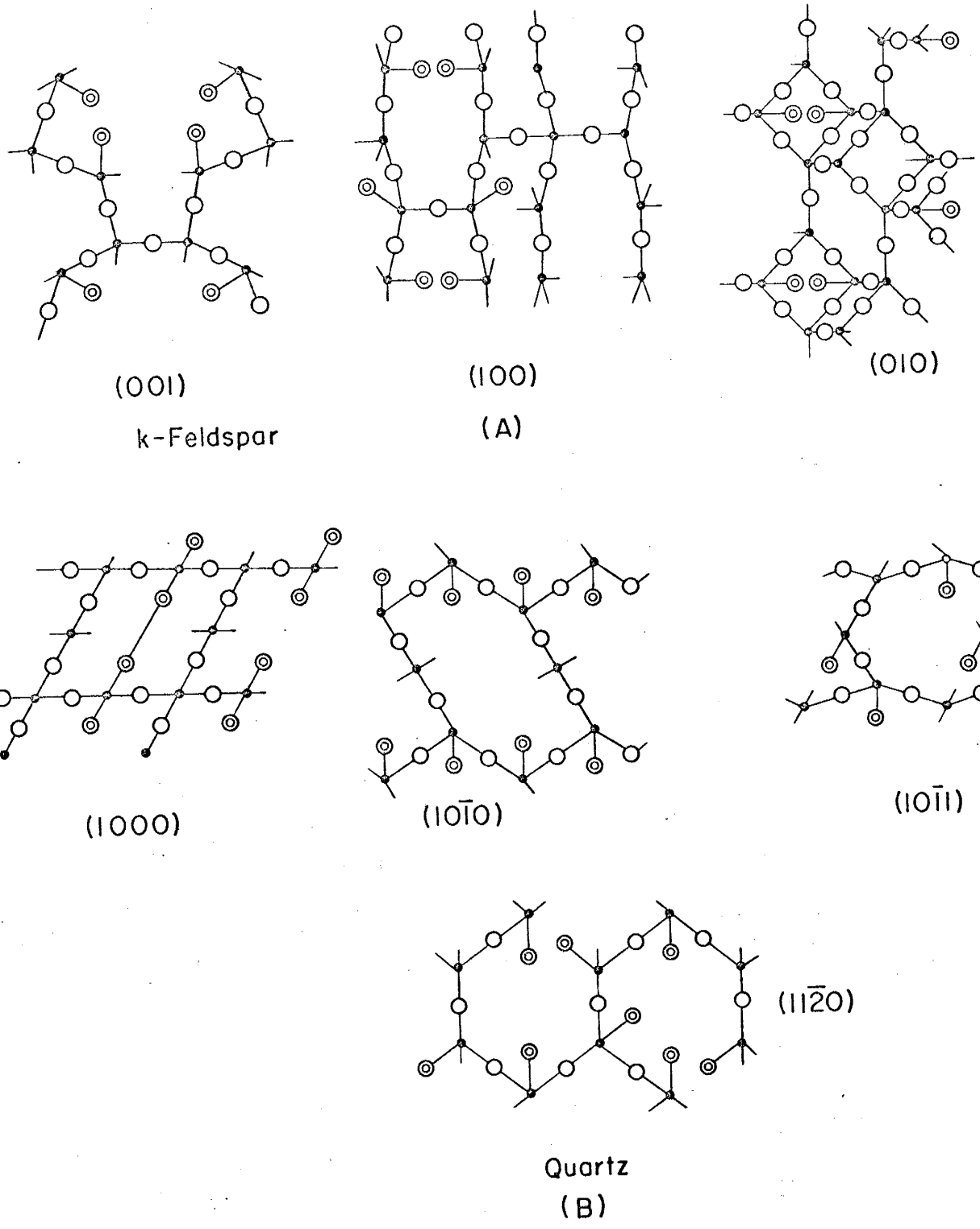

Figure 7. Atomic associations at quartz and K-feldspar surfaces. Symbols are the same as in the previous figure. (After DeVore, 1962.)

REFERENCES

Berry, L. G., and Mason, Brian (1959) Mineralogy (Concepts, Descriptions, Determinations), San Francisco: W. H. Freeman and Company

Dana, Edward S., (1955) A Textbook of Mineralogy, New York: John Wiley and Sons.

Deju, R. A., and Bhappu, R. B. (1965) Surface Properties of Silicate Minerals, Circular 82, State Bureau of Mines and Mineral Resources, New Mexico Institute of Mining and Technology.

DeVore, George W., (1962) Compositions of Silicate Surfaces and Surface Phenomena, publ. Dept. of Geology, Florida State Univ., Tallahassee, Fla.

Hartman, P., and Perdok, W. G. (1955) On the Relation Between the Structure and Morphology of Crystals, Act. Crystal., vol. 8, pp. 49-52, 521-529.

Ramberg, H. (1952) Chemical Bonds and the Distribution of Cations in Silicates, Journal of Geology, vol. 60, pp. 331-355.

Ramberg, H. (1954) Relative Stabilities of Some Simple Silicates as Related to the Polarization of the Oxygen Ions, Am. Mineral., vol. 39, pp. 256-271.

CHAPTER 2

MECHANISM OF SURFACE REACTIONS

In the previous chapter the properties of various silicate minerals were discussed from a mineralogical standpoint. Now the reactions which occur when these minerals are put in contact with water will be studied. These reactions occur almost entirely in the surface layer of the minerals (Deju and Bhappu, 1965) and are termed sorption reactions.

By sorption I mean the composite of all adsorption phenomena occurring between the silicate surface and the water in contact with it. For many years it has been common in the literature to classify all surface reactions as being specifically physical adsorption or chemical adsorption. However, for reactions like the ones outlined in this chapter it is impossible to attempt such a classification since both processes occur in a combined way and influence each other greatly.

In this chapter a model of sorption as seen from a chemical bond standpoint will be presented. On the basis of this model, one can study the surface reactions between deionized water and a silicate mineral. One can also study the system of polluted water and silicate. The polluted water will here be represented by water to which a given amount of alkyl benzene sulfonate (ABS) has been added. Finally, a general surface reaction for the water-silicate system will be postulated.

SORPTION MODEL

It is known that as the oxygen-silicon ratio increases from quartz to the olivines, a greater percentage of the oxygen bonding power is available for bonding to cations other than silicon. Hence, with an increasing oxygen-silicon ratio, there is increasing oxygen-to-metal bonding. Upon the fracturing of a silicate mineral crystal, the oxygen-metal bond breaks more easily than the stronger oxygen-silicon bond, resulting in a negatively charged surface. Then, if the mineral is immersed in a liquid containing hydrogen ions, the negatively charged surface should tend to be neutralized by hydrogen ions from solution, resulting in a change of the solution pH. Thus, an increase in the degree of sorption of hydrogen ions must occur as the oxygen-silicon ratio in the crystal structure increases.

Deju and Bhappu (1967) found that for a given silicate mineral the change of pH with time is given by

$$\Delta pH = C_o(1-e^{-C_1 t}) \qquad (1)$$

where C_o and C_1 are experimentally determined constants. C_o is readily determined since, when $t \to \infty$,

$$\Delta pH(\infty) = C_o = \lim_{t \to \infty} \Delta pH \ .$$

C_1 can be determined by differentiating (1) with respect to time.

EXPERIMENTAL PROCEDURE

Sorption Experimental Setup

Samples of each mineral used were placed in freshly deionized water previously adjusted to a desired pH with HCℓ. The beaker containing the solid sample and the water was placed under a bell jar from which the air was displaced at once by nitrogen gas from a tank. All experiments were carried out in a nitrogen atmosphere. The sample and solution were stirred gently but continuously during the entire experiment, the stirring speed being kept about the same for all runs. Changes in pH were followed with a Corning Model 12 pH meter and recorded on a Heathkit servo recorder (Figure 8).

Analytical Procedure

Samples of solution and solid were analyzed before and after each sorption experiment. Liquids were analyzed using the procedures outlined in Appendix 1. Solids were analyzed using an ARL Spectrographic Analyzer. Analyses for detergents in solution were carried out using a spectrophotometric procedure furnished by Shell Chemical Company (Paik, 1967), which is also listed in Appendix 1.

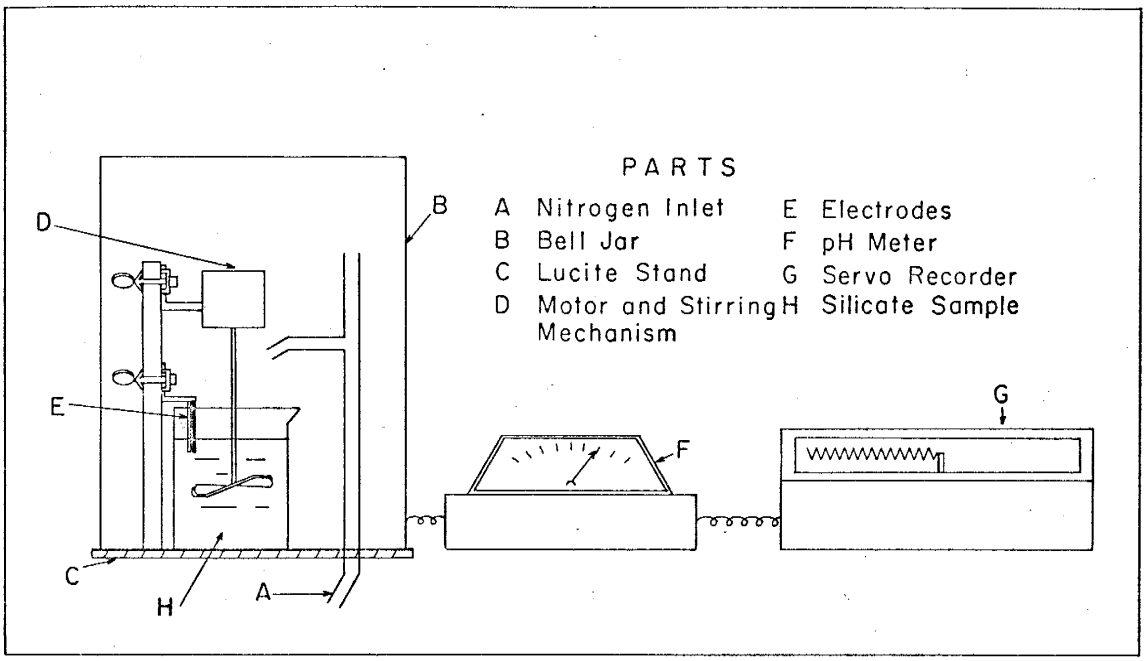

Figure 8. Experimental setup.

EXPERIMENTS ON SORPTION RATES

Following the experimental procedure outlined, the rate of sorption of H^+ ions from water solution by the silicate minerals under consideration was studied. The experimental results obtained were then correlated with theoretical results obtained using equation (1). Results obtained with water containing rather high concentrations of a common detergent (ABS) were also compared to the theoretical predictions.

The correlation between experimental and theoretical results is shown for a sample of glaucophane in Figure 9. Error analysis of the correlation gives a mean deviation of ± 1.2 per cent, which is well within accuracy limits. It is evident from Figure 9 that as the detergent concentration is increased the total change of pH decreases. This seems to indicate that the detergent is attaching to some of the metal cations present at the surface of the mineral, thus preventing the exchange of hydrogen for these cations.

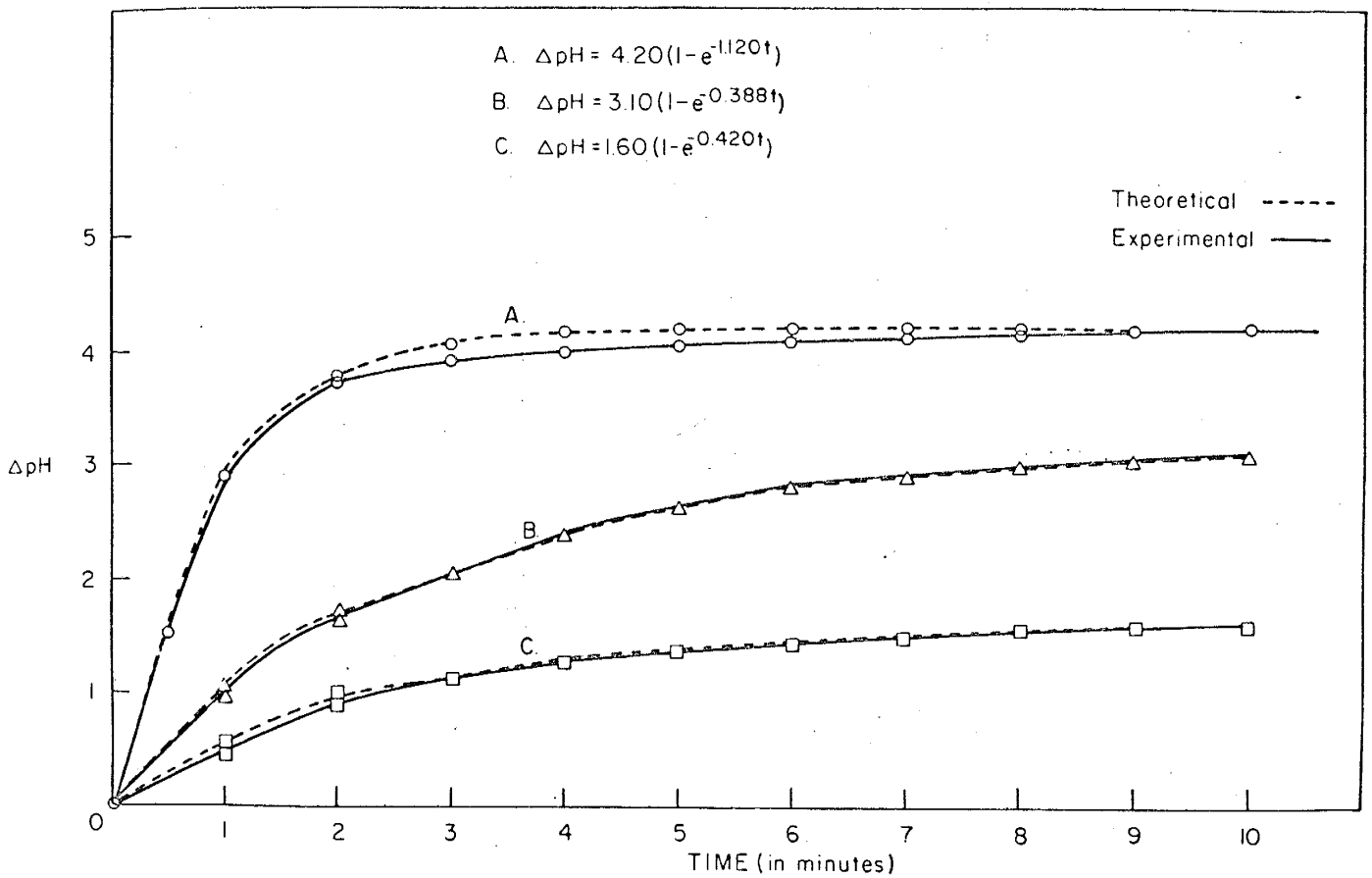

COMPARISON OF EXPERIMENTS AND THEORY FOR GLAUCOPHANE

Figure 9.

EFFECT OF DETERGENT CONCENTRATION

To further examine the effects of concentration on the total pH change, the maximum change of pH of each silicate mineral was plotted as a function of ABS concentration. Results are shown in Figure 10, the plot of which can be divided into three main regions as follows:

Region A. This is the region where the concentration of ABS is so high that a minimum number of hydrogen ions is sorbed on the surface. This region extends, in most instances, from concentrations of 10^{-2} M up. The pertinent equation is

$$\text{maximum} \quad \Delta \text{ pH} = \text{constant} \tag{2}$$

Region B. In this region, the concentration of ABS is less than in the previous one; therefore, some hydrogen ion sorption can take place. As the ABS concentration decreases, the hydrogen ion sorption increases. A maximum sorption of hydrogen ions finally occurs at the lower end of this region.

Region C. This part of the plot is also a horizontal line, that is, equation (2) is satisfied. At such low concentrations (below 5×10^{-7} M) of ABS, the role of the sulfonate ion is minimal, and thus maximum hydrogen sorption occurs.

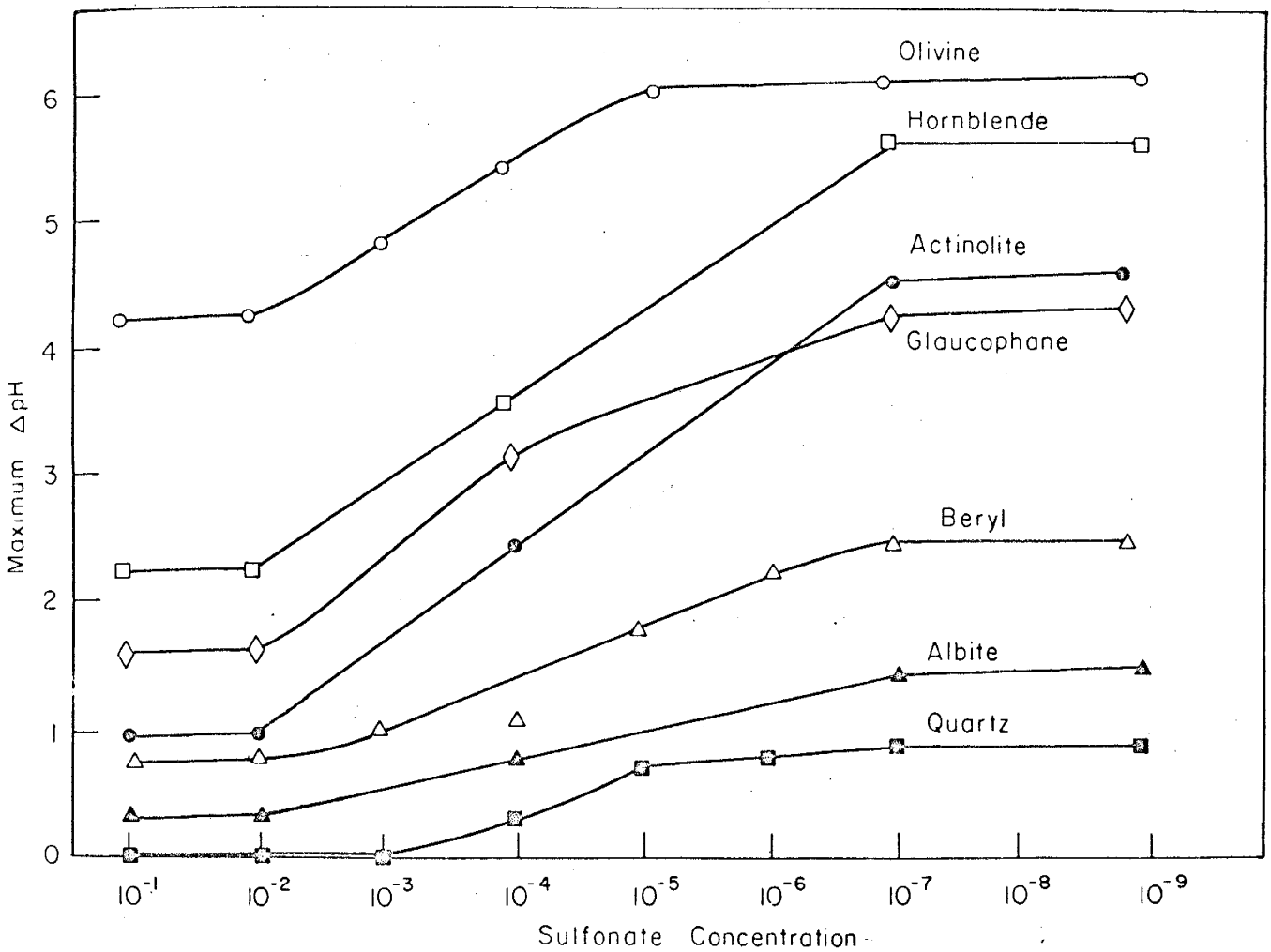

SULFONATE CONCENTRATION VERSUS MAXIMUM CHANGE IN pH
(INITIAL pH = 3.50)

Figure 10.

EXPERIMENTS TO RELATE OXYGEN-SILICON RATIO AND SORPTION

An increase in the change of pH, that is, in hydrogen ion sorption, takes place as the oxygen-silicon ratio in the crystal structure increases, the olivines experiencing the greatest change in pH while quartz shows almost no change (Fig. 11). Moreover, the greatest change in pH occurs during the first three minutes of the reaction. The results substantiate the sorption model proposed earlier in this chapter.

The attraction of hydrogen ions in some form or other to the surface of the mineral, however, does not fully explain what goes on during the reaction. There may also be an ion exchange (hydrolysis) between exposed metal ions of the lattice and hydrogen ions of water. For this reason, the crystal surface may gain additional hydrogen ions and the liquid phase may acquire further alkalinity.

In order to investigate further the mechanism behind the pH change, the escape of ions from the solid's surface into the solution phase was examined. The ions considered in this study were Ca, Mg, Fe, Al, Na, K, Li, and SiO_2. All silicates listed in Chapter 1 were investigated in this fashion. A typical result is shown in Figure 12 for the case of microcline. The plot for microcline shows that the rate at which H^+ ions are moving from the liquid into the surface of the solid is much faster than the rate at which the metal cations are coming from the solid's surface into the liquid. However, it is important to point out that at equilibrium the amount of metal ions that have left the solid surface (in milliequivalents) is very close to the amount of H^+ ions (in milliequivalents) that have come into the solid surface. Table 4 illustrates this point for various of the

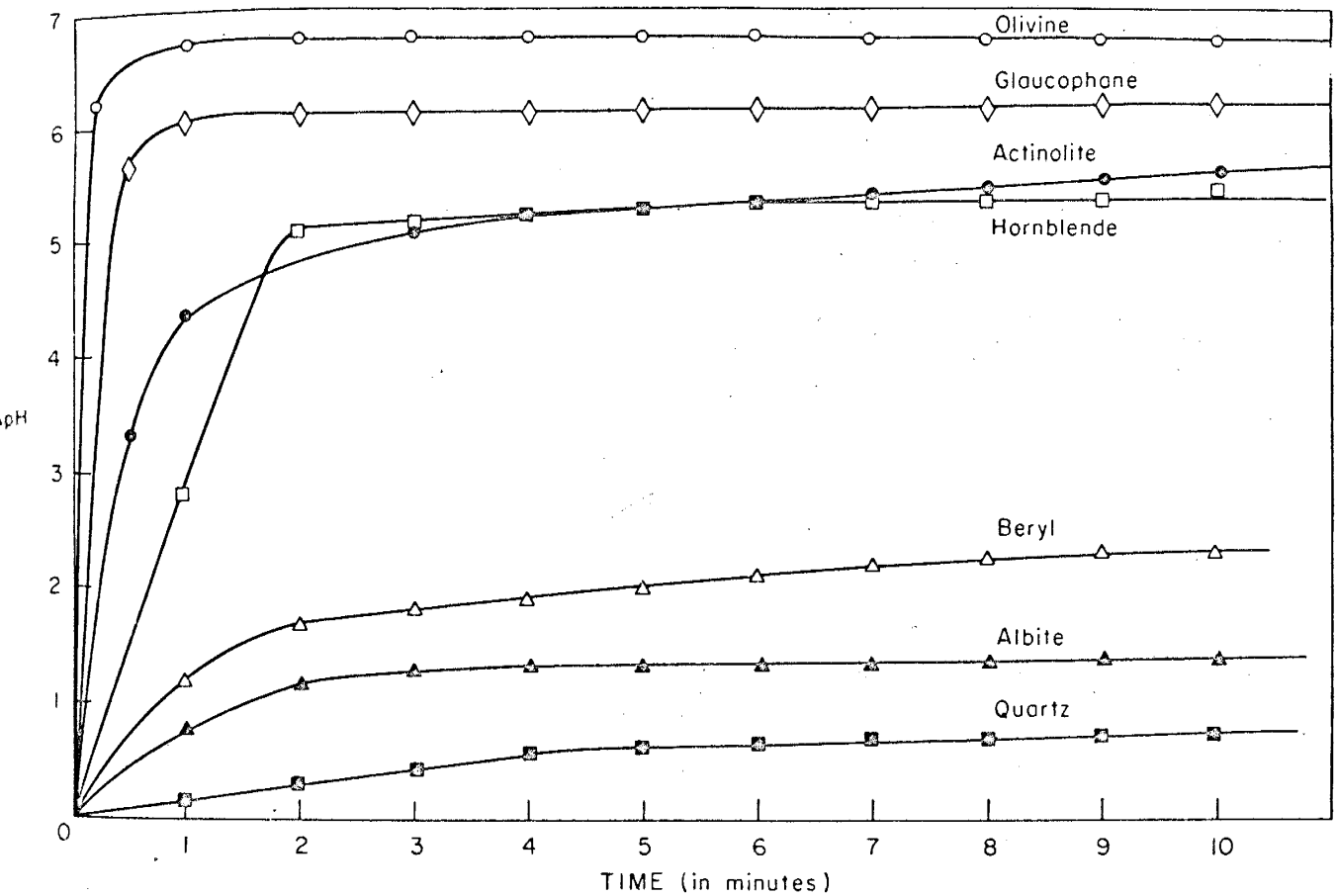

ADSORPTION ISOTHERMS IN WATER

Figure 11.

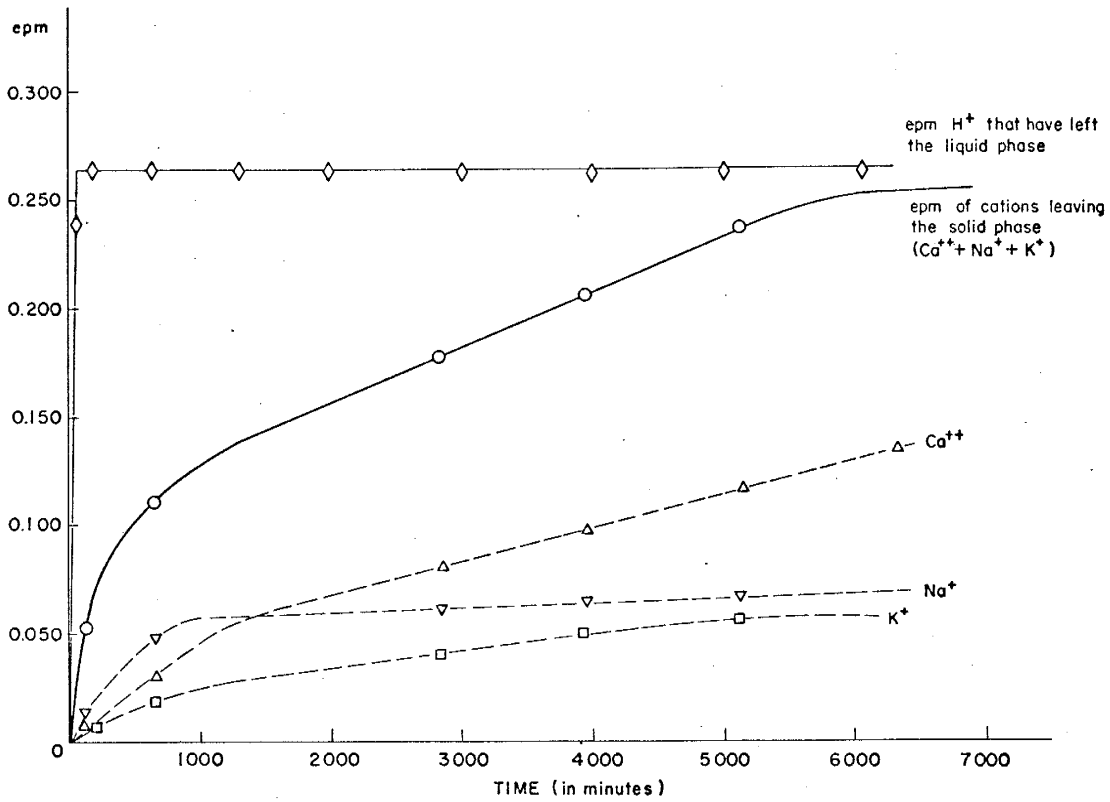

Figure 12. Isotherms for microcline.

minerals investigated. This table clearly shows that at equilibrium the number of ions that left the liquid phase is equal to the number of ions that entered it. Thus, one can conclude that the adsorption mechanism between silicate minerals and water is controlled by the physical and chemical properties of both phases and leads after a given time to a perfect exchange of ions between the two phases.

Table 4. Results of Ion Exchange Tests

ample	H^+ ions going into the solid surface per liter of solution †	Initial pH	Final pH	M^+ and M^{++} ions going into solution per liter of solution ††	Ions exchanged
ivine	1.06×10^{19}	4.75	10.50	1.02×10^{19}	Mg, Ca, K, Na
rnblende	1.06×10^{19}	4.75	9.80	1.29×10^{19}	Fe,Ca,Mg,K,Na
bite	1.06×10^{19}	4.75	6.01	0.92×10^{19}	Ca,K,Na,Fe,Mg
odumene	1.00×10^{21}	2.10	2.20	1.25×10^{21}	Li, Ca, Mg, Na
odumene	6.02×10^{20}	1.48	1.49	5.98×10^{20}	Ca, Na
odumene	1.90×10^{20}	3.50	8.75	1.80×10^{20}	Li, Ca, Na
gite	1.90×10^{20}	3.50	9.50	1.98×10^{20}	Na, K, Ca, Mg
gite	1.90×10^{20}	3.50	9.76	2.00×10^{20}	Na, K, Ca, Mg
gite	1.90×10^{20}	3.50	9.88	1.88×10^{20}	Na, K, Ca, Mg
ass Beads* (Feldspar)	2.35×10^{19}	4.40	7.90	2.36×10^{19}	Li, Na

3-M, Superbrite

† measured by a determination of pH

†† measured by a determination of ppm of ions in the liquid before and after the reaction

REACTION MECHANISM

On the basis of the results shown in this chapter one can postulate the following reactions to be occurring at the silicate-water interface.

$$pnH^{+} + \overline{M_pY_n} \rightarrow pM^{+n} + n\overline{H_pY}$$

$$pnH_2O + \overline{M_pY_n} \rightarrow pM^{+n} + (np)OH^{-} + n\,\overline{H_pY} \qquad (3)$$

where M^{+} is the metal cation, Y^{-} is the anionic part of the silicate sample, overbars represent surface products, and ions indicate species in aqueous phase. Also, n is the valence of M and p is the valence of Y.

This reaction mechanism has been further substantiated by Dejú and Bhappu (1966) and Faust and Hunter (1967).

SUMMARY

The reaction between the silicate mineral particles and the acidified water involves mainly an exchange of metal ions for hydrogen ions on the surface of the solid, leading to an increase in pH of the aqueous phase.

The degree of reaction depends directly on the oxygen-silicon ratio of the silicate structure, being greatest for the olivines.

The degree of reaction was also studied in the presence of pollutants (detergents). These studies indicate that the effect of the detergent is to attach to some of the metal cations present at the surface of the mineral thus preventing the exchange of hydrogen for these cations.

A model to explain the behavior of silicate minerals when immersed in water was presented. This model postulates that the reaction between the silicate mineral particles and water involves mainly an exchange of metal ions for hydrogen ions leading to an increase in pH of the aqueous phase. The model states that the actual reactions are of the form of equation (3).

REFERENCES

Dejú, R. A., and Bhappu, R. B. (1965) Surface Properties of Silicate Minerals, Circular 82, State Bureau of Mines and Mineral Resources, New Mexico Institute of Mining and Technology.

Dejú, R. A., and Bhappu, R. B. (1966) A Chemical Interpretation of Surface Phenomena in Silicate Minerals, Circular 89, State Bureau of Mines and Mineral Resources, New Mexico Institute of Mining and Technology.

Dejú, R. A., and Bhappu, R. B. (1967) A Correlation Between Surface Phenomena and Flotation in Silicates, Circular 90, State Bureau of Mines and Mineral Resources, New Mexico Institute of Mining and Technology.

Faust, Samuel D., and Hunter, J. V. (1967) Principles and Applications of Water Chemistry, New York: John Wiley & Sons, Inc.

Paik, Young H. (1967) Infrared and Flotation Studies of Adsorption of Sodium Alkylbenzenesulfonate on Olivine, Thesis, New Mexico Institute of Mining and Technology.

CHAPTER 3

ELECTRICAL PROPERTIES OF SILICATE MINERALS

The electrical phenomena occurring at the water-solid interface have been the subject of almost constant investigation for the past two centuries. The first breakthrough was accomplished by Reuss (1809) who found that if a potential is applied across a porous plug of wet clay, separating two portions of water, then a flow of water occurs from one side of the plug to the other. This phenomenon has been termed electroosmosis.

About 40 years later, Wiedemann (1852) made quantitative measurements of electroosmosis in his mass flow rate studies. Then Quinke (1861) discovered that if a liquid is forced through a porous plug of wet clay, a potential is created. This potential is now called streaming potential.

All of the above investigations were experimental in nature and the quantitative results derived from them were arrived at in an empirical fashion.

The development of the theory of electrical phenomena at the water-solid interface did not begin until the time of Helmholtz(1879) who based his theory on the existence of electrically charged layers of opposite sign at the water-solid boundary.

Since the early works of Helmholtz, theoretical investigations on the electrical properties of interfaces have received detailed consideration from many investigators; results indicate that a quantitative treatment presents many difficulties. Even though in most cases only approximations have been derived, these have proven to be of practical use.

In this chapter an attempt is made to begin with a set of simple and physically reasonable assumptions, and to build a model of the water-solid interface. The model is then tested by experimental means and its electrical properties are related to other properties of the water-solid system.

THEORETICAL CONSIDERATIONS

When a potential difference is externally applied to a liquid containing charged particles, it causes a migration of the particles to the pole carrying a charge opposite to that of the particles. If the particles are ions, the phenomenon is called ionic conduction; in the case of mineral particles, it is called electrophoresis. The present chapter is concerned only with electrophoresis and other electrical properties of a colloidal suspension of a mineral.

A Model of a Mineral Particle and Its Surrounding Electric Layers.

Generally, a mineral particle in suspension carries a charge on its surface. This surface charge, together with the ions in solution near the surface to maintain electroneutrality, form a series of electrical layers around the mineral particle. The ions responsible for the surface charge are termed surface-charge ions. The potential at the surface of the mineral is designated by ψ_0. Some of the ions near the surface of the mineral are anchored in a layer directly adjacent to the surface. These ions, which are said to be in the Stern layer, are strongly held to the surface. The potential of the periphery of this layer is called zeta potential (ψ_ζ). The remaining ions are loosely held by electrostatic forces and constitute the diffuse layer of counter ions that extends well into the solution. The surface layer and the Stern layer are grouped into what is called here the dipole layer. Figure 13 is a representation of all these layers.

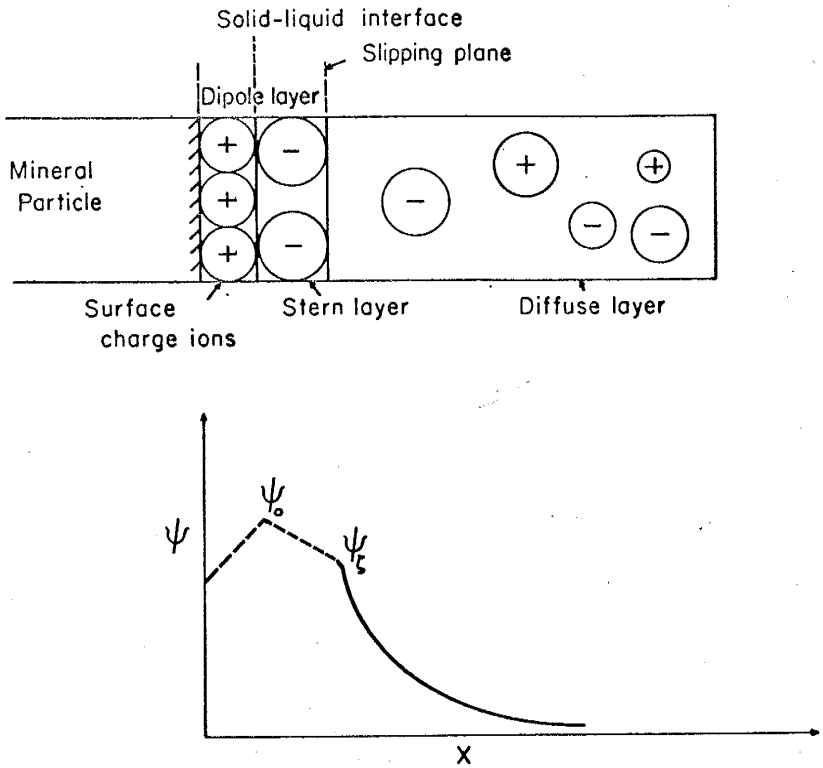

A Model of a Particle Surface and Its Surrounding Electric Layers

Figure 13.

To represent the electrical properties of a mineral particle surrounded by a dipole layer, the methods of potential theory are used.

The starting point is the divergence theorem

$$\int_T (\nabla \cdot A)\, dT = \int_\sigma A_n\, d\sigma$$

dT = volume element

$d\sigma$ = surface element.

Now we define two functions, $u = u(x,y,z)$ and $v = v(x,y,z)$, having continuous partial derivatives of the second order. Then, if we let $\vec{A} = \overrightarrow{u\nabla v}$, it follows that

$$\int_T (\nabla \cdot \overrightarrow{u\nabla v})\, dT = \int_\sigma (\overrightarrow{u\nabla v}) \cdot \vec{n}\, d\sigma$$

$$\nabla \cdot (\overrightarrow{u\nabla v}) = \left(\frac{\partial}{\partial x}\hat{i} + \frac{\partial}{\partial y}\hat{j} + \frac{\partial}{\partial z}\hat{k}\right) \cdot \left(u\left(\frac{\partial v}{\partial x}\hat{i} + \frac{\partial v}{\partial y}\hat{j} + \frac{\partial v}{\partial z}\hat{k}\right)\right)$$

$$\nabla \cdot (\overrightarrow{u\nabla v}) = u\nabla^2 v + \vec{\nabla u} \cdot \vec{\nabla v}$$

and

$$\vec{u\nabla v} \cdot \vec{n} = u\left(\frac{\partial v}{\partial x}\hat{i} + \frac{\partial v}{\partial y}\hat{j} + \frac{\partial v}{\partial z}\hat{k}\right) \cdot (\cos\alpha\, \hat{i} + \cos\beta\, \hat{j} + \cos\gamma\, \hat{k})$$

$$\overrightarrow{u\nabla v} \cdot \vec{n} = u\frac{\partial v}{\partial x}\cos\alpha + u\frac{\partial v}{\partial y}\cos\beta + u\frac{\partial v}{\partial z}\cos\gamma = u\frac{\partial v}{\partial n}.$$

Thus, we have

$$\int_T (u\nabla^2 v + \vec{\nabla u} \cdot \vec{\nabla v})\, dT = \int_\sigma u\, \frac{\partial v}{\partial n}\, d\sigma. \qquad (4)$$

Equation (4) is Green's first identity.

Interchanging u and v in (4), one obtains:

$$\int_T (v\nabla^2 u + \vec{\nabla v}\cdot\vec{\nabla u})\,dT = \int_\sigma v\,\frac{\partial u}{\partial n}\,d\sigma\ , \tag{5}$$

and subtracting (5) from (4) we get

$$\int_T (u\nabla^2 v - v\nabla^2 u)\,dT = \int_\sigma \left[u\,\frac{\partial v}{\partial n} - v\,\frac{\partial u}{\partial n}\right] d\sigma\ . \tag{6}$$

Equation (6) is Green's symmetric identity.

Consider a point P in x, y, z space and let there be a sphere of radius a with center at P. Then, we define a function f(Q) on the surface of the sphere (Q is an arbitrary point on the surface). The function f(Q) is a continuous function; also let c be a constant. Then

$$\int_{\sigma_1} \frac{f(Q)}{a^c}\,d\sigma = \int_{\sigma_1} \frac{f(P) + f(Q) - f(P)}{a^c}\,d\sigma =$$

$$\int_{\sigma_1} \frac{f(P)\,d\sigma}{a^c} + \int_{\sigma_1} \frac{f(Q) - f(P)}{a^c}\,d\sigma\ .$$

Let

$$I_1 = \int_{\sigma_1} \frac{f(P)}{a^c}\,d\sigma\ .$$

Thus,

$$I_1 = \frac{f(P)}{a^c}\int_{\sigma_1} d\sigma = \frac{f(P)}{a^c}\,4\pi a^2 = f(P)\,4\pi a^{2-c},$$

and in the limit as $a \to 0$, we obtain

$$\lim_{a \to 0} I_1 = \begin{cases} 4\pi f(P) & \text{for } c = 2 \\ 0 & \text{for } c < 2. \end{cases}$$

Now consider

$$I_2 = \int_{\sigma_1} \frac{f(Q) - f(P)}{a^c} \, d\sigma.$$

$$|I_2| \leq \frac{\max|f(Q) - f(P)|}{a^c} \int_{\sigma_1} d\sigma = \frac{\max|f(Q) - f(P)|}{a^c} 4\pi a^2$$

$$= \max|f(Q) - f(P)| 4\pi a^{2-c}.$$

Thus, $\lim_{a \to 0} |I_2| = 0$, since, as $a \to 0$, $f(Q) \to f(P)$, and therefore

$$f(Q) - f(P) \to 0.$$

It is now clear that

$$\lim_{a \to 0} \int_{\sigma_1} \frac{f(Q)}{a^c} \, d\sigma = \begin{cases} 4\pi f(P) & c = 2 \\ 0 & c < 2. \end{cases} \qquad (7)$$

Now, let us apply (6) to the function $v = 1/r$, where r is the distance from a fixed point P to the variable point of integration Q. The region of integration is to be the region inside a given closed surface and outside a small sphere σ_1 of radius $\underline{a}$ centered at P. The region of integration is depicted in Figure 14A.

In this region, r is not zero and (6) can be applied without hesitation. Since 1/r is a harmonic function, that is, satisfies Laplace's equation, it follows that

$$\nabla^2 v = \nabla^2 \frac{1}{r} = 0$$

and equation (6) becomes

$$-\int_T \frac{\nabla^2 u}{r}\, dT = \int_\sigma \left(u \frac{\partial}{\partial n}\left(\frac{1}{r}\right) - \frac{1}{r}\frac{\partial u}{\partial n}\right) d\sigma + I_0$$

where

$$I_0 = \int_{\sigma_1} \left(u \frac{\partial v}{\partial n} - v \frac{\partial u}{\partial n}\right) d\sigma.$$

Let $u = u(x,y,z)$ satisfy Poisson's equation. Then,

$$\int_T \frac{4\pi\rho}{r}\, dT = \int_\sigma \left(u \frac{\partial}{\partial n}\left(\frac{1}{r}\right) - \frac{1}{r}\frac{\partial u}{\partial n}\right) d\sigma + I_0. \tag{8}$$

Consider I_0

$$I_0 = \int_{\sigma_1} \left(u \frac{\partial}{\partial n}\left(\frac{1}{r}\right) - \frac{1}{r}\frac{\partial u}{\partial n}\right) d\sigma = \int_{\sigma_1} \frac{\left[u - a\frac{\partial u}{\partial n}\right]}{a^2}\, d\sigma$$

and therefore by virtue of (7) it follows that

$$\lim_{a \to 0} I_0 = \lim_{a \to 0} \int_{\sigma_1} \frac{\left[u - a\frac{\partial u}{\partial n}\right] d\sigma}{a^2} = 4\pi u(P).$$

Now, equation (8) becomes

$$\int_T \frac{4\pi\rho}{r}\, dT = \int_\sigma \left[u \frac{\partial}{\partial n}\left(\frac{1}{r}\right) - \frac{1}{r}\frac{\partial u}{\partial n}\right] d\sigma + 4\pi u(P)$$

or

$$u(P) = \int_T \frac{\rho}{r}\, dT + \frac{1}{4\pi}\int_\sigma \left[\frac{1}{r}\frac{\partial u}{\partial n} - u\frac{\partial}{\partial n}\left(\frac{1}{r}\right)\right] d\sigma. \qquad (9)$$

Equation (9) allows one to define physically the concept of the dipole layer. Let u be the electrostatic potential due to a charge distribution of surface density ρ. The potential satisfies Poisson's equation ($\nabla^2 u = -4\pi\rho$). Since q/r represents the potential due to a charge q at a distance r from the point of observation, the term $(1/r)\rho dT$ where $r = r(P,Q)$ and $\rho = \rho(Q)$ represents the potential at P due to charges within the volume element dT at Q. Hence, the first term of (9), $\int_T \frac{1}{r}[\rho dT]$, represents the potential at P due to charges within the body T.

Similarly, the second term in (9), $\int_\sigma \frac{1}{r}\left(\frac{1}{4\pi}\frac{\partial u}{\partial n}\right)d\sigma$, represents the potential at P due to a surface-charge distribution on the surface σ. To interpret the term

$$\int_\sigma \left[\frac{\partial}{\partial n}\left(\frac{1}{r}\right)\right]\left[-\frac{u}{4\pi}\, d\sigma\right]$$

in (9), let us consider the configuration shown in Figure 14B. Here a charge $-q$ is introduced at the point Q on the surface and a charge $+q$ is introduced at a distance $\Delta N << r$ at the point Q_1 along the outward normal $\vec{N}$ to σ. The distance from $-q$ to P is r_0 and the distance from $+q$ to P is denoted by r. If we take $q = m/\Delta N = \frac{\text{dipole moment}}{\text{charge separation}}$ where m is constant, the potential at P is

$$q\left(\frac{1}{r} - \frac{1}{r_0}\right) = q\Delta\left(\frac{1}{r}\right) = \frac{m\Delta\left(\frac{1}{r}\right)}{\Delta N} \underset{\Delta N \to 0}{\to} m\frac{\partial}{\partial n}\left(\frac{1}{r}\right).$$

The limiting configuration of the figure is a dipole; the constant m is the dipole moment. Thus, the term

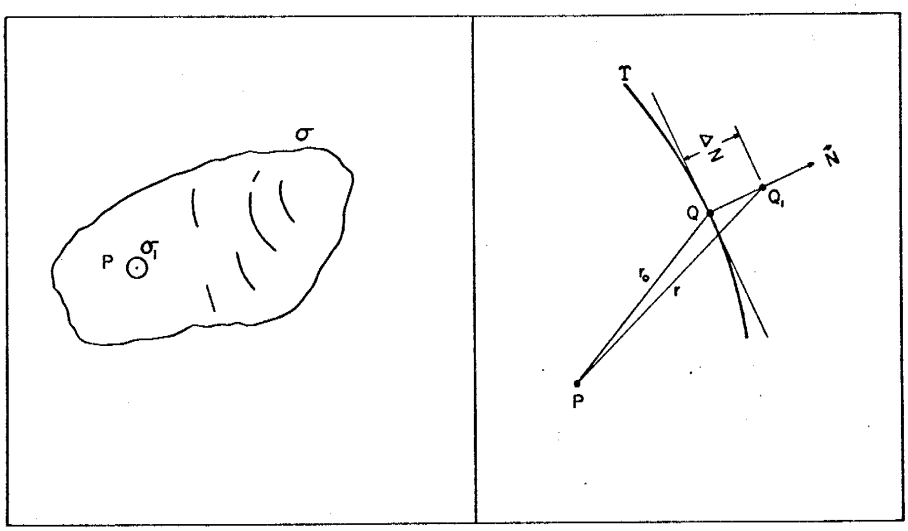

A. Regions of integration

B. Dipole configuration at the surface

Figure 14.

$$\int_{\sigma} \left(\frac{\partial}{\partial n}\frac{1}{r}\right)\left(-\frac{u}{4\pi}\, d\sigma\right)$$

represents the potential due to a surface distribution of dipoles having the moments $-\frac{u\, d\sigma}{4\pi}$. A surface distribution of dipoles such as this we will call a dipole layer.

Since the volume integral in (9) is extended only over T, it does not take account of the charges outside σ. That purpose is served by the surface integral in (9). From this viewpoint, (9) shows that the charges outside σ can be replaced by a suitable surface charge and dipole layer on σ, without changing the potential within σ. If T increases beyond all bounds, the limiting value of the surface integral can be thought to represent the influence of the charges at infinity.

A Simplified Close-up View of the Dipole and Diffuse Layers.

As was mentioned in the previous section, our model of a mineral particle in suspension involves three layers: the surface layer, the Stern layer, and the diffuse layer. These layers are shown in Figure 13. The surface layer is the outer layer of ions in the solid phase. The Stern layer is a layer adjacent to the surface layer but carrying opposite charge. The diffuse layer can be regarded as the layer of ions extending from the Stern layer's outer boundary deep into the liquid phase.

The diffuse layer is very important but difficult to treat, and therefore it has not been so extensively studied in the literature as the other two layers.

Gouy (1917) assumed that the ions in the liquid phase followed a Boltzmann distribution function up to the surface of the particle. This

assumption is rather inaccurate close to the particle's surface. In the present treatment we begin by assuming that a Boltzmann function governs the distribution of ions up to the boundary between the Stern and the diffuse layers,

$$\eta_i = \eta_{i_0} \exp\{-\theta_i \, e\psi(kT)^{-1}\} \tag{10}$$

where η_i is the concentration of ions of type $\underline{i}$ at a point $\underline{x}$ where the potential is $\psi(x)$, η_{i_0} is the concentration in the bulk of the solution, θ_i is the valence of ions of type i, $\underline{e}$ is the electronic charge, $\underline{k}$ is Boltzmann's constant, and T is the temperature.

The diffuse layer also satisfies Poisson's equation, which here is written

$$\nabla^2\psi = -\frac{4\pi\rho}{D}, \tag{11}$$

where ∇^2 is the Laplace operator, ψ is the potential a distance $\underline{x}$ away from the boundary between the dipole and the diffuse layer, D is the dielectric constant, and ρ is the space charge per unit volume. ρ is given by

$$\rho = \sum_{i=1}^{n} \theta_i \, e \, \eta_i. \tag{12}$$

Combining equations (10), (11), and (12), we get

$$\nabla^2\psi = -\frac{4\pi}{D} \sum_{i=1}^{n} \theta_i \, e \, \eta_{i_0} \exp\{-\theta_i \, e \, \psi(kT)^{-1}\}. \tag{13}$$

The solution to (13) in its general form is analytically possible but very complicated. To simplify the solution, we assume that the particle acts as an infinitely large plane surface and we average all θ_i and η_i. Then, equation (13) can be solved to obtain the solution

$$\psi = \psi_\zeta \exp(-\kappa x) \tag{14}$$

where ψ_ζ is the zeta potential and κ is the well known Debye-Hückel function which is defined by the expression

$$\kappa = \frac{8\pi\theta^2 e^2 \eta}{DkT}$$

where θ is an average of all θ_i and η is an average of all η_i.

This model gives an approximation to the potential as a function of distance. The potential drops exponentially as we move outward from the plane separating the Stern and the diffuse layers.

Complications in the Theory.

There are many complications in the detailed theory of the electric layers, especially for particles moving in an electric field (Kruyt, 1952; Overbeek, 1959; Frumkin, 1946). The effective viscosity in the diffuse layer is affected by the fact that the ions in it are also moving because of the field applied. This gives rise to electrophoretic retardation. Briefly, since net charge in the fluid region close to the surface is opposite in sign to that of the surface, these ions on the whole move relative to the solution in a direction opposite to that of the surface. In turn, they entrain solvent with them (for example, through their hydration shells and atmospheres) so that there is a local motion of the medium opposing the motion of the charged particle or surface. Therefore, a more realistic model of the electric layers as a particle moves in an electric field must also include a consideration of the local medium velocity.

There is also a relaxation effect which consists in that, because of the motion of the particle, the dipole layer lags somewhat behind; again, the effect is one of retarding the motion of the particle. Deryagin and

co-workers (1966) studied this relaxation effect and showed that differential diffusion of ions in the vicinity and toward the surface of a moving particle may give rise to an added contribution to the electrical potential which is independent of and perhaps superposed on the zeta potential.

Another point is that the dipole layer region is a source of conductance and so is the surface of the particle itself. This conductance is difficult to evaluate. LeFebre (1967) has studied conductance for the ice-solution interface.

Derivation of the Zeta Potential Equation.

The diffuse layer satisfies Poisson's equation

$$\nabla^2\psi = -\frac{4\pi\rho}{D} \tag{15}$$

where ∇^2 is the Laplace operator, ψ is the potential at a point located a distance x from the outer boundary of the Stern layer, ρ is the space charge per unit volume at that same point, and D is the dielectric constant of the medium.

Assume that the liquid under consideration is undergoing laminar flow, that its viscosity, μ, and dielectric constant, D, are uniform throughout the mobile part of the diffuse layer, and that the bulk of the potential drop in the diffuse layer takes place in a distance which is small compared to the radius of curvature of the surface.

When an external field of strength E is applied, each volume element in a layer of liquid of thickness dx at a distance x from the surface will experience a force

$$F_1 = E\rho\ dx, \tag{16}$$

where F_1 has the dimensions of force per unit area.

The viscous drag on the liquid layer is contributed by adjacent layers that are moving at a different velocity. The side of the layer at a distance x from the surface will be retarded by a force given by:

$$f_x = - \mu \left(\frac{dv}{dx} \right)_x , \tag{17}$$

where v is the liquid velocity; the side at a distance x + dx from the surface will be accelerated by a force

$$f_{x+dx} = \mu \left(\frac{dv}{dx} \right)_{x+dx} . \tag{18}$$

Thus, the net frictional force per unit area on the layer in question is

$$F_2 = \mu \left(\frac{dv}{dx} \right)_{x+dx} - \mu \left(\frac{dv}{dx} \right)_x . \tag{19}$$

At steady state, the total force per unit area on the layer is zero:

$$E \rho \, dx = \mu \frac{d^2v}{dx^2} dx. \tag{20}$$

We know that for a plane surface

$$\nabla^2 \psi = \frac{d^2\psi}{dx^2} . \tag{21}$$

Thus, by (15) and (21) we have

$$- \frac{4\pi\rho}{D} = \frac{d^2\psi}{dx^2} \tag{22}$$

or

$$\rho = - \frac{D}{4\pi} \frac{d^2\psi}{dx^2} . \tag{23}$$

By (20) and (23) we get

$$- \frac{ED}{4\pi} \frac{d^2\psi}{dx^2} = \mu \frac{d^2v}{dx^2} . \tag{24}$$

Since at $x = \infty$, $v = v_e$ (electrophoretic velocity), $\psi = 0$, and at $x = 0$, $v = 0$, $\psi = \psi_\zeta$, equation (24) gives

$$v_e = \frac{ED\,\psi_\zeta}{4\pi\mu} . \tag{25}$$

A possible use of this equation is in determining the so-called zeta potential. We can define zeta potential as the electrical potential in the slipping plane between the fixed and flowing liquid, that is, the potential at the outer edge of the Stern layer. In order to determine the zeta potential, we measure the electrophoretic velocity v_e under a certain electric field of strength E and, knowing D and μ for the case under consideration, we can determine ψ_ζ.

EXPERIMENTAL

The quantity which we measure in electrokinetic studies is electrophoretic mobility, that is, the velocity at which a given particle moves when a suspension of these particles is placed in an electric field. The electrophoretic mobility, as shown in the previous section, depends on the strength of the field, the viscosity of the fluid, the dielectric constant of the fluid, and the zeta potential. The zeta potential is highly dependent on some of the ions present in the dipole layer. Such ions are usually termed potential-determining ions. In the case of the experiments with silicate minerals to be described in this paper, the potential-determining ions are H^+ and OH^-. Thus, zeta potential is a function of the pH of the solution in which the particles are immersed.

The isoelectric point of charge of a given solid sample whose potential-determining ions are H^+ and OH^- can be defined as the point on the pH scale at which the sample possesses zero net surface charge and the adsorption densities of H^+ and OH^- are equal. At the isoelectric point of charge both the electrophoretic mobility and the zeta potential are zero.

The isoelectric point of charge is a very important parameter influencing surface phenomena. It determines the range of pH in which a surface reaction will be likely to occur. For example, beryl has its isoelectric point of charge at pH 3.00, being positively charged below this pH. Thus, if a sample of beryl is immersed in water at a pH below 3.00, the H^+ ions in the water will not be attracted to the positively charged beryl surface, and any surface exchange of H^+ for metal cations would be highly improbable under these circumstances.

Instrumentation

Moving Boundary Cell

Moving-boundary methods were among the earliest to be used for the determination of electrophoretic mobilities. The Burton cell uses a traveling telescope to measure the moving boundary. With this technique, it is essential to have equilibrium between the suspended particles and the liquid. Also, careful consideration must be given to the type of liquid used in the experiment.

The Burton cell is highly reliable and has been widely used. However, experiments with it are very tedious and require several hours to complete. This may cause errors due to diffusion not detectable with the telescope. A very complete discussion of the Burton cell is given by Alexander and Johnson (1949).

Mass Transport Cell

Long and Ross (1965) developed a method for determining electrophoretic mobilities in an effort to obtain an instrument well adapted for fundamental research, while retaining the main features of earlier mass-transport cells.

The setup of the Long-Ross cell is shown in Figure 15. This cell is made of an acrylic resin (Lucite, Plexiglas), which is machinable. The cell is very simple in design and construction. For electrophoretic mobility measurements, the main circuit components are two electrode probes and a recorder with a voltage-divider circuit.

In this cell, the amount of solids transported, a (in grams), is given by the equation

$$a = MGAv_e t, \tag{26}$$

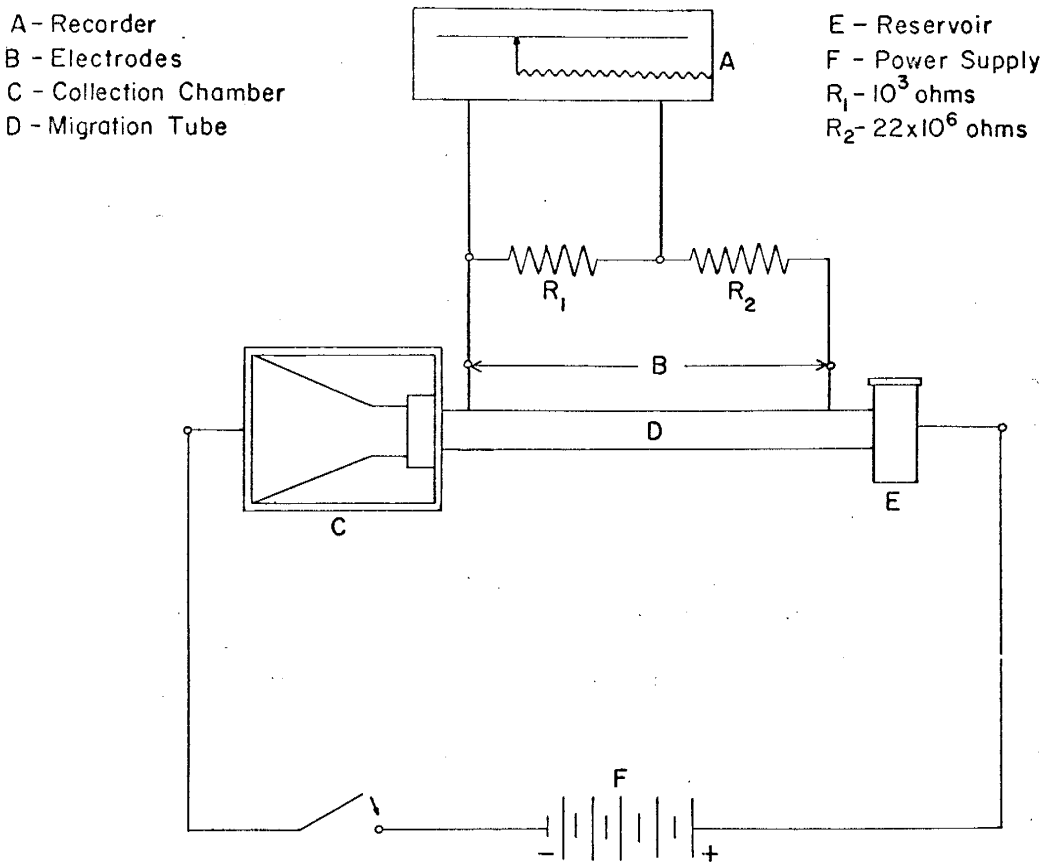

Batteries connected to electrodes. Voltage divider circuit attached to platinum probes.

(after Journal of Colloid Science, v. 20, 438-447 (1965))

Figure 15. The Long-Ross mass transport cell.

where M is the concentration of the solids (gm/ml), G is the potential gradient (volts/cm), A is the area of cross section of the migration tube (cm^2), v_e is the electrophoretic mobility (cm sec^{-1}/volt cm^{-1}), and t is the time (sec).

This apparatus is most reliable for colloidal particles of high specific gravity. Comparison of the Long-Ross method with the Burton cell shows mobility differences of no more than 4 percent.

Errors using this apparatus may be ascribed to convection currents due to Joule heating of the particles or of the supporting electrolyte, counterflow effect, convection currents created by the gravitational fall of particles, and thermal conductivity properties of and electrostatic charge effects on Plexiglas. The advantages of this method are many more than its shortcomings, and reproducible measurements of electrophoretic mobilities of dispersed particles can easily be made using the Long-Ross cell.

Streaming Potential

Streaming potential is also frequently used in measuring zeta potential and isoelectric point of charge. This is an indirect way of measurement. Zeta potentials (ψ_ζ) can be calculated by determining the difference in potential between the two ends of a porous plug of particles as a liquid is forced through the plug. The equation that relates zeta potential to streaming potential is given by Gaudin and Fuerstenau (1955). For aqueous systems at 25° C, this equation is

$$\psi_\zeta = 9.69 \times 10^4 \frac{S\lambda}{P} \qquad (\psi_\zeta \text{ in millivolts}) \tag{27}$$

where S is the streaming potential in millivolts, P is the driving pressure in centimeters of mercury, and λ is the specific conductance of the solution contained inside the plug in $ohms^{-1}cm^{-1}$.

To determine zeta potentials by this procedure, it is necessary experimentally to measure driving pressure, specific conductance, and streaming potential. The error in zeta potential values measured in this manner has been less than 1 percent. Further discussion of streaming potential studies is given by Fuerstenau (1956) and Korpi (1960).

Electrophoresis Cell

The apparatus used for the electrophoresis experiments described below is shown in Figures 16 and 17. The cell and glassware were designed and built in the laboratories of the New Mexico Bureau of Mines and Mineral Resources, and the projection apparatus was a Rayoscope.

This apparatus consists of three main parts: A power supply unit, a conducting unit, and an optical system. The power supply used has a range of 0 to 300 v dc and 0 to 50 milliamps dc.

The conducting unit is composed of a series of glass tubes that allow the solution with the particles to pass through the observation region and then to drain at the other end of the unit. This conducting unit is supplied with two sets of electrodes: An inner permanent platinum electrode for measurements of electrophoretic mobility when high accuracy is needed (the electrode separation can be determined extremely accurately) and an outer removable set of electrodes for rapid isoelectric point of charge measurements.

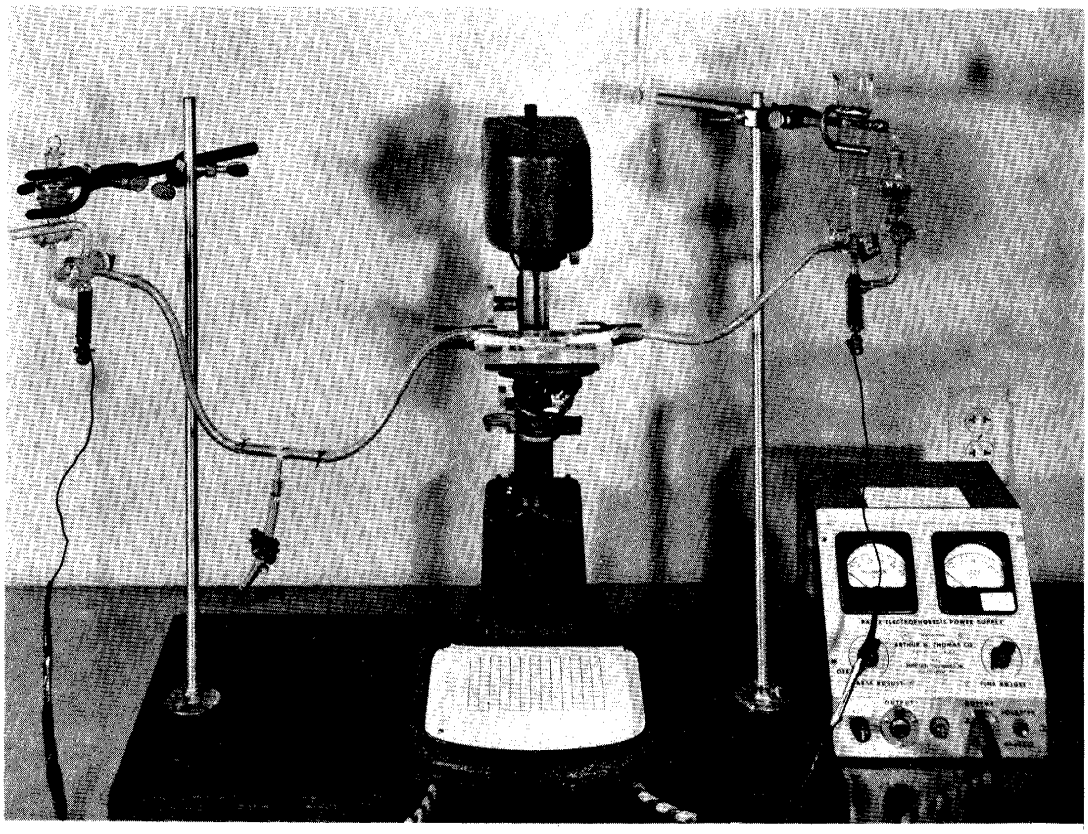

Figure 16. Photograph of electrophoresis apparatus.

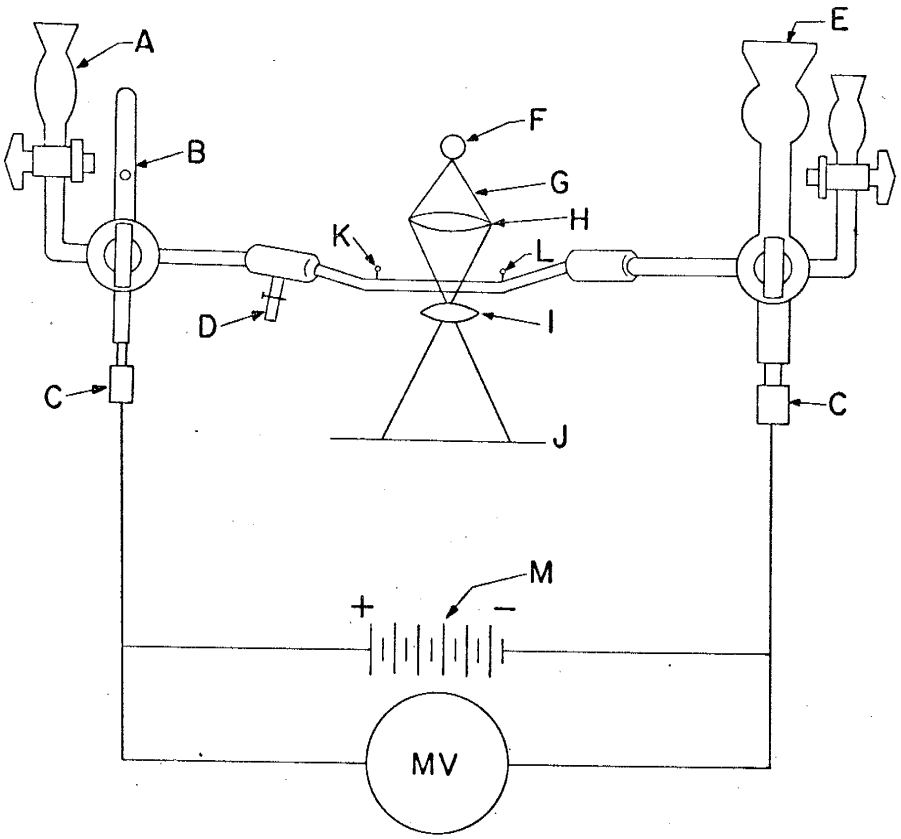

A - $CuSO_4$ or KCl reservoir
B - Drainage outlet
C - Cu-Zn electrode
D - Drainage outlet
E - Particles in solution
F - Light
G - Heat and color filters
H - Lens
I - Lens
J - Screen
K - Pt Electrode
L - Pt Electrode
M - Battery

Figure 17. Diagram of electrophoresis apparatus.

The optical system itself consists of two parts: A projector and a lens filter system. This modification, not previously used, allows the projection of the images of particles on a screen, thus eliminating the need for tedious microscopic observations. The heat absorption and blue (color) filters added to the projector allow the experimenter to minimize convection currents inside the cell. It was shown by Whitney and Blake (1904) that suspended particles and not the glass itself are heated.

The author also developed a second modified electrophoresis cell based partly on the design by Zeta-Meter Corporation (Riddick, 1961) and partly on the cell discussed above. This second electrophoresis cell is shown in Figure 18. Although less reliable than the electrophoresis apparatus above, it is more convenient for rapid routine measurements of isoelectric point of charge. Measurement errors using this cell are caused mainly by the thermal conductivity properties of Plexiglas and by convection inside the tube.

Experiments, Results, and Discussion.

The samples studied are shown in Table 5. All samples were hand picked and then dry-crushed in a ceramic ball mill and screened to obtain a minus 400-mesh size fraction. The sized samples were then run through the electromagnetic separator to remove iron-bearing materials. Finally, the samples were crushed in an automatic mortar to obtain a size fraction 2 to 10 microns in diameter. Final particle sizes were determined to an accuracy of ±1.5 percent, using a Fisher subsieve sizer. One gram of this size fraction of a mineral was mixed with about a gallon of deionized water. From this stock suspension, 10 samples of 100 milliliters each were taken,

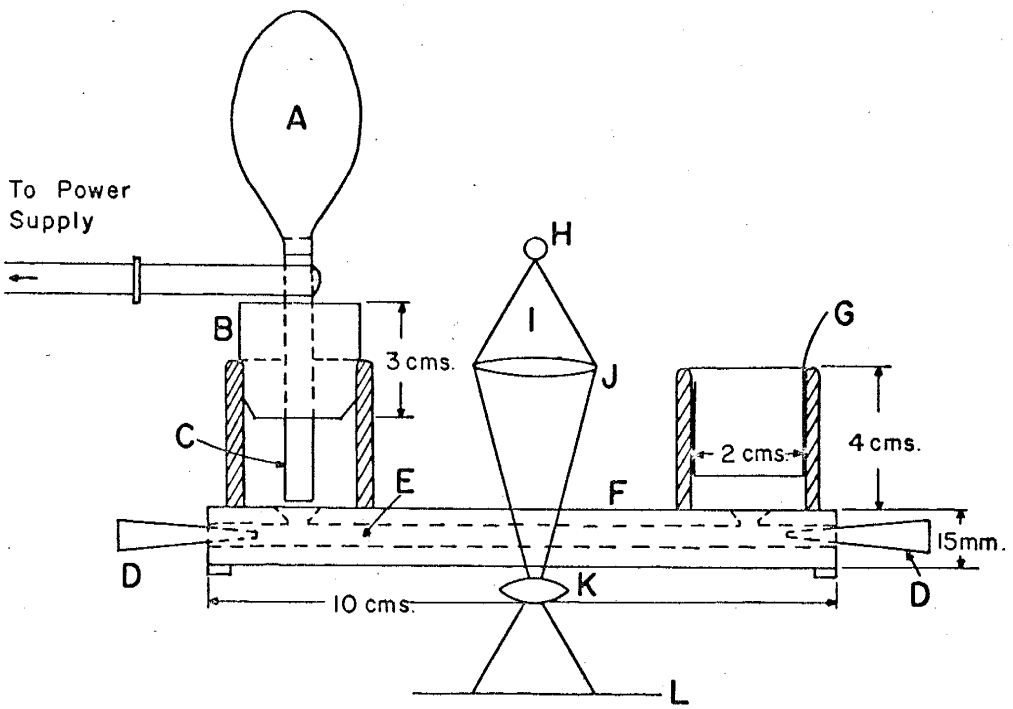

A - Rubber Bulb, 11ml. capacity
B - Foam Latex Plug
C - Electrode
D - Plexiglass Plugs
E - Drill Hole, 4.4mm. diameter
F - Type II UVA Plexiglass
G - Open Electrode
H - Light Source
I - Heat and Color Filters
J - Lens
K - Lens
L - Screen

Figure 18. Modified electrophoresis cell.

Table 5. Results of Electrophoresis Experiments

Mineral	Formula	Location	History	O:Si ratio	Zero Charge (pH)	Specific Gravity
Forsterite	Mg_2SiO_4	Twin Sisters Range, Wash.	very pure, dry crushed, iron-free sample, unleached	4:1	4:10	3.26-3.40
Enstatite	+Fe, Bronzite $MgO \cdot SiO_2$	Near Webster, Jackson County, North Carolina	very pure, dry crushed, iron-free sample, unleached	3:1	3.75	3.10-3.40
Augite	$Ca(Mg \cdot Fe)(SiO_3)_2$ $((Al \cdot Fe)_2O_3)_x$	Mexico	very pure, dry crushed, iron-free sample, unleached	3:1	3.80	3.20-3.50
Augite	$Ca(Mg \cdot Fe)(SiO_3)_2$ $((Al \cdot Fe)_2O_3)_x$	Mexico	bulk ore sample, dry crushed, unleached	3:1	4.45	3.20-3.50
Spodumene	$Li_2O \cdot Al_2O_3 4SiO_2$	Harding Mine Dixon, N. Mex.	very pure, dry crushed, iron-free sample, unleached	3:1	2.60	2.64
Beryl	$3BeO \cdot Al_2O_3 6SiO_2$	Harding Mine Dixon, N. Mex.	very pure, dry crushed, iron-free sample, cleaned with 1M HCl	-	3.00	2.63-2.91
Microcline	$K_2OAl_2O_3 6SiO_2$	Harding Mine Dixon, N. Mex.	very pure, dry crushed, iron-free sample, unleached	2:1	2.40	2.54-2.57
Albite	$Na_2OAl_2O_3 6SiO_2$	Harding Mine Dixon, N. Mex.	very pure, dry crushed, iron-free sample, unleached	2:1	2.00	2.61-2.64
Quartz	SiO_2	Harding Mine Dixon, N. Mex.	sample of high purity, cleaned by leaching in concentrated HCl and washed in conductivity H_2O	2:1	1.80	2.59-2.66
Quartz	SiO_2	Brazilian crystals	sample of Brazilian hand-picked crystals, cleaned by leaching in concentrated HCl, 8 hrs. treatment in Soxhlet	2:1	1.50	2.59-2.66
Quartz	SiO_2	Harding Mine Dixon, N. Mex.	7-day leached sample, highly purified	2:1	1.40	2.59-2.66
Quartz	SiO_2	Harding Mine Dixon, N. Mex.	bulk sample, untreated	2:1	3.70	2.59-2.66

each having approximately the same degree of particle dispersion. Every sample was then adjusted to desired pH with HCℓ or NaOH, and its isoelectric point of charge was determined.

The isoelectric point of charge was determined by observing the particles as they moved through the electrophoresis cells described previously. First, the velocity of the particles was statistically measured using 20 determinations. Then, the electrophoretic mobility was plotted as a function of pH to determine the isoelectric point of charge.

Results obtained for the isoelectric point of charge experiments are shown in Table 5 and Figure 19. It can be seen from Table 5 that for a series of very pure silicate samples the oxygen-silicon ratio increases as the isoelectric point of charge increases.

An important point to consider is the observed difference in isoelectric point of charge between a leached and an unleached sample of the same mineral, as shown in Table 5. An explanation may be obtained by using the model described in the previous chapter for the reaction of these silicates when they are in contact with an acid solution.

Let M^+ be the metal cation, Y^- be the anionic part of the silicate sample; overbars represent surface products, and ions indicate species in aqueous phase. The surface reactions may be indicated by the following equations:

$$H^+ + \overline{MY} \rightleftarrows M^+ + \overline{HY} \tag{28}$$

$$H_2O + \overline{MY} \rightleftarrows M^+ + \overline{HY} + OH^- \ . \tag{29}$$

During a leaching process, a large number of the M^+ ions may leave the surface, an equivalent amount of H^+ ions replacing them. The number of

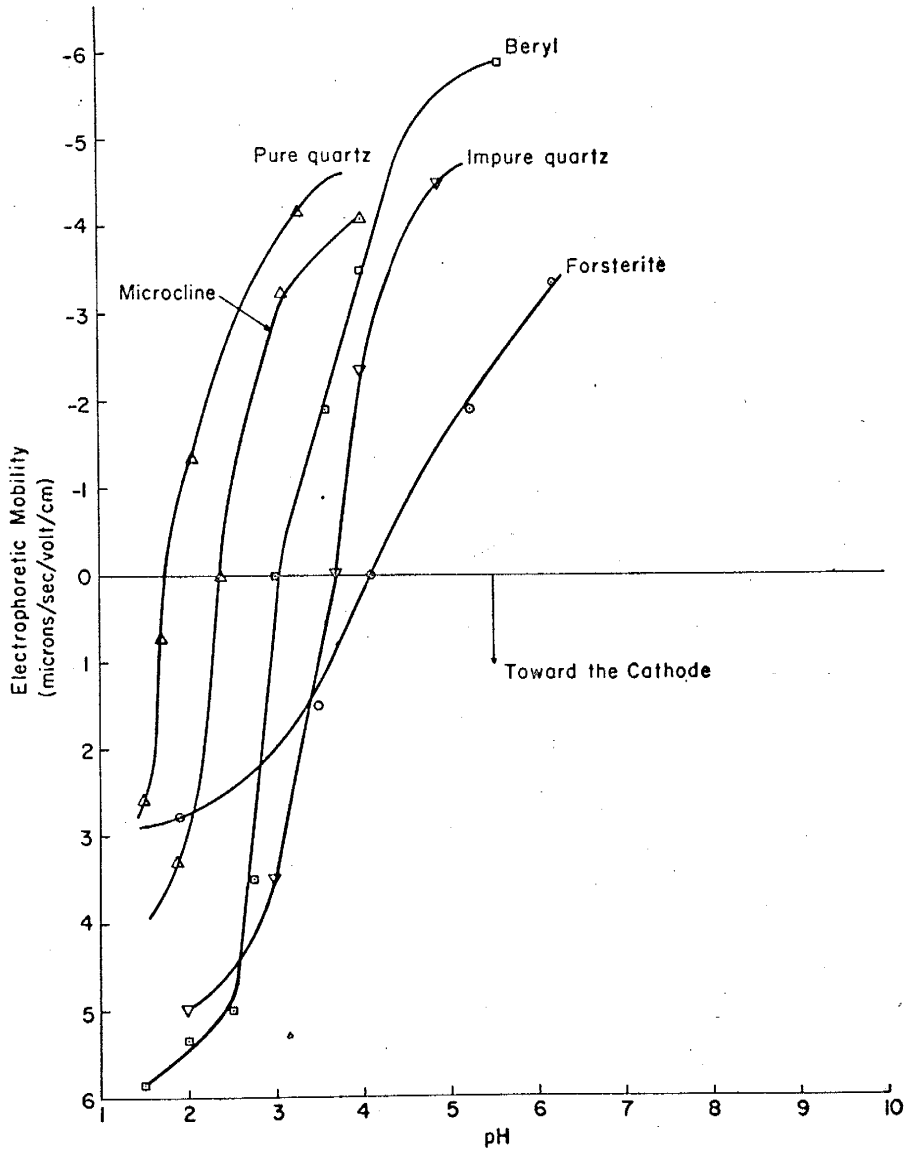

Figure 19. Results of isoelectric point of charge experiments.

M^+ ions present on the surface will then be substantially less than for an unleached sample and the amount of OH^- ion formed as an end product will also be much less. If the leached sample is denoted by A and the unleached sample by B, it follows that

$$[OH^-]_A < [OH^-]_B \tag{30}$$

and therefore,

$$[H^+]_A \text{ final} > [H^+]_B \text{ final} . \tag{31}$$

Since, for the silicates used, H^+ is the potential-determining factor, as shown by Dejú and Bhappu (1965a, b),

$$\text{ip} = \text{isoelectric point} = k/[H^+], \tag{32}$$

where k is the proportionality constant. Thus (31) becomes

$$\text{ip}_A < \text{ip}_B. \tag{33}$$

For this reason, the isoelectric point of charge of the leached and purified sample may be less than that of the impure sample, as is observed experimentally.

In reality, equations (28) and (29) probably do not represent the only reactions occurring on the surface of the mineral. There may be an entire set of reactions simultaneously occurring, as indicated in general form by

$$\begin{aligned} &pnH^+ + \overline{M_pY_n} \rightleftarrows pM^{+n} + n\,\overline{H_pY} \\ &pnH_2O + \overline{M_pY_n} \rightleftarrows pM^{+n} + (np)OH^- + n\,\overline{H_pY} \end{aligned} \tag{3}$$

where n is the valence of M and p is the valence of Y in the silicate mineral.

The model discussed in the first section of this chapter completes the picture of phenomena occurring at the silicate-solution interface. By electrophoresis experiments the electrophoretic mobility of various silicate minerals was measured (microns/sec/volt/cm). Using equation (25) and recalling that, at 25° C, D=78.54 and μ=0.00894 poises, the value of the zeta potential of the minerals under consideration was determined as a function of solution pH. Then, using equation (14), the potential ψ was plotted as a function of relative distance (κx) for several values of $[H^+]$ concentration. Such a plot is shown in Figure 20 for the case of beryl. Similar plots were made for other minerals. This type of plot gives a quantitative view of the electrical potential surrounding a mineral particle in suspension. Such plots, together with the predicted type of chemical reaction between water and silicates, and the concept of isoelectric point of charge, describe the phenomena occurring at the water-silicate interface.

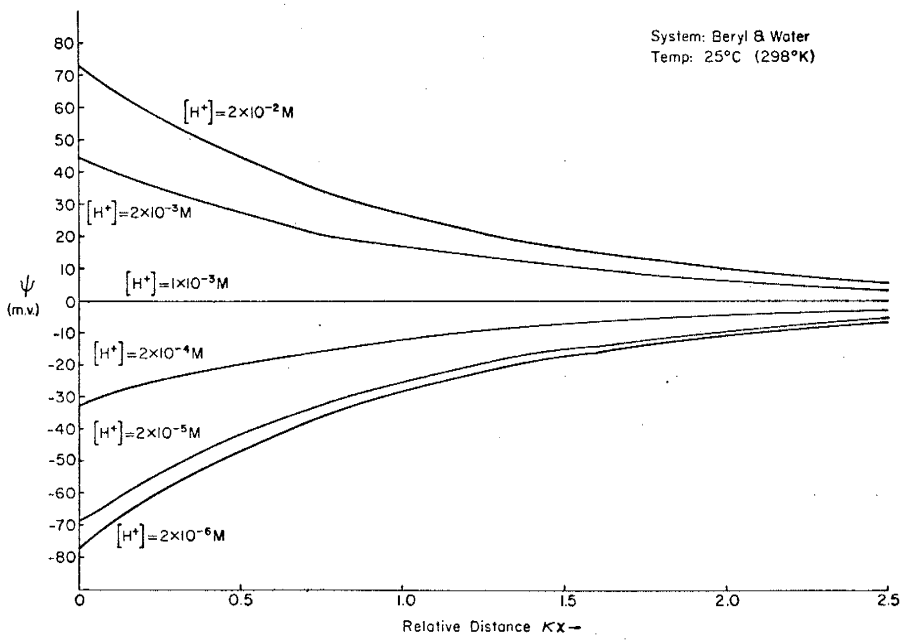

Figure 20. ψ versus κx for the system beryl-water.

SUMMARY

A model of a mineral particle and its surrounding electric layers has been developed. The model shows that the charges outside the particle's surface σ can be replaced by a suitable surface charge and dipole layer on σ, without changing the potential within σ.

The electric layers surrounding a mineral particle in suspension were also closely studied and a model of potential as a function of distance was constructed.

Phenomena such as electrophoretic retardation, relaxation effects, and dipole layer conductance are briefly discussed, and their possible effects on the model are mentioned.

Beginning with the assumption that potential satisfies Poisson's equation in the diffuse layer, the equation

$$v_e = \frac{ED\psi_\zeta}{4\pi\mu}$$

was derived.

The various instruments which are used for electrokinetic studies were briefly discussed. These are: The moving boundary cell, mass transport cell, streaming potential apparatus, and electrophoresis cell.

Experiments using some of the above instruments were performed using silicate minerals suspended in water. The isoelectric point of charge was determined by observing the particles as they moved in the presence of an electric field. Their velocity was then statistically measured.

The isoelectric point of charge increases with the oxygen-silicon ratio.

The isoelectric point of charge of a leached sample is less than that of an unleached sample. This same result can be derived qualitatively from knowledge of the surface reactions at the water-silicate interface.

Electrophoresis experiments combined with the model described at the beginning of the chapter were used to determine the electric layers for several minerals and led to a better understanding of the reactions at the water-silicate interface.

The isoelectric point of charge of a given sample tells us the range of pH in which any surface reactions between water and that sample will occur.

SYMBOLS

ψ_ζ = zeta potential

ψ_0 = surface potential

$d\tau$ = volume element

$d\sigma$ = surface element

r = radius

ρ = density of charge

q = charge

η_i = concentration of ions of type i at a point x where the potential is $\psi(x)$

η_{i_0} = concentration of ions of type i in the bulk of the solution

θ_i = valence of ions of type i

e = electronic charge

k = Boltzmann's constant

T = temperature

x, y, z = space variables

t = time

D = dielectric constant

θ = average of all θ_i

η = average of all η_i

κ = Debye-Hückel function

E = strength of electric field

F = force

f = component forces

v_e = electrophoretic velocity

μ = viscosity

m = dipole moment

a = amount of solid transported in Long-Ross cell

M = concentration of solids (gm/ml)

G = potential gradient (volts/cm)

A = area of cross section of the migration tube (cm^2)

S = streaming potential (mv)

P = driving pressure

λ = specific conductance

M^+ = metal cation (in general) of valence n

Y^- = anion of valence p

ip = isoelectric point

overbars = surface products

REFERENCES

Alexander, A. E., and Johnson, P. (1949) Colloid Science, London: Oxford University Press, vol. 1, p. 321.

Deju, R. A., and Bhappu, R. B. (1965a) Design of an Apparatus for Determining Isoelectric Point of Charge, Circular 79, State Bureau of Mines and Mineral Resources, New Mexico Institute of Mining and Technology.

_____, and _____ (1965b) Surface Properties of Silicate Minerals, Circular 82, State Bureau of Mines and Mineral Resources, New Mexico Institute of Mining and Technology.

Deryaguin, B. V. (1966) Research in Surface Forces (2 vols) Consultants Bureau, New York.

Frumkin, A. (1946) Journal of Colloid Science, vol. 1, pp. 277-291.

Fuerstenau, D. W. (1956) Measuring Zeta Potential by Streaming Potential Techniques, Min. Eng., vol. 8, n. 8, pp. 834-835.

Gaudin, A. M., and Fuerstenau, D. W. (1955) Quartz Flotation with Anionic Collectors, Min. Eng., vol. 7, n. 1, pp. 66-72.

Gouy, G. (1917) Ann. Phys., vol. 7, n. 9, p. 129.

Helmholtz, H. (1879) Wied. Ann., vol. 7, p. 337.

Korpi, G. K. (1960) Measuring of Streaming Potentials, M. S. Thesis, Massachusetts Institute of Technology.

Kruyt, H. R. (1952) Colloid Science, New York: Elsevier Publishing Co.

LeFebre, Vernon (1967) The Freezing Potential Effect, Journal of Colloid Science, vol. 25, p. 263.

Long, R. P., and Ross, S. (1965) An Improved Mass Transport Cell for Measuring Electrophoretic Mobilities, Journal of Colloid Science, vol. 20, pp. 438-447.

Overbeek, J. T. (1959) Advances in Colloid Science, New York: Interscience Publishers.

Quinke, G. (1861) Pogg. Ann., vol. 113, p. 513.

Reuss, F. F. (1809) Mem. Soc. Imperiale Natural, Moscou, vol. 2, p. 327.

Riddick, T. M. (1961) Zeta Potential New Tool for Water Treatment, Chem. Eng., vol. 68, n. 13, pp. 121-126.

Whitney, W. R., and Blake, J. C. (1904) Jour. Am. Chem. Soc., vol. 26, pp. 1339-1387.

Wiedemann, G. (1852) Pogg. Ann., vol. 76, p. 321.

CHAPTER 4

MATHEMATICAL TREATMENT OF SORPTION

Having defined and described the mechanism of the reaction which takes place at the water-silicate interface, we are now in a position to solve the equations of flow as they apply to the water-silicate system. In this chapter we will derive a mathematical model of flow through porous media which couples the hydrodynamic considerations with the mechanism of reaction postulated in the previous two chapters. The model will be one-dimensional and will neglect dispersion.

DEFINITIONS

Sorption is a term used to describe the composite of all surface reactions which take place when two phases are put in contact with one another.

Dispersion is a term used to include all phenomena which tend to cause spreading of one phase, say a fluid stream, into, or onto, another phase, say a porous medium.

Diffusion is a process which tends toward an equalization of concentrations within a single phase. It is usually expressed in terms of amount of substance passing perpendicularly through a given region of unit area per unit time.

KINETICS

In Chapter 2 we showed that the reaction occurring when a silicate is placed in contact with a solid is given by equation (3). We also showed that the rate of forward reaction between a liquid and the silicate surface does not necessarily equal the rate of the backward reaction.

Consider a system where liquid-deionized water passes at a uniform rate through a homogeneous bed of a given silicate mineral. Let

S = concentration of solute in the solid phase (mass of solute/volume of solid material),

C = concentration of solute in the liquid phase (mass of solute/volume of liquid),

K_i = proportionality (rate) constants,

t = time, and

γ = porosity.

Then, the rate equation for the reaction between water and a silicate is given by

$$\frac{\partial S}{\partial t} = \gamma(K_1 C - K_2 S) \tag{34}$$

From equation (34) it follows that if $K_2 S > K_1 C$, then $\frac{\partial S}{\partial t}$ is negative, and hence a diminution of solute in the solid phase occurs. Basically, equation (34) states that sorption and desorption can occur together and at different rates in a continuous injection system; that is, there can exist in such a system a mass-transfer resistance that controls any gains or losses of the solute concentration in the solid phase.

MASS CONSERVATION

From a macroscopic point of view, we can write the law of conservation of mass as

$$V \frac{\partial C}{\partial y} + \frac{\partial C}{\partial t} + \frac{1}{\gamma} \frac{\partial S}{\partial t} = 0, \tag{35}$$

where V = average fluid velocity.

Equation (35) was first derived by Klotz (1946) and assumes no dispersion. However, Hendricks (1965) proved that in a liquid-solid system, at the beginning, sorption exceeds dispersion but under conditions of continued injection, sorption (and therefore surface free energy) decreases with time until the relative magnitudes of dispersion and sorption may be of the same order. Thus, equation (35) becomes

$$D \frac{\partial^2 C}{\partial y^2} - V \frac{\partial C}{\partial y} = \frac{\partial C}{\partial t} + \frac{1}{\gamma} \frac{\partial S}{\partial t}, \tag{36}$$

where D = coefficient of dispersion.

The discussions in this work are restricted to the sorption-desorption system without dispersion.

BOUNDARY AND INITIAL CONDITIONS

If we take a point, y_1, on a porous bed, the concentration, S, at y_1 will be a function of space, not of time, before the fluid reaches y_1. In mathematical form, we say

$$S(y,t) = S_o(y) \qquad t \leq y/V. \tag{37}$$

Equation (37) serves as the initial condition. To obtain a boundary condition, consider the interface between the fluid and the top of the porous bed. Certainly, along this interface,

$$C(y,t) = C_o(t) \qquad y = 0. \tag{38}$$

MATHEMATICAL SOLUTION

To solve the system under consideration, we use equations (34) and (35) and side conditions (37) and (38) and apply the transformations

$$\alpha = y/V, \tag{39}$$

and

$$\beta = \gamma(t - y/V). \tag{40}$$

Then (35) becomes

$$\frac{\partial C}{\partial \alpha} = - \frac{\partial S}{\partial \beta}. \tag{41}$$

Equation (41) implies that there exists a function, $F(\alpha,\beta)$, with total differential defined such that

$$dF(\alpha,\beta) = Sd\alpha - Cd\beta.$$

Thus,

$$S = \frac{\partial F}{\partial \alpha}, \quad \text{and} \quad C = - \frac{\partial F}{\partial \beta}. \tag{42}$$

Transforming (34), using (39) and (40), we get

$$\frac{\partial S}{\partial \beta} = K_1 C - K_2 S, \tag{43}$$

and the initial and boundary conditions become

$$C(o,t) = C_o(\beta/\gamma) = C_1(\beta) \quad \text{when} \quad \alpha = 0, \tag{44}$$

and

$$S(y,t) = S_1(\alpha) \quad \text{when} \quad \beta = 0. \tag{45}$$

Now, using (42) we can change (43) into a differential equation in F:

$$\frac{\partial^2 F}{\partial \beta \partial \alpha} + K_1 \frac{\partial F}{\partial \beta} + K_2 \frac{\partial F}{\partial \alpha} = 0. \tag{46}$$

Let $F(\alpha,\beta) = e^{C_1\alpha} e^{C_2\beta} \phi(\alpha,\beta)$, where C_1 and C_2 are constants to be determined and ϕ is a new function in α and β.

Thus, (46) becomes

$$\frac{\partial^2\phi}{\partial\alpha\partial\beta} + (K_2+C_2)\frac{\partial\phi}{\partial\alpha} + (K_1+C_1)\frac{\partial\phi}{\partial\beta} + K_1C_2\phi + K_2C_1\phi + C_2C_1\phi = 0. \tag{47}$$

If $C_1 = -K_1$, $C_2 = -K_2$, then (47) becomes

$$\frac{\partial^2\phi}{\partial\alpha\partial\beta} = K_1K_2\phi(\alpha,\beta). \tag{48}$$

From equations (42) and (45) and the definitions of F and ϕ, we obtain

$$S_1(\alpha) = \left(\frac{\partial F}{\partial\alpha}\right)_{\beta=0} = -K_1e^{-K_1\alpha}\phi(\alpha,0) + e^{-K_1\alpha}\frac{\partial\phi(\alpha,0)}{\partial\alpha}.$$

Letting $\phi(\alpha,0) = f(\alpha)$ gives

$$f'(\alpha) - K_1f(\alpha) = e^{K_1\alpha}S_1(\alpha). \tag{49}$$

Equation (49) can easily be solved by the method of quadratures to obtain

$$\phi(\alpha,0) = f(\alpha) = e^{K_1\alpha}\int_0^\alpha S_1(\xi)d\xi \quad . \tag{50}$$

Similarly we can obtain

$$\phi(0,\beta) = g(\beta) = e^{K_2\beta}\int_0^\beta -C_1(\lambda)d\lambda. \tag{51}$$

Also, $\phi(0,0) = 0.$ (52)

Thus, we must now simultaneously solve equations (48), (50), (51), and (52). This can be done with a method illustrated by Sokolnikoff and Redheffer (1958), using an example involving the theory of forced oscillations and resonance.

After tedious manipulation, we find that

$$S(\alpha,\beta) = e^{-(K_1\alpha+K_2\beta)}\{-K_1\{\int_0^\alpha f'(\xi)I_0(2\sqrt{K_1K_2\beta(\alpha-\xi)})d\xi$$

$$+\int_0^\beta g'(\lambda)I_0(2\sqrt{K_1K_2\alpha(\beta-\lambda)})d\lambda\}$$

$$+\int_0^\alpha f'(\xi)\sqrt{\frac{K_1K_2\beta}{\alpha-\xi}}\,I_1(2\sqrt{K_1K_2\beta(\alpha-\xi)})d\xi$$

$$+\int_0^\beta g'(\lambda)\sqrt{\frac{K_1K_2(\beta-\lambda)}{\alpha}}\,I_1(2\sqrt{K_1K_2\alpha(\beta-\lambda)})d\lambda + f'(\alpha)\}, \qquad (53)$$

and

$$C(\alpha,\beta) = -e^{-(K_1\alpha+K_2\beta)}\{-K_2\{\int_0^\alpha f'(\xi)I_0(2\sqrt{K_1K_2\beta(\alpha-\xi)})d\xi$$

$$+\int_0^\beta g'(\lambda)I_0(2\sqrt{K_1K_2\alpha(\beta-\lambda)})d\lambda\} + \int_0^\alpha f'(\xi)\sqrt{\frac{K_1K_2(\alpha-\xi)}{\beta}}\,I_1(2\sqrt{K_1K_2\beta(\alpha-\xi)})d\xi$$

$$+\int_0^\beta g'(\lambda)\sqrt{\frac{K_1K_2\alpha}{\beta-\lambda}}\,I_1(2\sqrt{K_1K_2\alpha(\beta-\lambda)}d\lambda + g'(\beta)\}, \qquad (54)$$

where I_0 and I_1 are the zeroth and first-order modified Bessel functions of the second kind with imaginary arguments; $f'(\alpha)$ and $g'(\beta)$ can be obtained by differentiation of equations (50) and (51).

Thus, the solution to our problem is given by equations (53) and (54), together with the transformation equations (39) and (40) and definition equations (50) and (51).

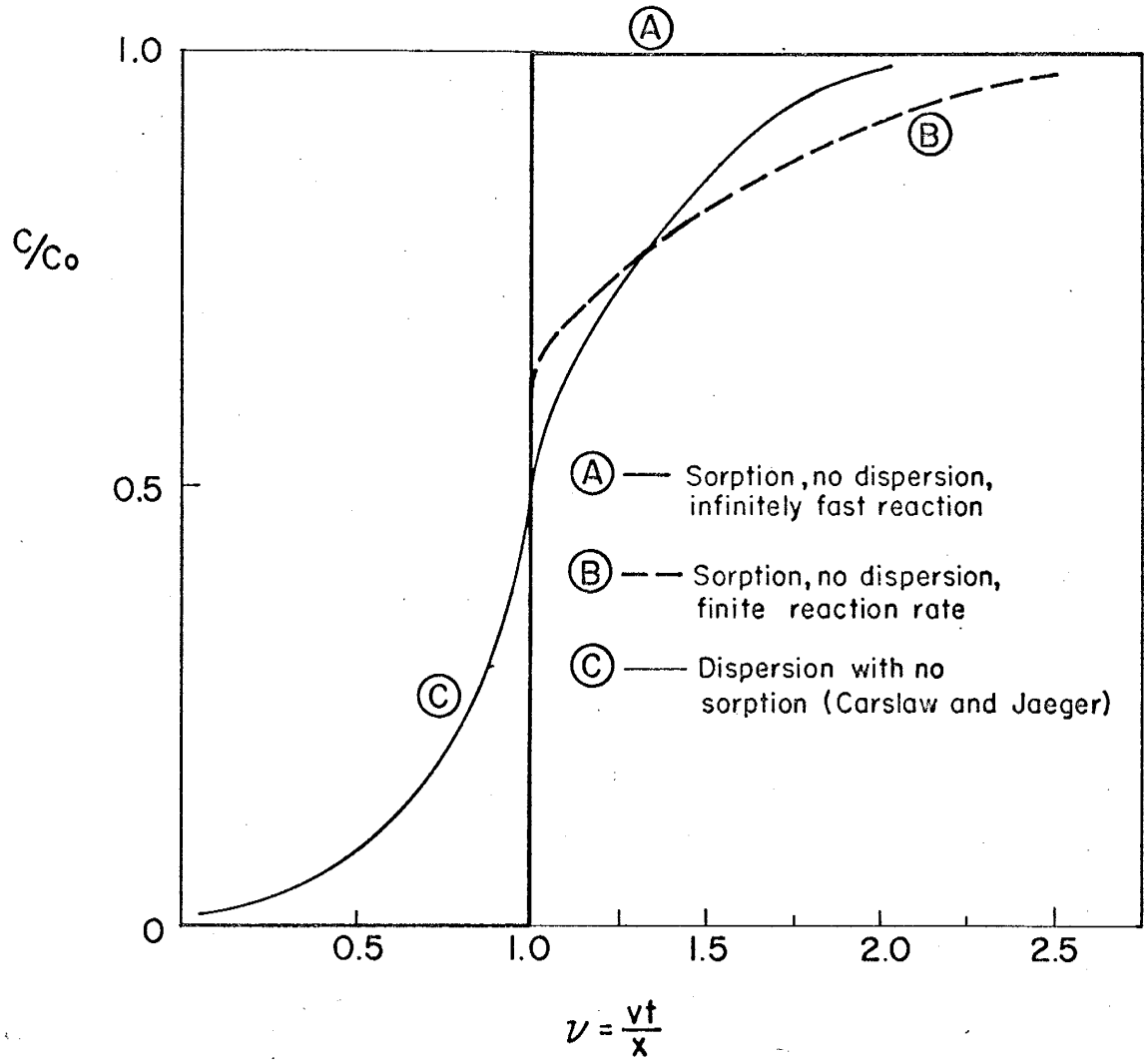

Figure 21. C/C_o versus ν.

This solution is rather complex because our original assumptions were rather general. To use these equations it is best to employ a numerical approach with a digital computer (Banks and Ali, 1964). Thus, we now consider the nondimensional ratio C/C_o versus $\nu = vt/y$; S/S_o will not be considered since it is rather difficult to treat experimentally, and thus of no great practical value.

Figure 21 shows the result of the computer analysis. It is important to examine the figure qualitatively and notice that if the exchange of ions takes place infinitely fast and with no dispersion (curve A), the change in concentration due to the exchange reaction is preserved without distortion as the interface moves through the column. Thus, at $\nu = 1$ (that is, at $t = x/v$) the concentration jumps from $C/C_o = 0$ to $C/C_o = 1$. If the reaction requires a finite length of time, then one obtains curves of type B. These results can be compared with curve C, which gives the behavior of dispersion with no sorption (Ogata, 1958; Carslaw and Jaeger, 1959; Banks and Ali, 1964). Figure 21 clearly shows the difference between a chemical phenomenon such as sorption and a purely mechanical phenomenon such as dispersion. This difference should be easy to see in an experimental check of the model presented here.

SUMMARY

In the previous two chapters we established the reaction mechanism at the silicate-water interface. Once we have established that the reaction mechanism is given by equation (3) we can translate the mechanism into differential equation form, that is,

$$\frac{\partial S}{\partial t} = \gamma(K_1 C - K_2 S), \tag{34}$$

where S = concentration of solute in the solid phase (mass of solute/ volume of solid material),

C = concentration of solute in the liquid phase (mass of solute/ volume of liquid),

K_i = proportionality (rate) constants,

t = time, and

γ = porosity.

Then, solving equation (34) together with the differential form of the law of conservation of mass and with appropriate boundary and initial conditions, we can obtain a solution which gives us the changes of concentration of solute as the water passes through the bed as a function of both space and time. Figure 21 depicts these changes for the mechanism proposed and compares them to the changes expected for a dispersion mechanism without a chemical reaction.

SYMBOLS

S = concentration of solute in the solid phase (mass of solute/volume of solid material)

C = concentration of solute in the liquid phase (mass of solute/volume of liquid)

K_i = proportionality (rate) constants

t = time

γ = porosity

V = average fluid velocity

D = coefficient of dispersion

y = vertical space coordinate

I_o = zeroth order modified Bessel function of the second kind with imaginary argument

I_1 = first order modified Bessel function of the second kind with imaginary argument

REFERENCES

Banks, Robert B., and Ali, Iqbal (1964) Dispersion and Adsorption in Porous Media Flow, Journal of the Hydraulics Division--Proceedings of the ASCE, vol. 90, n. HY5, pp. 13-31.

Carslaw, H. S., and Jaeger, J. C. (1959) Conduction of Heat in Solids (2nd ed) Oxford Univ. Press: New York, p. 388.

Hendricks, D. W. (1965) Sorption in Flow Through Porous Media, Ph. D. Dissertation, Univ. of Iowa.

Klotz, I. M. (1946) Chem. Revs. vol. 39, p. 241.

Ogata, Akio (1958) Dispersion in Porous Media, Ph. D. Dissertation, Northwestern University.

Sokolnikoff, I. S., and Redheffer, R. M. (1958) Mathematics of Physics and Modern Engineering, McGraw-Hill: New York.

CHAPTER 5

EXPERIMENTAL TREATMENT OF SORPTION

In the previous chapter a model of sorption was presented. This model was valid for first order kinetics and ion exchange where the rate of forward sorption was not necessarily equal to the rate of backward sorption (desorption). This model will now be experimentally checked for the system silicate-water. In this system forward sorption will be the movement of hydrogen ions from the solution phase to the solid surface. Backward sorption (desorption) will refer to the motion of cations from the solid surface to the liquid phase. The rates of sorption and desorption are not considered equal and in most cases differ considerably.

In this chapter the results of column experiments with the systems glass beads-water, soda microcline-water, spodumene-water, and forsterite-water are reported. The four systems used cover the whole range of silicates and vary considerably in properties. The attempt in this chapter will be to look at trends in general rather than specific details applicable only to a given silicate family.

EXPERIMENTAL

Set-up

To substantiate the theoretical discussion and the models presented in the previous chapters column experiments were conducted. Figure 22 depicts the set-up. The column was three inches in outside diameter and was made of quarter-inch Lucite; the shower head on top minimizes any dispersion effects.

The water used in the experiments was first distilled and then passed through two beds of mixed resin ion exchanger. (Water produced in this fashion is comparable to triple-distilled water.) It was then acidified to the desired pH, using HCℓ prior to its entrance into the column.

The pH monitoring equipment consisted of two Corning Model 12 pH meters, two sets of Corning pH electrodes and two Heathkit servo recorders.

All cation and chloride monitoring was done using the analytical techniques presented in Appendix 1.

Materials

Column experiments were conducted with samples of glass beads, soda microcline, spodumene, and forsterite. Mineralogical data on these samples appear in Table 1. Chemical analyses were run on the four solids used and are reported in Table 6.

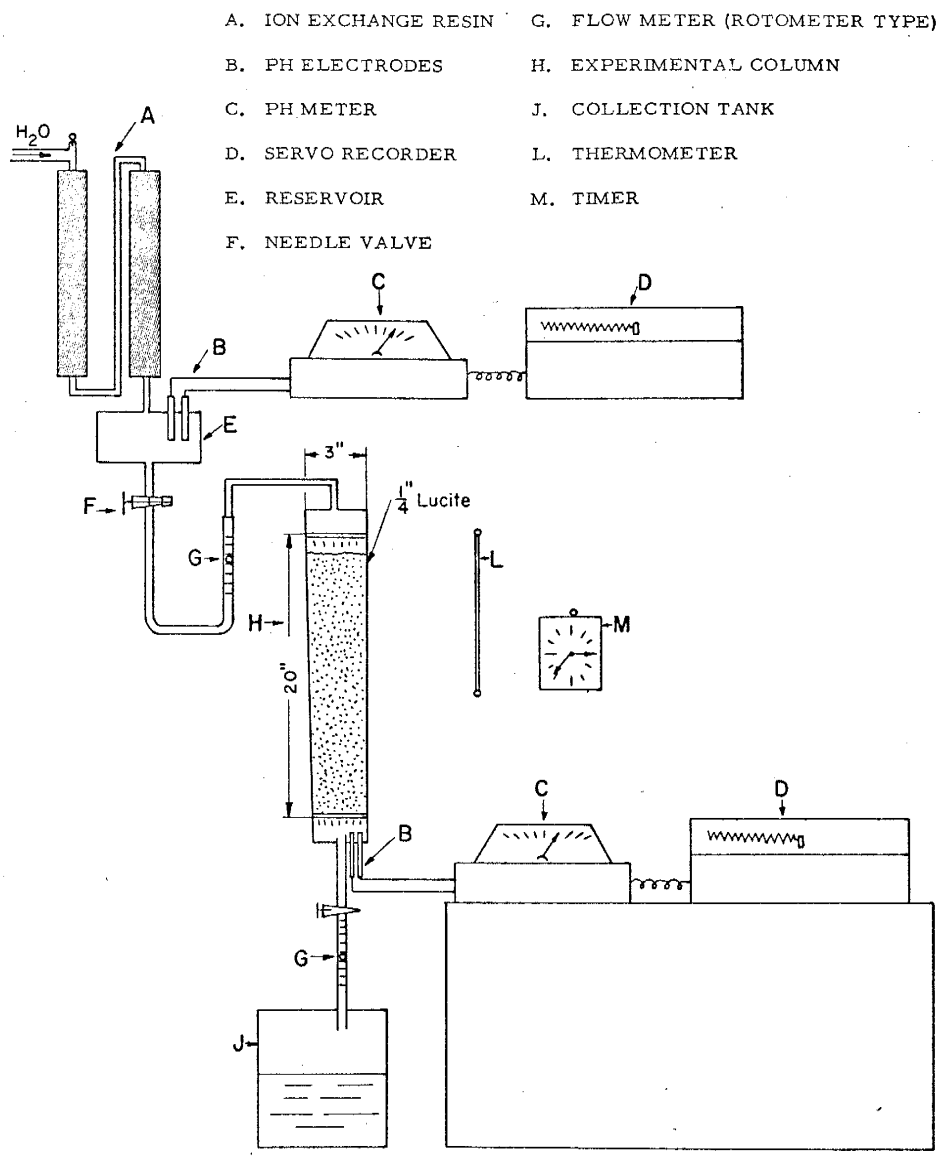

Figure 22. Setup for column experiments.

Table 6. Chemical Analyses

Constituent	Glass Beads Percent	Glass Beads Normalized Percent	Soda Microcline Percent	Soda Microcline Normalized Percent
SiO_2	71.20	72.11	67.02	66.22
Al_2O_3	0.60	0.61	19.86	19.62
FeO	0.42	0.43	0.06	0.06
K_2O	0.19	0.19	8.13	8.03
CaO	9.63	9.75	0.04	0.04
Na_2O	14.34	14.52	5.10	5.04
MgO	2.21	2.24	0.00	0.00
Li_2O	0.00	0.00	0.00	0.00
H_2O	0.15	0.15	1.00	0.99
BeO	0.00	0.00	0.00	0.00
TiO_2	0.00	0.00	0.00	0.00
MnO	0.00	0.00	0.00	0.00
Total	98.74	100.00	101.21	100.00

Constituent	Spodumene Percent	Spodumene Normalized Percent	Forsterite Percent	Forsterite Normalized Percent
SiO_2	64.24	63.03	38.60	37.76
Al_2O_3	25.52	25.04	4.76	4.66
FeO	0.17	0.17	8.00	7.83
K_2O	0.84	0.82	0.16	0.16
CaO	0.12	0.12	2.92	2.86
Na_2O	3.08	3.02	4.38	4.28
MgO	0.01	0.01	39.14	38.29
Li_2O	6.14	6.02	0.00	0.00
H_2O	1.80	1.77	3.89	3.81
BeO	0.00	0.00	0.00	0.00
TiO_2	0.00	0.00	0.25	0.24
MnO	0.00	0.00	0.11	0.11
Total	101.92	100.00	102.21	100.00

In all experiments the column was filled with a nearly homogeneous sample of the solid being used. The size distribution in all samples, determined by sieve analysis, follows:

Mesh Size U.S. Sieve Number	% Fraction
+80	0
-80+100	50
-100+140	50
-140	trace

HYDROGEN SORPTION

Samples of all four materials used were packed in equal columns to a height of 13.20 cms. Acidified water at an initial pH of 3.00 was passed through the column at a constant rate of 10.5 cc/min. The result of monitoring the pH on all four samples is shown on figures 23, 24, 25, and 26. These figures depict the behavior of the non-dimensional ratio $[H^+] / [H_0^+]$ as a function of time and $\nu = vt/x$, where $[H_0^+]$ is the concentration of hydrogen ions in the inflowing water, $[H^+]$ is the concentration of hydrogen ions in the effluent at time t, v is the flow velocity, and x is the bed length.

Figures 23 and 24 resemble the sorption behavior described by the model of the previous chapter. The rate of sorption of soda microcline is also seen to be less than that of the glass beads. In the case of the two higher silicates investigated (spodumene and forsterite) the rates of hydrogen ion sorption are extremely slow, being less for forsterite than for spodumene. This is to be expected since it was pointed out in Chapter 2 (page 19) that for a silicate mineral the higher the oxygen-silicon ratio the greater the amount of hydrogen sorption possible and thus it takes longer to achieve surface equilibrium.

Similar sorption curves were obtained for various experiments where beds of different lengths were used. As the bed length is reduced, however, the experimental error increases maximizing any dispersion effects.

On the basis of the derivation of the previous chapter and figures 23, 24, 25 and 26, one can conclude that the phenomenon occurring between the solid and the liquid is one of sorption and not a purely mechanical

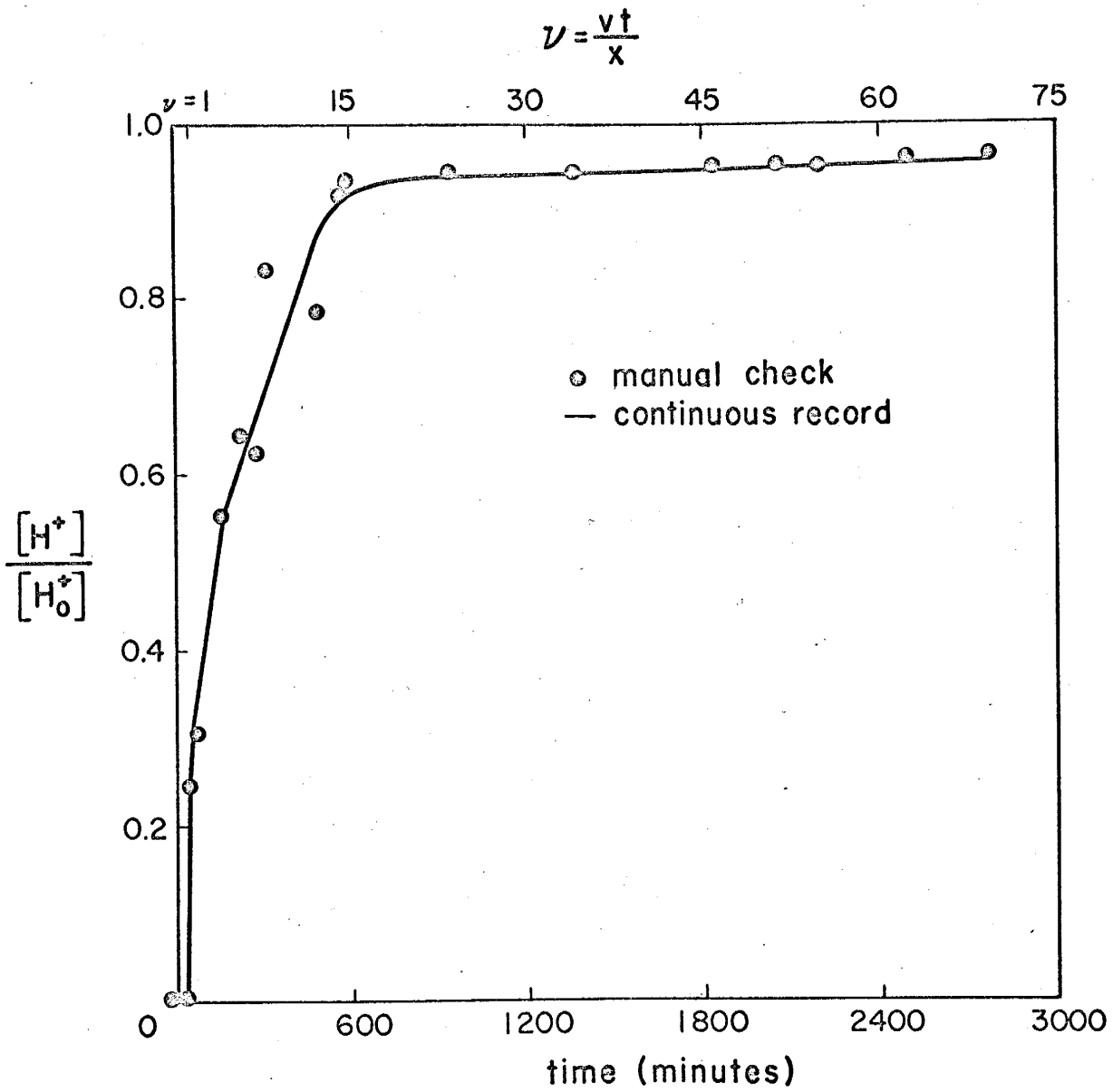

Figure 23. Sorption isotherm for glass beads.

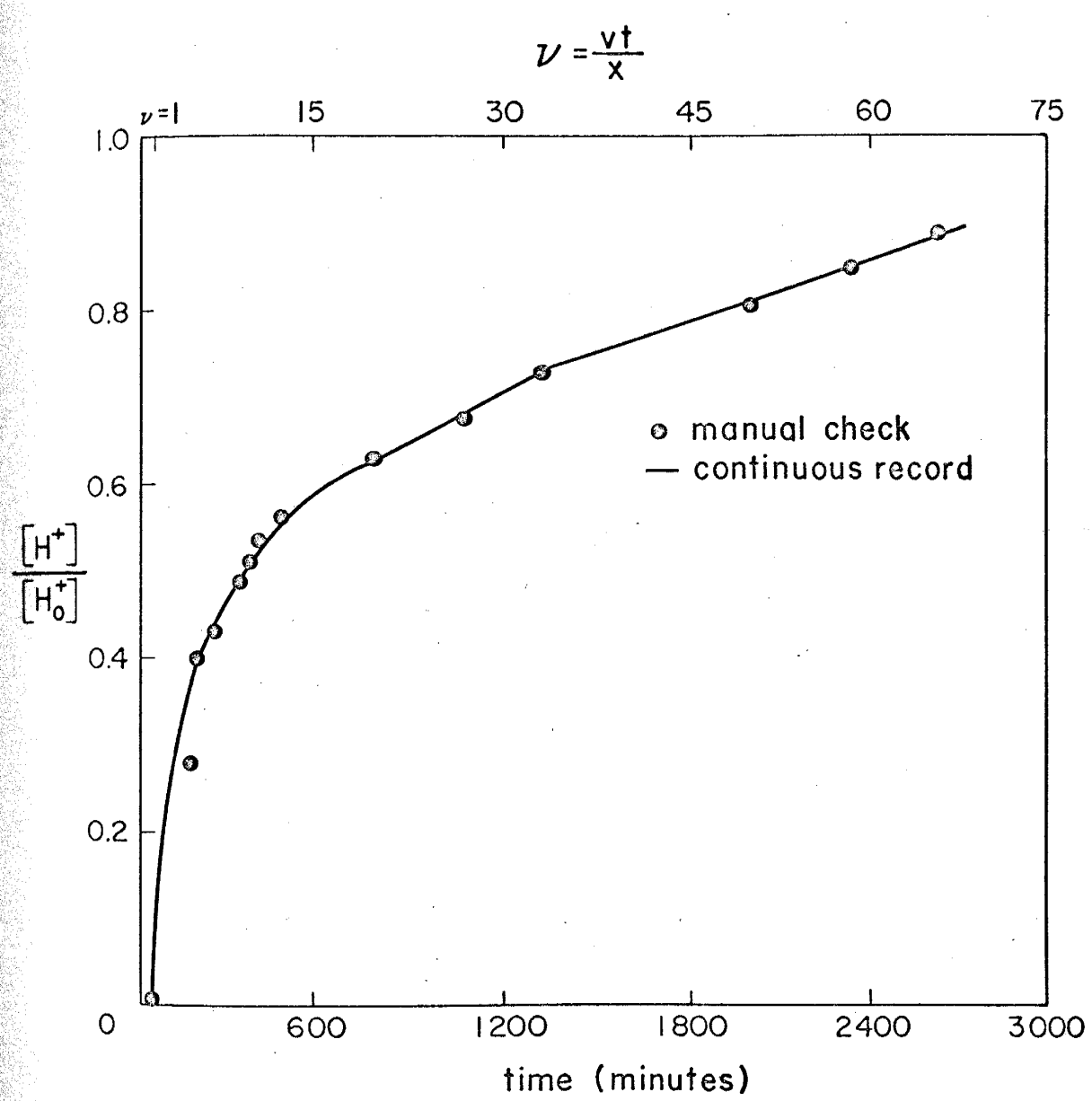

Figure 24. Sorption isotherm for soda microcline.

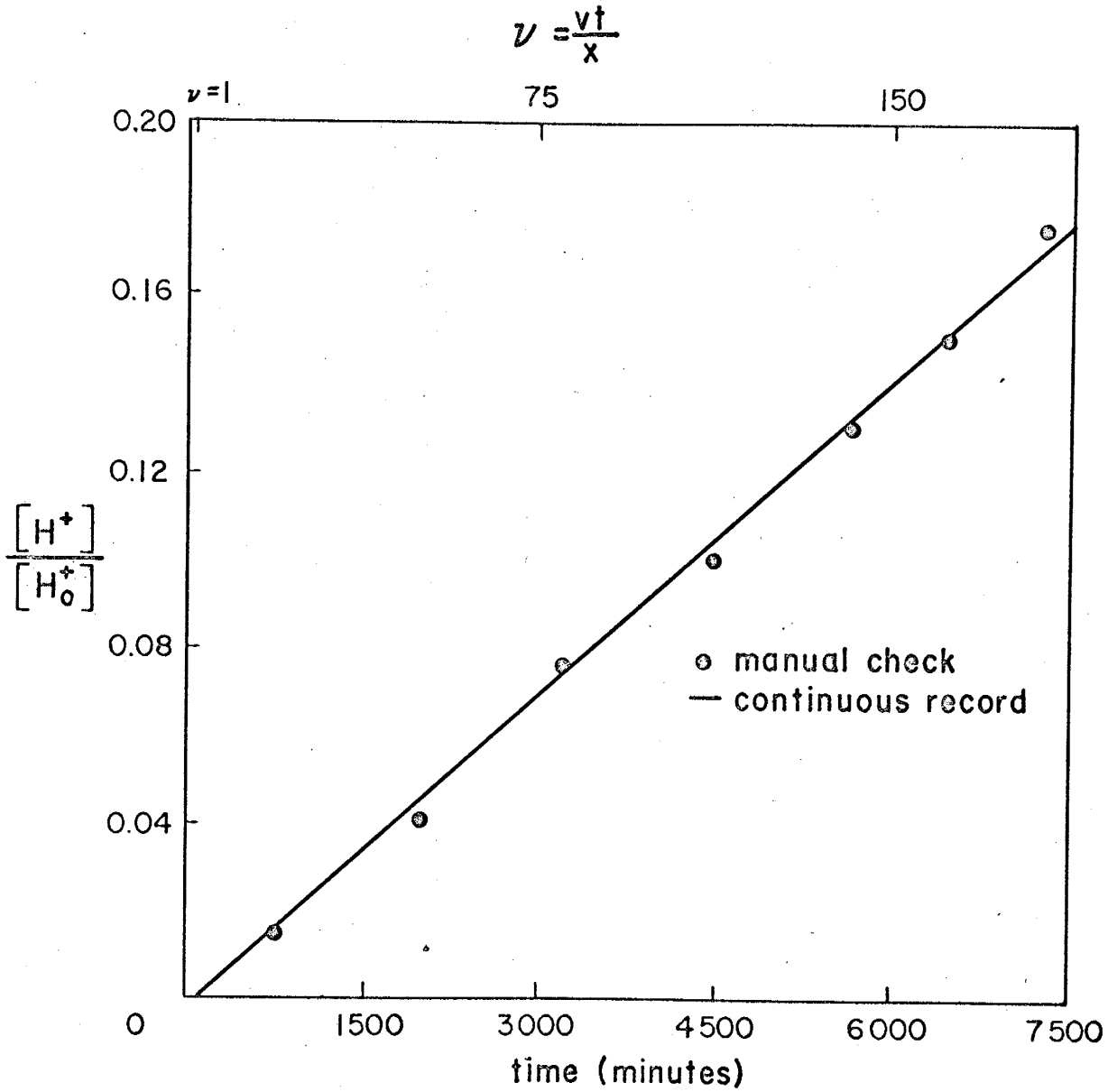

Figure 25. Sorption isotherm for spodumene.

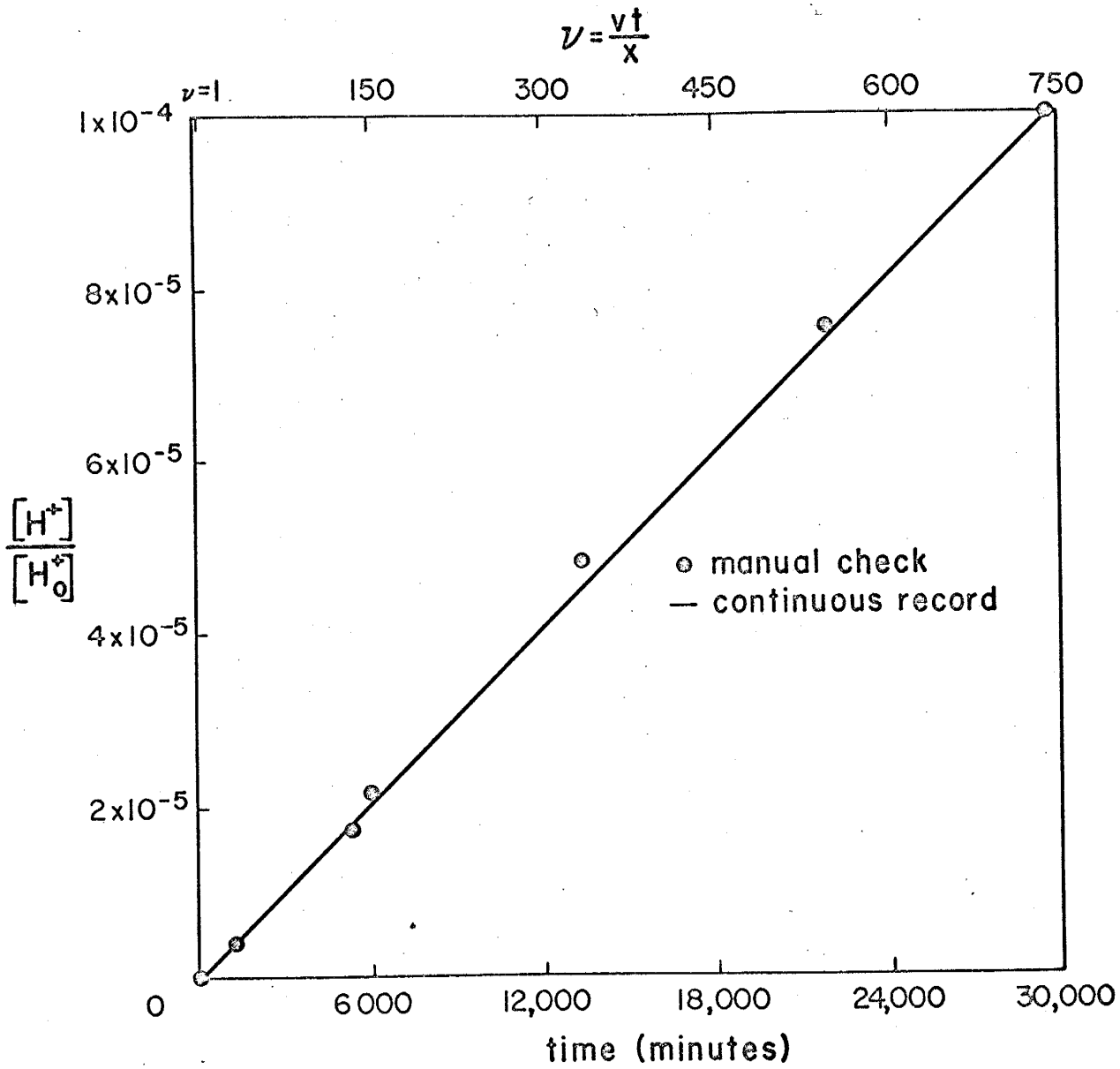

Figure 26. Sorption isotherm for forsterite.

phenomenon such as dispersion. If the phenomenon in question were dispersion, then C/Co must equal 0.5 when $\nu = 1$ and from the experiments this is clearly not so.

Dejú and Bhappu (1969) have further discussed how one can experimentally distinguish dispersion and sorption using the theoretical model and column experiments with glass beads.

Chloride in the water due to HCℓ addition was monitored using both a chloride electrode and the chloride analysis procedure reported in Appendix 1. No changes in the chloride concentration were observed in any of the experiments reported.

DESORPTION

In the previous section the movement of hydrogen ions from the liquid to the solid surface was discussed. In order for these ions to occupy positions on the solid surface some of the cations originally present on the solid surface must move into the liquid phase. This latter movement is termed desorption.

The main cations showing desorption in this study are Na^{+}, K^{+}, Li^{+}, Ca^{++}, Mg^{++}, Al^{+++}, Fe^{++}, and Fe^{+++}. The amounts of these cations in the water percolating through a solid bed were determined by the analytical methods outlined in Appendix 1. Samples of the percolating water were analyzed at relatively close intervals of time. Specific ion electrodes were tried for Ca^{++} but failed due to interference from other cations. Thus, all analyses reported were done chemically in most cases immediately or within a short time after withdrawing the sample.

Figure 27 shows the desorption curves for sodium, potassium, calcium, and magnesium on glass beads. The corresponding sorption isotherm is shown in Figure 23. As was pointed out in Table 6 these beads had 14.34% Na_2O, 9.63% CaO, 2.21% MgO. They also contained small traces of K_2O, FeO, and Al_2O_3. Figure 27 shows that considerable desorption of both Na^{+} and Ca^{++} occurred with smaller desorption of Mg^{++} and only a trace of K^{+} appeared in the effluent. The desorption of monovalent cations seems to occur prior to that of divalent cations. In the case of trivalent cations no desorption occurred until the desorption of divalent cations was completed.

The sample of soda microcline contained 8.13% K_2O and 5.10% Na_2O. Its desorption curves are shown in Figure 28. Even though potassium is present

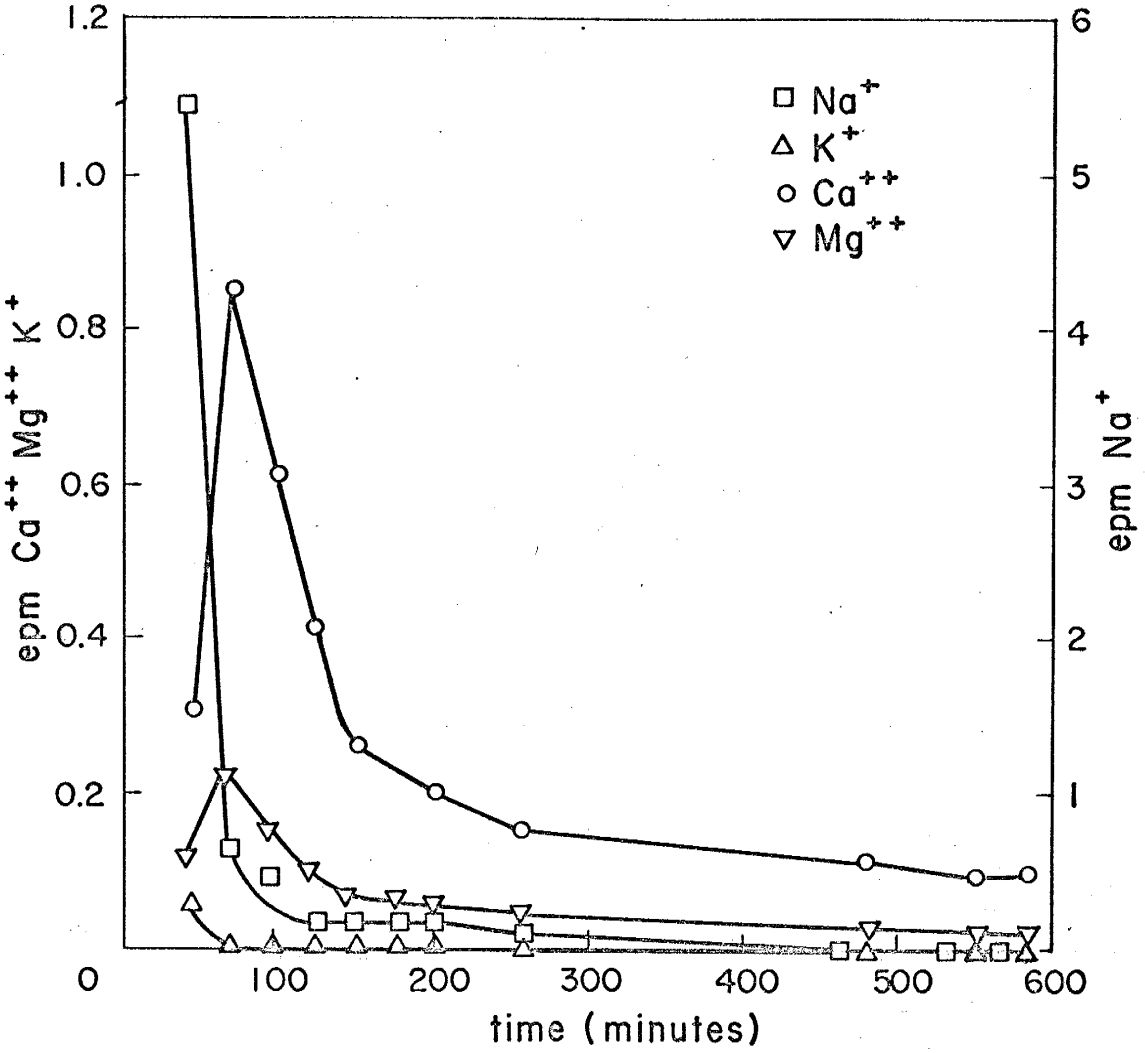

Figure 27. Na^+, K^+, Ca^{++}, and Mg^{++} desorption curves for glass beads.

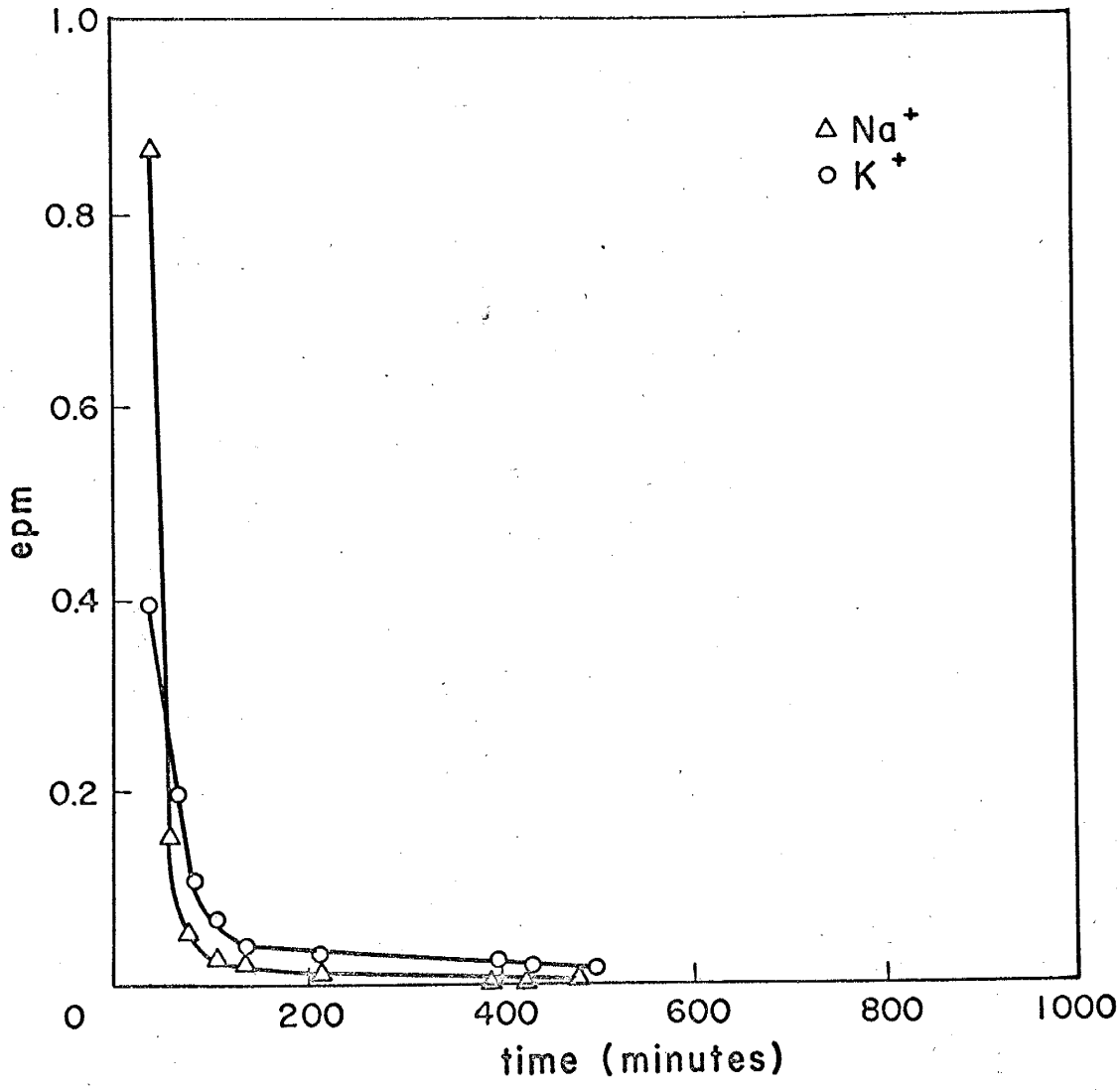

Figure 28. Na^+ and K^+ desorption curves for soda microcline.

in larger amount than sodium, the sodium desorbed faster and to a greater extent than the potassium. This may be due to:

(1) a tighter bonding of the potassium ions to the the crystal lattice, and/or

(2) the larger ionic mobility of sodium.

Figure 28 shows that the desorption of monovalent cations was almost complete after 100 minutes. Figure 29 shows the desorption curve of Al^{+++} for the same soda microcline. Al^{+++} desorption did not start until after about 100 minutes at which point the pH was about 4. A peak in the Al^{+++} desorption curve did not occur until about 400 minutes. As was pointed out before, this shows that Al^{+++} does not desorb considerably until the divalent and monovalent cations have completed their desorption. In the case of Al^{+++} the phenomena described can be similarly explained by a consideration of ionic mobilities or of the solubility of $Al(OH)_3$ in the pH range in question.

Figures 30, 31, and 32 for spodumene and forsterite show the same order of desorption described above for the glass beads and the soda microcline.

On the basis of all the experiments performed, an order of desorption from faster to slower can be established as follows:

monovalent cations	>	divalent cations	>	trivalent cations

or more specifically,

$$Li^{+} > Na^{+} > K^{+} > Mg^{++} > Ca^{++} > Fe^{++} > Al^{+++} > Fe^{+++}$$

which is the same order of relative ionic mobilities worked out for ion exchange resins (Dow Chemical Co., 1959).

In the case of the forsterite sample, even though there was 8 per cent FeO, the desorption of iron was very minimal and at best only in the range

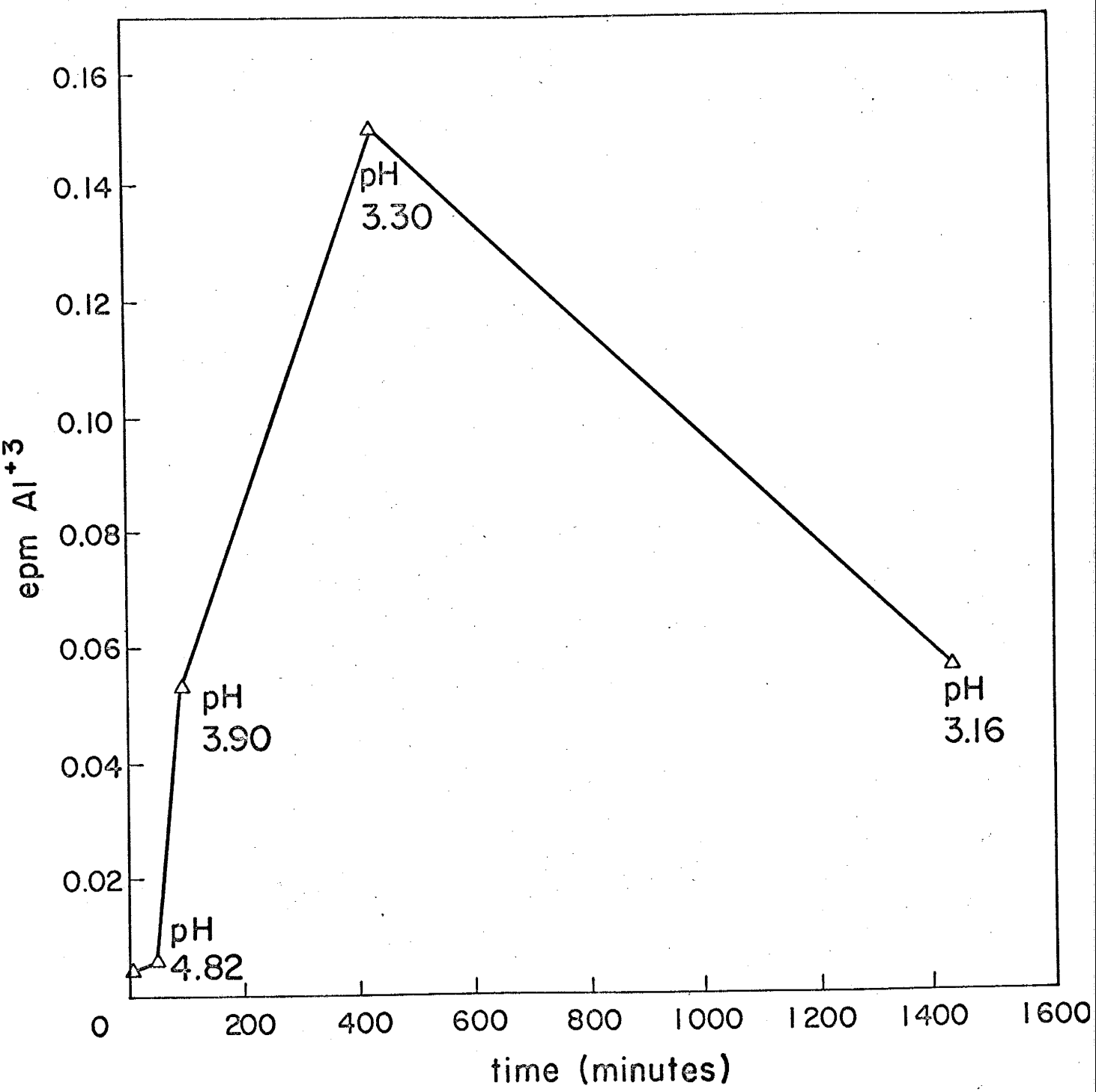

Figure 29. Al^{+3} desorption curve for soda microcline.

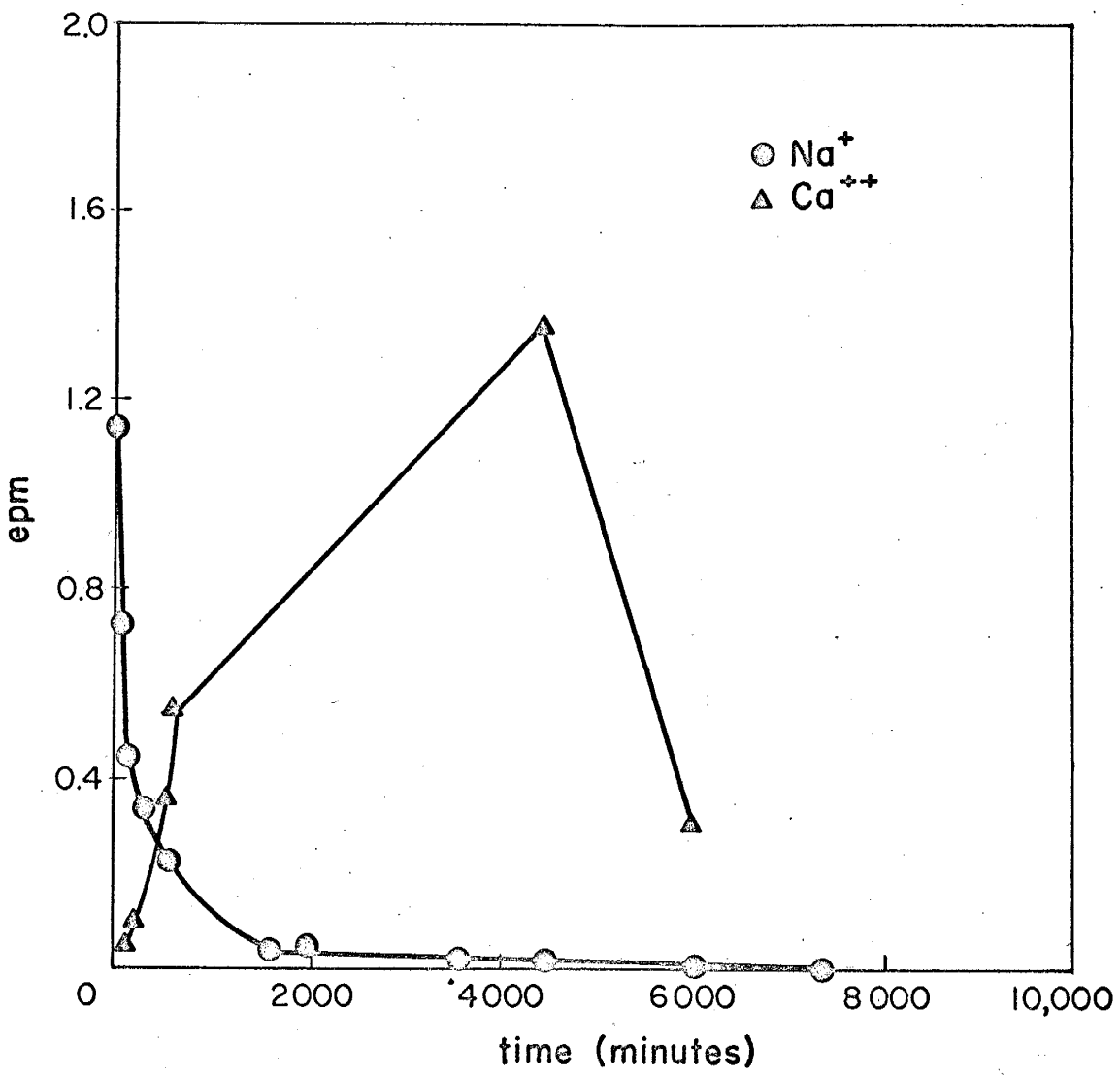

Figure 30. Na^{+} and Ca^{++} desorption curves for spodumene.

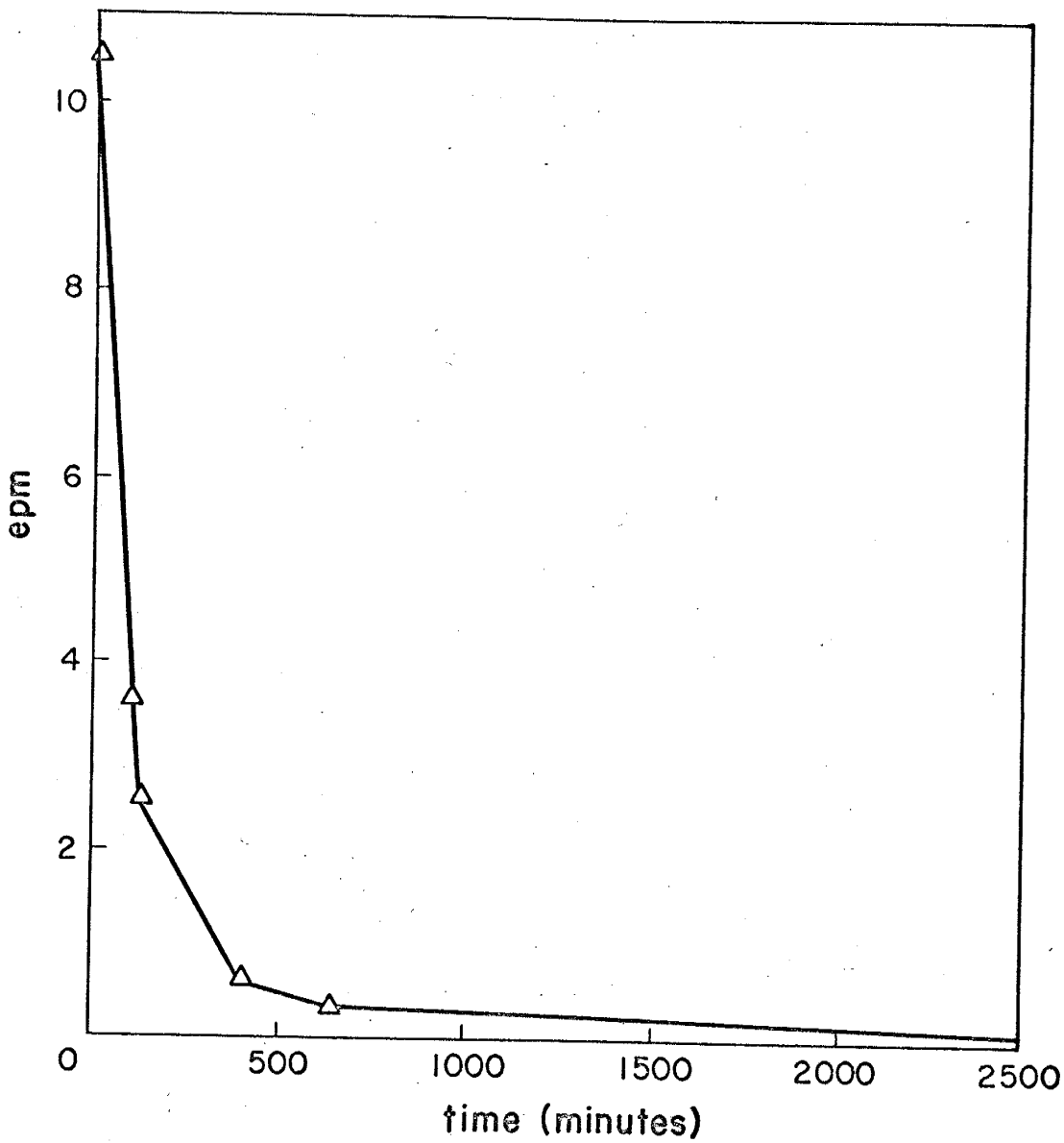

Figure 31. Li^+ desorption curve for spodumene.

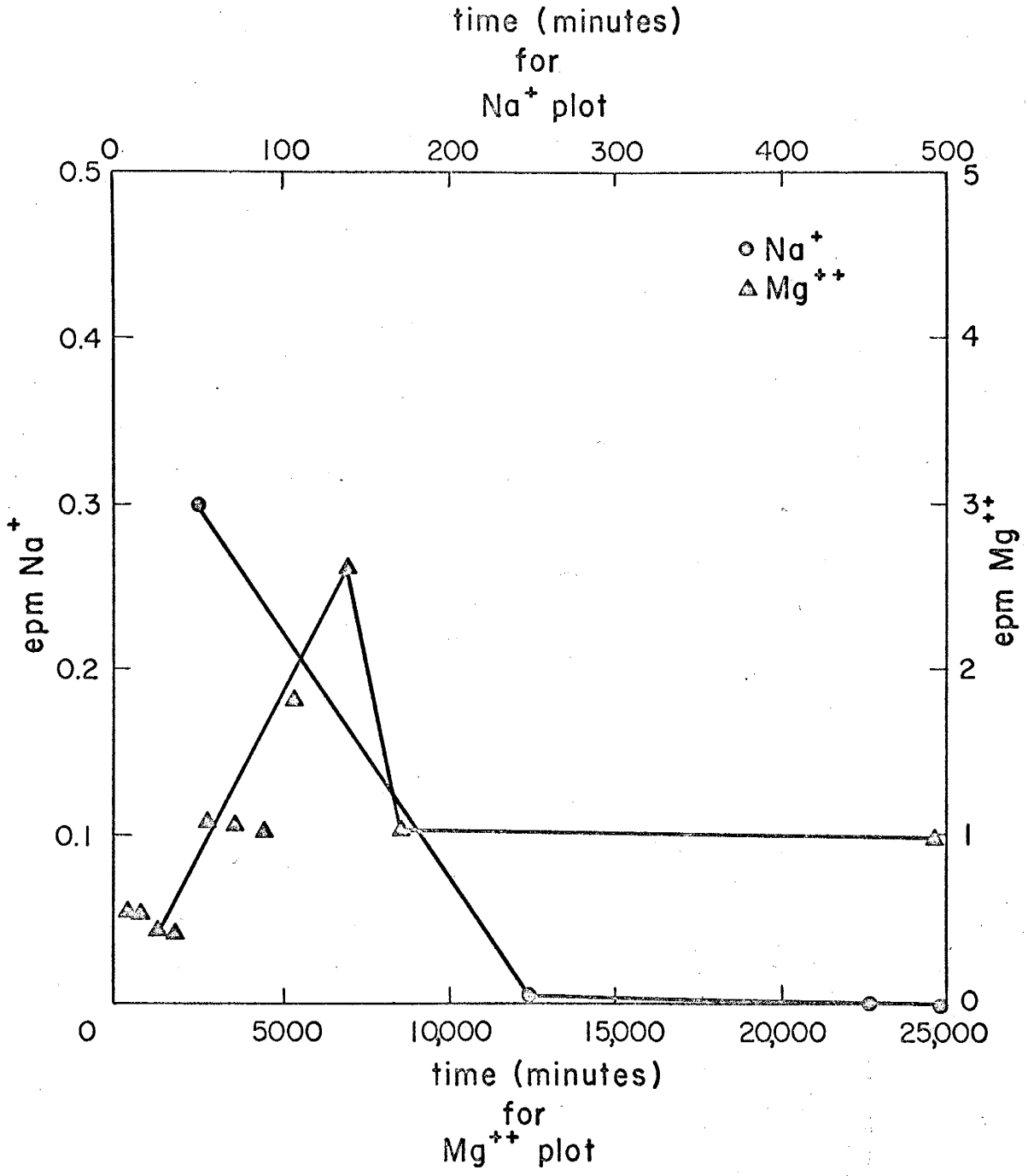

Figure 32. Na^{+} and Mg^{++} desorption curves for forsterite.

of a few parts per billion. Most of the iron found in solution was in the form of Fe^{++} and traces of Fe^{+++} were found once the pH went below 4. This is, of course, what one would expect from the solubility of the various iron complexes as a function of pH. Bhappu, Johnson, Brierley, and Reynolds (1968) have worked out such solubility curves for the iron system and their curves well agree with the extent of iron desorption in my experiments. However, since the iron desorption was so small, I would not like to make any quantitative statement in this respect because of possible inaccuracies in the method of analysis for such low concentrations of iron.

Silica behaved almost identically in all column experiments regardless of the bed being used. Silica dissolved initially up to about 6.45 ppm when the outflowing water was at pH values larger than 9. Then, its solubility declined slowly until it leveled off at about 2 ppm when the pH reached about 4.

SUMMARY

Column experiments consisting of water percolating through beds of glass beads, soda microcline, spodumene, and forsterite were conducted to verify and expand the theoretical model presented in the previous chapter.

The experimental curves of hydrogen sorption for glass beads and soda microcline resemble the theoretical curve of the previous chapter. The surface reaction between water and glass beads is much faster than that between water and microcline. For the two higher silicates used, the rates of reaction were so slow that no correlation with the theory was practical since surface equilibrium could not be achieved in a reasonable time for laboratory observation.

No changes in the chloride content of the water were observed in the experiments conducted.

In order for the hydrogen ion to occupy positions in the solid surface, desorption must occur and some of the cations originally present on the solid surface will move into the liquid phase. Desorption curves were plotted for each of the four systems under consideration. A correlation was found between rates of desorption and ionic mobilities, the greater the mobility, the faster the desorption.

Iron does not come into solution very easily and even in a forsterite sample where the FeO content was close to 8 per cent, no water sample was found to have more than a few parts per billion, mostly in the form of Fe^{++}.

Silica (at high pH values) initially dissolved up to about 6.45 ppm but, as the pH decreased, its solubility went down to about 2 ppm, at which point it leveled off.

The experiments performed in this chapter, together with the theoretical model in the previous chapter, confirm that sorption does occur at the water-silicate interface and allow a clear distinction between sorptive and dispersive behavior. No correlation of rate constants between model and experiment was attempted due to the experimental difficulties involved in determining rate constants, especially in reactions involving mineral systems.

REFERENCES

Bhappu, R. B., Johnson, P. H., Brierley, J. A., and Reynolds, D. H. (1968) Theoretical and Practical Studies on Dump Leaching, State Bureau of Mines and Mineral Resources Publication.

Deju, R. A., and Bhappu, R. B. (1969) A Kinetic Study of the Mechanism of Flow Through Porous Media, paper presented at the AIME National Meeting, Washington, D. C., Feb. 1969.

Dow Chemical Company (1959) Dowex: ION Exchange, R. R. Donnelley and Sons Company: Chicago, Ill.

GENERAL SUMMARY AND CONCLUSIONS

The purpose of this work was to investigate the reactions taking place between water and the porous medium through which it flows. The elements considered are the surface reactions at the liquid-solid interface and the flow equations. The theoretical model developed, coupled with the column experiments, helps in the understanding of the mechanism of surface reactions occurring when water percolates through a porous bed. The results presented show that sorption is the controlling process effecting changes in water quality. The silicate-water system is used because of the abundance and importance of the silicate minerals.

All sorption phenomena at the silicate-water interface can be conceived as adjustments to produce a minimum of free energy difference between the crystal, the surface, and the external environment.

The reactions between the silicate mineral particles and acidified water involve an exchange of metal ions for hydrogen ions on the surface of the solid leading to an increase of pH of the aqueous phase.

The degree of exchange as measured by the change of hydrogen ion activity of the water is related to the O:Si ratio of the minerals.

The rate of sorption of cations from the mineral surface is determined by the ionic mobility which is an index dependent on both the ionic size and the cation valence. The rate of sorption decreases from the monovalent to the trivalent cations and from smaller to larger cations. This is the same behavior as has been observed with ion exchange resins.

In addition to the chemical characteristics, the electrical properties of the interface are very important. The isoelectric point of charge

of a given silicate sample determines the range of pH in which surface reactions will occur. For this reason, a model of the electric layers surrounding a mineral particle in suspension is constructed and the resulting equations are used to obtain a better understanding of the reactions at the water-silicate interface.

Next, a model of flow through porous media with sorption is developed. This model shows the difference between sorption and dispersion. The column experiments with various minerals substantiate the model and furnish information about rates of sorption.

In brief, this work shows how important it is to consider surface reactions in studying hydrochemistry, especially when considering minerals containing metal cations.

RECOMMENDATIONS FOR FUTURE STUDY

The hydrochemical model presented here should be further generalized by extending it to two and three dimensions.

An interesting but complex problem would be to combine the model of sorption presented here with diffusion and dispersion.

An experimental set-up to study surface reactions at a solid-liquid boundary under pressure and at high temperatures should be devised.

More minerals with various cations on the surface should be studied to further expand the scheme of desorption rates presented here.

The hydrochemical results presented here should be used to predict hydrochemical behavior in the field.

Systems other than water and silicates should be studied.

APPENDIX 1. CHEMICAL ANALYSES PROCEDURES

1.1 Procedure for Aluminum Analysis in Water Samples

Type of method: colorimetric

Optimum range: 0-3.0 ppm

Reagents: AluVer - Hach #799 pkts.
Bleach - Hach #940 pkts.

Technique: (1) Measure 50 mls of sample into a 125 ml erlenmeyer flask, 50 mls of distilled water into a second, and 50 mls standard solution (2 ppm Aℓ) into a third.

(2) To each flask add contents of 1 pkt. AluVer and swirl to solution. A pink color will develop if Aℓ is present.

(3) Immediately divide each sample into two 25 ml parts.

(4) To one portion of each add contents of 1 pkt. bleach (#940) and swirl to mix. The pink color should disappear.

(5) Let stand 30 minutes and read A525 for each sample against its bleached counterpart as reference solution, recording as A, B, and C for pairs 1, 2, and 3, respectively.

$$Aℓ \text{ (ppm)} = 2(A-B)/(C-B)$$

Interference: This method is subject to slight interference from iron (10 ppm Fe = 1 ppm Aℓ).

1.2 Procedure for Calcium Analysis in Water Samples

EDTA method, calcein indicator, indirect titration based on H. Diehl, "Calcein, Calganite and 90-dihydroxybenzene," G.F.S. #199 p. 29 (1963).

1. Measure aliquot to contain less than 10 mg Ca into a 500 ml conical (Phillips) flask.

for Ca < 100 ppm, take 100 mls
100-200 ppm, 50 mls
200-400 ppm, 25 mls
400-1000 ppm, 10 mls

2. Add 5 mls each (concentrated) nitric and perchloric acids and 0.2 gms KCℓ and evaporate to dryness. Add 5 mls HCℓ (concentrated) and evaporate just to dryness. Do not bake.

3. Cool, add 2-3 drops (conc.) HCℓ and 10 mls of distilled H_2O and warm to solution. Dilute to 100 mls with distilled water.

4. Add, swirling to mix after each addition:
   (a) 0.2-0.3 mg ascorbic acid powder
   (b) excess standard (0.005 M) EDTA solution (1 ml = 0.2 mg Ca)
   (c) 5 mls of 20% triethanolamine in distilled water
   (d) 5 mls KOH-KCN buffer
   (e) 0.05 g of modified calcein indicator powder

A lavender (orchid) color should develop in 1-2 minutes.

5. Add standard (0.005 M) Ca solution until the violet color fades and a fluorescent green color appears.

6. Back titrate dropwise with the standard (0.005 M) EDTA solution until the green color vanishes and the non-fluorescent purple reappears. (Sensitive to 0.05 ml (1 drop) or less EDTA sln.)

Calculations: V = vol. EDTA sln - f x vol. Ca sln. where f = (vol EDTA soln)$_{std}$/(vol Ca soln)$_{std}$

Ca ppm = V x 401 M (100 ml sample aliquot)
= V x 802 M (50 ml sample aliquot)
= V x 1604 M (25 ml sample aliquot)
= V x 4010 M (10 ml sample aliquot)

There are no interfering elements.

Solutions Required: 1. KOH-KCN Buffer - dissolve 224 gms KOH and 40 gms KCN in water and dilute to 4 liters. Store in 1-gallon polyethylene bottle (160 g NaOH + 30 gms NaCN may be used to make 4 liters buffer).

2. Standard Calcium Solution - 500 ppm. Dissolve 2.498 gms primary-standard grade $CaCO_3$ in minimum HCl and dilute to two liters. Use to check standardization of standard EDTA solution.

3. Standard Ca solution - 0.005 M. Dissolve 2.000 gms primary-standard grade $CaCO_3$ in 10 mls HCl, boil off CO_2, and dilute to 4 liters. Store in a 1-gallon polyethylene bottle. Determine ratio, f, of concentration of standard EDTA solution to the concentration of the Ca solution by pipetting 10, 15, 20, and 25 ml, respectively, into 500 ml erlenmeyer flasks, diluting to 100 mls and titrating as directed for sample, starting at step #4.

f = (vol EDTA sln)$_{std}$/(vol Ca soln)$_{std}$
(use average of the 4 values determined)

4. Standard EDTA solution - 0.005 M. Dissolve 7.446 gms primary-standard-grade disodium ethylenediaminetetra-acetate dihydrate (GFS #365) in distilled water and dilute to 4 liters. Store in a 1-gallon polyethylene bottle. Check the molality against 10 mls aliquots of the 500 ppm standard calcium solution. Pipet the 10 ml aliquot (= 5.0 mg Ca) into a 500 ml erlenmeyer flask. Dilute to 100 mls and treat as sample starting in step 4.

1.3 Procedure for Chloride Analysis in Water Samples

To 25 ml sample add 3 drops of diphenyl carbazone bromophenyl blue indicator. Neutralize the sample with 0.05 N HNO_3 until blue indicator color goes to weak yellow. If the indicator color is not blue, add a drop of NaOH to obtain the blue color. Titrate slowly with mercuric nitrate to first permanent pink-violet color.

Indicator: .5 gms diphenylcarbazone + .05 gms bromophenol blue + 100 mls of 95% ethyl alcohol (keep in a dark bottle).

Calculations: ppm = 20 (ml titration)

1.4 Procedure for Iron Analysis in Water Samples

TPTZ - Extraction Method of Collins and Diehl (Journal of Marine Research, 1960).

Reagents: 2, 4, 6 - Tripyridyl-s-triazine (TPTZ) 0.001 M. Dissolve 0.321 gms ot TPTZ (GFS #291) in a few drops of HCl and dilute to 1 liter with deionized water.

Hydroxylammonium Chloride 10% (iron free) solution. Dissolve 10 gms of hydroxylammonium chloride in 100 mls of water. Add 1 ml of 0.001 M TPTZ and 1 gm of sodium perchlorate. Add 10 ml of nitrobenzene and shake the mixture for 1 minute. Allow the mixture to stand in a separatory funnel for a few minutes and then draw off the lower nitrobenzene layer and discard it. Store the water solution of the iron-free hydroxylammonium chloride in a glass bottle with a plastic cap with a polyethylene liner.

Sodium Acetate-Acetic Acid Buffer. 2 M Sodium Acetate-2 M Acetic Acid (iron free). Dissolve 16.4 gms of sodium acetate and 11.5 mls of acetic acid in 100 mls of H_2O. Add 1 ml of 0.001 M TPTZ, 1 ml of 10% hydroxylammonium chloride solution, and 1 gm of sodium perchlorate. Add 10 ml of nitrobenzene and shake the mixture for 1 minute. Allow the mixture to stand in a separatory funnel for a few minutes and then draw off the lower, nitrobenzene layer and discard. Store the solution in a glass bottle with a plastic cap with a polyethylene liner.

Sodium Perchlorate 10% (iron free) solution. Dissolve 10 gms of sodium perchlorate in 100 mls of water. Add 1 ml of 0.001 M TPTZ and 1 ml of 10% hydroxylammonium chloride solution. Add 10 mls of nitrobenzene and shake the mixture for one minute. Allow the mixture to stand in a separatory funnel for a few minutes and then draw off the lower nitrobenzene layer and discard. Store the solution in a glass bottle with a plastic cap with a polyethylene liner.

Standard Iron Solution (1) 10.0 µg Fe per ml; 1.00 µg Fe per ml. Weigh carefully 0.0702 g of ferrous ammonium sulfate and transfer to a 1-liter volumetric flask. Add iron-free water to dissolve the salt, add 2-5 mls of concentrated sulfuric acid, dilute exactly to the mark with iron-free water and mix well. Pipet 100.0 ml of this solution into a second 1-liter volumetric flask, add 2.5 ml of sulfuric acid, dilute to

the mark with iron-free water, and mix well. The first of these solutions contains 10 µg of iron per ml, the second contains 1 µg of iron per ml.

Standard Iron Solution (2) 0.050 µg Fe per ml. Pipet 50.0 ml of the standard iron solution containing 1.00 µg Fe per ml into a 1-liter volumetric flask. Add 2.5 ml of sulfuric acid, dilute to the mark with deionized water and mix well. This solution will contain 0.05 µg Fe per ml.

Cleaning of Glassware: Clean the glassware to be used with concentrated nitric or concentrated hydrochloric acid or a mixture of the two, preferably by soaking the glassware overnight.

Procedure. Pipet 100.0 ml of the water into a 125-ml separatory funnel. Add 2.0 ml of 10%, iron-free hydroxylammonium chloride solution, 2.0 ml of 10%, iron-free sodium perchlorate solution, 5.0 ml of 0.001 M TPTZ, and 5.0 ml of 2 M sodium acetate-2 M acetic acid buffer. If the previous treatment of the sample, such as wet ashing, has introduced much acid, neutralize with ammonium hydroxide to pH 4 to 5 as determined with a bit of indicator paper. Add 10 ml of nitrobenzene, shake for one minute, allow the phases to separate and gently swirl the funnel to dislodge any drops of nitrobenzene clinging to the upper walls. Drain the nitrobenzene layer into a 25-ml volumetric flask and repeat the extraction with another 10-ml portion of nitrobenzene. Dilute the combined extracts to 25.0 ml with ethanol. Measure the absorbancy of the solution at 595 mµ using a 5-cm cell and a mixture of nitrobenzene and ethanol (4:1) in the solvent cell. Run a reagent blank through the entire operation and subtract the absorbancy found for it from that of the unknown solution.

Then, prepare a calibration curve following the above procedure but using various volumes from 0 to 50 ml of the standard iron solution containing 50.0 µg Fe per liter.

The above procedure gives total iron values. For Fe^{++} analysis omit the addition of 10% iron-free hydroxylammonium chloride solution. However, standards must be reduced.

Taken from: The Iron Reagents: Bathophenanthroline, 2, 4, 6-Tripyridyl-S-Triazine, Phenyl-2-Pyridyl Ketoxime by Harvey Diehl, and G. Frederick Smith (GFS C.C. 1960).

1.5 Procedure for Lithium Analysis in Water Samples Using Atomic Absorption Spectrophotometry

Analytical Solutions

Stock Solution - 1000 ppm lithium in aqueous solution

Lithium Standards - 25-ml solutions containing 2.5, 5, 7.5, and 10 ppm lithium

Optimum Working Range - 1 to 10 ppm (in aqueous solution)

OPERATING CONDITIONS

Instrument Settings

	Model 303	Model 290
Wavelength - 6708 A	RANGE - VIS WAVELENGTH - 335	COARSE SELECT ELEMENT - 951.6
Slit	SLIT - 5 (3 mm, 40 A)	7 A
Source - Hollow cathode	SOURCE - 15 ma	LAMP CURRENT - 5 ma
Fuel - Acetylene (Oxidizing Flame)	FLOW[1] - 9.0	FUEL FLOW - 14.0
Oxidizer - Air	FLOW[2] - 9.0	AIR FLOW[2,3] - 14.0
Filter	FILTER - IN	Red (290-1070)

Footnotes:

[1]On fuel flowmeters having two float balls, flow is indicated by the upper (plastic) ball when the oxidant is air.

[2]Oxidant flow is the sum of the flows through the nebulizer and the auxiliary orifice.

[3]On early instruments, ADJUST FLAME control is set to 14.00.

Acetylene pressure should be 8 psig. Oxidant pressure should be set to 30 psig at the burner regulator for the Model 303, when either air or nitrous oxide is used.

ADDITIONAL ANALYTICAL INFORMATION

Sample Preparation - The samples should be diluted to put the lithium within the range from 1 to 10 ppm in aqueous solutions.

Sensitivity and Detection Limit - The standard conditions provide a sensitivity better than 0.07 ppm lithium for 1% absorption. It is not difficult to achieve a detection limit of 0.005 ppm lithium in aqueous solutions.

Other Analytical Lines - Gatehouse and Willis list a sensitivity of 15 ppm Li/1% absorption at 3233 A.

Flame - Lower temperature flames than the air-acetylene specified here will improve the sensitivity somewhat (2 times for air-coal gas) and will reduce the interaction with other alkali metals. See the discussion under cesium for more information.

Lamps - Absorption depends very little on lamp current, but the current must not be too high or the cathode will melt.

The Perkin-Elmer bismuth lamp has a bismuth-lithium alloy cathode and can be used for lithium determinations. The neon fill gas in this lamp, used for high bismuth emission, requires the use of narrow slits in lithium determinations, however, because several neon lines are close to the lithium 6708 A line. For routine lithium determinations, therefore, the single-element, argon-filled lithium lamp is to be preferred.

	Model 303		Model 290
Bi-Li Lamp Current	30 ma	Source	12 ma
Slit	2 (0.1 mm, 1.3 A)	Slit	2 A

1.6 Procedure for Magnesium Analysis in Water Samples Using Atomic Absorption Spectrophotometry

ANALYTICAL SOLUTIONS

Stock Solution - 1000 ppm magnesium in aqueous solution

Magnesium Standards - 25 ml solutions containing 0.5, 1.0, 1.5, and 2.0 ppm magnesium

Optimum Working Range - 0.2 to 2 ppm (in aqueous solution)

OPERATING CONDITIONS

Instrument Settings

	Model 303	Model 290
Wavelength - 2852 A	RANGE - UV WAVELENGTH - 285	COARSE SELECT ELEMENT - 209.5
Slit	SLIT - 5 (3 mm, 20 A)	7 A
Source - Hollow cathode	SOURCE - 6 ma	LAMP CURRENT - 4 ma
Fuel - Acetylene (Reducing flame)	FLOW[1] - 9*	FUEL FLOW - 14.0*
Oxidizer - Air	FLOW[2] - 8	AIR FLOW[2,3] - 14.0

Footnotes:

[1]On fuel flowmeters having two float balls, flow is indicated by the upper (plastic) ball when the oxidant is air.

[2]Oxidant flow is the sum of the flows through the nebulizer and the auxiliary orifice.

[3]On early instruments, ADJUST FLAME control is set to 14.00.

Acetylene pressure should be 8 psig. Oxidant pressure should be set to 30 psig at the burner regulator for the Model 303, when either air or nitrous oxide is used.

*Use a standard solution of 1 ppm magnesium and adjust the acetylene flow to obtain maximum absorption.

ADDITIONAL ANALYTICAL INFORMATION

Sample Preparation - Almost any material can be analyzed for magnesium by simply putting the sample into solution and diluting until the magnesium content is in the 0.2 to 2 ppm range. If aluminum is present at high levels, it may be necessary to use lanthanum or strontium to remove the potential interference.

Sensitivity and Detection Limit - When the standard conditions are used, the sensitivity is usually about 0.01 ppm Mg for 1% absorption. The signal-to-noise ratio is very favorable and it is possible to achieve a detection limit of 0.003 ppm in aqueous solutions.

Other Analytical Lines - In unpublished data, D. C. Manning has found that the magnesium ground state line at 2025 A has a sensitivity of about 2 ppm magnesium for 1% absorption.

Flame - A rich air-acetylene flame is preferable for the determination of magnesium by atomic absorption. The sensitivity of the magnesium analysis is about the same in the air-acetylene and the air-hydrogen flames. Experience with calcium indicates that the anionic interferences will be smaller in an air-acetylene flame. The sensitivity is less in liquid petroleum gas glames and the tendency toward anionic interferences is much increased.

Lamps - The absorption of magnesium in an air-acetylene flame decreases considerably as the lamp current is increased.

A Ca-Mg lamp is available and will save analysis time when a number of such dual determinations must be run. The operating currents for this lamp are as follows:

Model 303	Model 290
15 ma	5 ma

1.7 Procedure for Potassium Analysis in Water Samples Using Atomic Absorption Spectrophotometry

ANALYTICAL SOLUTIONS

Stock Solution - 1000 ppm potassium in aqueous solution

Potassium Standards - 25-ml solutions containing 2.5, 5, 7.5, and 10 ppm potassium

Optimum Working Range - 1 to 10 ppm (in aqueous solution)

OPERATING CONDITIONS

Instrument Settings

	Model 303	Model 290
Wavelength - 7665 A	RANGE - VIS WAVELENGTH* - 383	COARSE SELECT ELEMENT* - 1167.6
Slit	SLIT - 4 (1 mm, 13 A)	7 A
Source - Arc discharge	SOURCE - 350 ma+	LAMP CURRENT - 350 ma+
Fuel - Acetylene (Oxidizer - Air)	FLOW[1] - 9.0	FUEL FLOW - 14.0
Oxidizer - Air	FLOW[2] - 9.0	AIR FLOW[2,3] - 14.0
Filter	FILTER - IN	Red (290-1070)

Footnotes:

[1]On fuel flowmeters having two float balls, flow is indicated by the upper (plastic) ball when the oxidant is air.

[2]Oxidant flow is the sum of the flows through the nebulizer and the auxiliary orifice.

[3]On early instruments, ADJUST FLAME control is set to 14.00.

Acetylene pressure should be 8 psig. Oxidant pressure should be set to 30 psig at the burner regulator for the Model 303, when either air or nitrous oxide is used.

*Wait a few minutes after the source is turned on before making the wavelength setting. A bright argon line near the potassium line appears earlier and may lead to confusion if the wavelength is set immediately.

+If drift or instability is observed after lamp warmup (20 to 30 min.), use the next higher lamp current setting available.

ADDITIONAL ANALYTICAL INFORMATION

Sample Preparation - A wide variety of industrial and biological materials can be analyzed for potassium by putting them into solution in a suitable solvent. The dilution should provide a potassium concentration in the range from 1 to 10 ppm in solution. If an acetylene flame is used, sodium

may interfere slightly if present at much higher levels than the potassium. This effect can be avoided by approximately matching the sodium content of the potassium standards with that of the sample. The match need be no better than 20% of the amount present.

Sensitivity and Detection Limit - Under the standard conditions, the sensitivity is about 0.1 ppm potassium for 1% absorption. The detection limit is less than 0.005 ppm potassium when scale expansion is used. Gatehouse and Willis indicate that the potassium determination is more sensitive in a rich low-temperature flame.

Other Analytical Lines - Gatehouse and Willis list a sensitivity of 5 ppm for 1% absorption at the potassium line at 4044 A.

Interferences - Potassium absorption is enhanced in the presence of Na, Li, and Cs, especially in a high-temperature flame. This is discussed in more detail in connection with cesium.

Lamps - A hollow cathode lamp is also available for potassium determination but the detection limit is poorer. Lamp currents:

Model 303	Model 290
25 ma	10 ma

1.8 Procedure for Silica Analysis in Water Samples

All samples in this study contained low amounts of silica. The colorimetric procedure below applies only to samples in the low range (< 12 ppm preferably 0-5 ppm).

(1) Pipet 25 ml of sample into each of two erlenmeyer flasks, and 25 ml standard (2 ppm) into a third.
(2) To each add 1 pkt molybdate powder (Hach #759) and 1 pkt acid powder (Hach #735).
(3) Swirl to dissolve and let stand 10 minutes.
(4) To each add 1 pkt of 0.1 gm oxalic acid (Hach #763), swirl to solution and let stand two minutes.
(5) To #1 and #3 add 1 pkt amino acid powder (Hach #804), swirl to mix and let stand 5 minutes.
(6) Read A700 for sample and standard against the blank (Flask #2).

Silica (ppm) = 2A(sample)/(A standard)

1.9 Procedure for Sodium Analysis in Water Samples Using Atomic Absorption Spectrophotometry

REAGENTS

Sodium chloride
Water, freshly distilled in an all-glass still and stored in polyethylene.

ANALYTICAL SOLUTIONS

Stock Solution - 1000 ppm sodium in aqueous solution

Sodium Standards - 25-ml solutions containing 1, 2, and 3 ppm sodium

Optimum Working Range - 0.3 to 3 ppm sodium

OPERATING CONDITIONS

Instrument Settings

	Model 303	Model 290
Wavelength - 5890 A	RANGE - VIS WAVELENGTH - 295	COARSE SELECT ELEMENT - 780.8
Slit	SLIT - 3 (0.3 mm, 4 A)	7 A
Source - Arc discharge	SOURCE - 700 ma*	LAMP CURRENT - 700 ma*
Fuel - Acetylene (Oxidizing flame)	FLOW[1] - 9.0	FUEL FLOW - 14.0
Oxidizer - Air	FLOW[2] - 9.0	AIR FLOW[2,3] - 14.0

Footnotes:

[1]On fuel flowmeters having two float balls, flow is indicated by the upper (plastic) ball when the oxidant is air.

[2]Oxidant flow is the sum of the flows through the nebulizer and the auxiliary orifice.

[3]On early instruments, ADJUST FLAME control is set to 14.00.

Acetylene pressure should be 8 psig. Oxidant pressure should be set to 30 psig at the burner regulator for the Model 303, when either air or nitrous oxide is used.

*If drift or instability is observed after lamp warmup (20-30 min.), use the next higher lamp current setting available.

ADDITIONAL ANALYTICAL INFORMATION

Sample Preparation - If soluble in aqueous solvents, almost any material can be analyzed for sodium by simply putting the material into solution and diluting it to the optimum analytical range of 0.3 to 3 ppm. Non-aqueous solutions require standards in the same solvent.

Sensitivity and Detection Limit - Under the standard conditions, the sensitivity is about 0.04 ppm sodium per 1% absorption. An increase of about two times will result from the use of a low-temperature flame. Since there is very little noise associated with this analysis, it is easy to achieve a detection limit of less than 0.005 ppm sodium with the Model 303. A detection limit of 0.02 ppm sodium has been obtained with the Model 290. Slight improvements in these detection limits are obtainable by use of the Boling burner heads to reduce noise due to dust particles in the flame.

Other Analytical Lines - The 3302 A resonance line of sodium yields a sensitivity of about 5 ppm sodium for 1% absorption and provides a convenient way to avoid the need to dilute more concentrated solutions of sodium.

Interferences - Robinson shows no interference from 5000 ppm Li or K on the determination of sodium. Experience with other alkali metals in the air-acetylene flame indicates that large concentrations of another alkali metal will alter the proportion of the metal that is ionized, and since for the alkalis a considerable fraction of the metal is ionized at the temperature of an air-acetylene flame, a significant quantitative error can result. This is a problem only if another alkali is present at a much higher concentration than the sodium. Sodium can be determined at levels of less than 1 ppm, even in calcium salts, without any interference from the calcium present.

Lamps - The arc discharge lamp used for the determination of sodium usually requires about twenty to thirty minutes to warm up. Some lamps require higher currents than the recommended 700 ma to produce a stable discharge. Other lamps require a higher current for starting but will operate at a lower lamp current. No current available from the Lamp Power Supply will damage the lamp. Increase the lamp current until the arc has the characteristic yellow-orange color of the sodium discharge.

A hollow cathode lamp is available for sodium. It requires a warmup time of only five minutes, but does not provide the energy available from the arc discharge lamp. Use the following operating conditions:

	Model 303	Model 290
Slit	4 (1 mm, 13 A)	20 A
Lamp current	25 ma	10 ma

1.10 Procedure for Surfactant (Anionic) Analysis

SCOPE

1. This method describes a procedure for the determination of anionic surfactants such as sodium alkyl aryl sulfonates, petroleum sulfonates, and sodium or ammonium alkyl sulfates. Because of the small

quantity of compound required for a determination, 0.1 to 0.4 mg, the method is applicable to dilute solutions and to highly colored materials such as new or used engine oils. Carboxylic acids and their salts do not interfere.

METHOD SUMMARY

2. The surfactant is allowed to react with an aqueous solution of methylene blue chloride and the resulting colored methylene blue-surfactant salt is extracted with chloroform. After the extracts are washed with water the surfactant is determined colorimetrically.

APPARATUS

3. Photoelectric Colorimeter. Any spectrophotometer or photoelectric colorimeter equipped with an interference filter transmitting light at 650 mμ may be used. This procedure is written for a Beckman Model B Spectrophotometer equipped with 1 cm cells.

REAGENTS

4. (a) Chloroform, cp.

(b) Methylene Blue Solution. Dissolve 0.1 g of methylene blue chloride (USP) in 100 ml of distilled water.

(c) Hydrochloric Acid, cp, 6 N.

APPARATUS STANDARDIZATION

5. (a) Prepare 4 standards, using a material which contains a previously determined (see Note 1) amount of the particular surfactant for which analysis is to be made, by accurately weighing out portions to contain approximately 0.0002, 0.0004, 0.0006, and 0.0008 meq (approximately 0.1 to 0.4 mg). Continue as directed in Sections 6(b) and 6(c).

Note 1. Analysis of surfactants for use in preparation of standards can be made most rapidly by the Methylene Blue Titration method.

(b) If the material is colored, weigh out another portion, to contain between 0.0002 and 0.0008 meq, for use as a color blank. Treat as in Sections 6(b) and 6(c) but omitting the methylene blue solution.

(c) Obtain a corrected absorbance for each standard by use of the calculations in Section 7(a). Plot the corrected absorbances against milliequivalents of surfactant.

PROCEDURE

6. (a) Weigh an amount of sample into distilled water or chloroform, whichever is more appropriate, so that after suitable dilution, an aliquot portion of 20 ml or less will contain between 0.0002 and 0.0008 milliequivalents.

(b) Measure this portion into a 125-ml separatory funnel and add water and/or chloroform until approximately 20 ml of each is present. Neutralize the mixture by adding 6 N hydrochloric acid dropwise, using an indicator paper, and add 3 or 4 drops in excess. Add 1 ml of the methylene blue solution, stopper the funnel, and shake gently for 1 minute, venting the funnel occasionally. Allow the funnel to stand for 5 minutes and carefully drain the lower (chloroform) layer into a second 125-ml separatory funnel containing approximately 20 ml of distilled water. Stopper the second funnel, shake it for one minute and allow it to stand for five minutes. Carefully drain the chloroform layer through a plug of cotton in the vortex of a filter funnel into a 100-ml volumetric flask. Make three additional extractions with 20-ml portions of chloroform. Each time, transfer the chloroform layer to the second funnel, wash with 20 ml of fresh distilled water as before and collect in the volumetric flask. Wash the filter funnel and cotton with chloroform and dilute to the mark.

(c) Within one hour measure the absorbance relative to distilled water using the Beckman Model B Spectrophotometer adjusted to transmit light at 650 mμ and covered 12 x 12 x 46-mm rectangular cells.

(d) Make a blank determination on the reagents by repeating the entire procedure but omitting the sample.

(e) If the sample is colored, make a color blank determination by repeating the entire procedure on a similar sized portion of sample but omitting the methylene blue solution.

CALCULATION

7. (a) Correct the absorbance obtained for the sample by subtracting the absorbance of the reagent blank (Section 6(d)) and the absorbance of the blank color blank by means of the following expression:

$$\text{Corrected Absorbance} = A - \frac{B \times D}{C} - E$$

where:

A = absorbance obtained for the sample,
B = absorbance obtained for the sample color blank,
C = weight of sample taken for sample color blank, grams,
D = weight of sample taken for analysis, grams, and
E = absorbance obtained for the reagent blank.

(b) Obtain the milliequivalents of surfactant present from the calibration curve. Calculate the surfactant content of the sample by means of the following expression:

$$\text{Anionic Surfactant content, milliequivalents/100 g} = \frac{(F)(100)}{(W)}$$

where:
F = surfactant present, obtained from calibration curve, milliequivalents, and
W = weight of sample contained in portion extracted.

APPENDIX 2. PPM-EPM CONVERSIONS

Li^{+}	ppm x 0.14411 = epm
Na^{+}	ppm x 0.04350 = epm
K^{+}	ppm x 0.02558 = epm
Ca^{++}	ppm x 0.04990 = epm
Mg^{++}	ppm x 0.08224 = epm
Fe^{++}	ppm x 0.03582 = epm
Fe^{+++}	ppm x 0.05373 = epm
Al^{+++}	ppm x 0.11160 = epm
Cl^{-}	ppm x 0.02820 = epm
HCO_3^{-}	ppm x 0.01639 = epm
CO_3^{--}	ppm x 0.03333 = epm
SO_4^{--}	ppm x 0.02082 = epm

This thesis is accepted on behalf of the faculty of the Institute by the following committee:

E. Jacobs

Roland B. Schaffer

Gerhard Wolfgang Groves

R. Wayne Ohline

Date: 3 March '69